

**Super-resolved imaging reveals insights  
into the NK cell immune synapse and  
can validate expansion microscopy**

# Dissertation

zur Erlangung des  
Doktorgrades der Naturwissenschaften (Dr. rer. nat.)

Der

Naturwissenschaftlichen Fakultät I  
Biowissenschaften

der Martin-Luther-Universität  
Halle-Wittenberg,

vorgelegt

von Herrn Maximilian Lothar Wilhelm Büttner

Datum der Verteidigung: 12.Januar.2024





---

**Super-resolved imaging reveals  
insights into the NK cell immune  
synapse and can validate expansion  
microscopy**

---

Academic supervision:

Prof. Dr. med. Heike Kielstein  
Prof. Dr. rer. nat. Ingo Heilmann

## Table of Contents

### The effect of leptin on the natural killer cell immune synapse and lytic granule exocytosis machinery

Introduction	6
<i>Role of natural killer cells</i> .....	7
<i>NK cell activating receptors and the cases of NKp30 and NKG2D</i> .....	7
<i>Adhesion and inhibitory receptors</i> .....	8
<i>Cytokines and the adipocytokine leptin</i> .....	9
<i>Interest in NK cell biology for immunotherapy</i> .....	10
<i>How does a kill through degranulation work?</i> .....	12
<i>NK cell functional assays</i> .....	13
<i>Influence of differential protein expression due to external stimuli</i> .....	14
<i>Confluence of activating and inhibitory signals</i> .....	14
<i>Manifold influences can only result in a binary outcome</i> .....	16
<i>Minimal models</i> .....	16
<i>Microscopy techniques</i> .....	17
<i>Choice of in vitro model</i> .....	19
Results	21
<i>Validating the cell model and induction of degranulation</i> .....	21
<i>Modifying the LAMP1 degranulation assay for the minimal model</i> .....	23
<i>STED imaging of leptin-simulated NK-92 cells</i> .....	25
<i>Colocalization of NKp30 receptor clusters and lytic granules</i> .....	27
<i>Rac1 and CDC42 pulldown assay</i> .....	31
<i>Rho-family kinase activity</i> .....	32
<i>Bottom-up proteomics approach for target identification</i> .....	33
<i>Changes in protein expression</i> .....	34
<i>Phosphorylation in response to leptin</i> .....	36
<i>Jak/STAT, MAPK/Erk- pathway and signaling proteins regulating actin-modifying proteins</i> .....	36
<i>Leptin alters phosphorylation of actin-modifying proteins and proteins coordinating exocytosis</i> .....	37
Discussion	50
<i>Validity of the model system</i> .....	50
<i>Utility of the model</i> .....	51
<i>STED-Imaging shows differences in actin density</i> .....	52
<i>Lytic granules preferentially localize to NKp30 protein clusters</i> .....	52
<i>Leptin affects Rho-family proteins and further regulatory pathways</i> .....	54
<i>Alterations in the exocytosis machinery</i> .....	56
Methods	59

## Challenges of using expansion microscopy for super-resolved imaging of cellular organelles

Introduction	67
<i>The peroxisomal import machinery</i> .....	68
<i>Expansion microscopy can increase resolution</i> .....	68
Results	70
<i>Expansion of the nucleus</i> .....	70
<i>Comparison of cell area and the mitochondrial network</i> .....	70
<i>Peroxisomal membrane and matrix</i> .....	73
Discussion	75
<i>The nucleus expands anisotropically</i> .....	75
<i>Signal loss can impair detection confidence</i> .....	75
<i>The peroxisomal membrane expands more than the peroxisomal matrix</i> .....	76
<i>Direct comparison of individual cells</i> .....	77
<i>Alternative approaches to increasing the fluorescence intensity</i> .....	78
<i>Conclusion</i> .....	78
Methods	79
References	82



# **The effect of leptin on the natural killer cell immune synapse and lytic granule exocytosis machinery**

## **Introduction**

### **Role of natural killer cells**

Natural killer cells (NK cells) perform a key function in innate immunosurveillance. They patrol the human body in search of virally infected or malignantly transformed cells. Having found these, such a target cell can be forced to undergo apoptosis by the cytotoxic effector functions of an NK cell. They can also secrete inflammatory cytokines to alert other components of the immune system.[1] What determines the strength of NK-cell cytolytic functions has been the subject of considerable research. The biochemical underpinnings of how an NK cell decides which cell it sends into apoptosis or leaves unharmed remain incompletely understood still.

There are a number of commonalities between the cytotoxic function of NK cell and their far more intensely researched counterpart in the specific immune system: T-cells. The main distinguishing feature is the T-cell receptor (TCR), which is specific to an antigen that is knowingly associated with disease. If the TCR of a T-cell binds to a protein motif displayed on the human leucocyte antigen-1 complex (HLA-1) of another cell, there is certainty that this cell is diseased and must be forced into apoptosis.[2] This certainty in recognition is possible only because the T-cell with this specific TCR was previously selected for and activated by contact with an antigen-presenting-cell.[3]

NK cells perform the same cytotoxic effector functions, they however require no priming nor prior education what a diseased cell looks like in terms of a single, definitive antigen. Instead, they have a complex array of mechanisms that allow them to sense the state of a cell they are in contact with. One of the earliest discovered mechanism is described by the concept of the ‘missing self’: Every human cell expresses the HLA-I complex, which is laden with peptides from the cellular interior. It is this complex that is bound by the TCR in search of its antigen.[4] Thus, if HLA-I expression of a cell is abolished due to infection or transformation, this cell can evade T-cells. NK cells perform a complimentary function here: If a cell does not express the ‘self’- HLA-I complex, it is killed by NK cells. [5, 6] Another complement to the adaptive immune system can be found in NK-cell mediated antibody-dependent cytotoxicity: NK cells detect other cells opsonized with Immunoglobulin G1 (IgG1) through their Fc $\gamma$ RIIIA receptor and force them into apoptosis.[7, 8]

### **NK cell activating receptors and the cases of NKp30 and NKG2D**

Although these two functions were discovered first, they are only one facet of NK-cell activity. Their main capability is the killing of diseased cells without the need for prior education. NK cells can judge the state of cells that they come into contact with through a wide array of receptors, generally split into the two categories of activating and inhibitory NK-cell receptors. The activating receptors are capable of binding so-called stress-induced ligands on their target cells.[1] An overview of NK-cell receptors and their cognate ligands can be found in Fig. 1 of the aforementioned publication.

Most of these ligands are not constitutively expressed by normal cells, but their expression can be induced via various forms of cellular stress. A well-studied example is the receptor NKG2D with its ligands. After DNA damage, the DNA-damage-response-pathway attempts to mitigate: The ATM and ATR kinases are activated by double strand breaks and in turn phosphorylate several proteins related to the DNA damage checkpoint. ATR can also be activated by a stalled replication fork. They concomitantly induce the expression of the NKG2D ligands MICA, MICB and ULBP1-3. A number of tumor diseases trigger this mechanism and, to a lesser extent, some viral infections do as well.[9] Thus, a cell can signal its woes in maintaining genetic integrity to the immune system.

While the previous example relates to DNA-damage specifically, the sensory function of an NK cell receptor is often multifunctional, because the receptor-ligand binding is degenerate: One receptor is able to bind several different ligands. The activating NK-cell-receptor NKp30 can, for one, bind to B7-H6. This stress-induced ligand is not expressed by healthy tissue but has been shown to be expressed by several tumors.[10] The mechanism leading to its induction are currently not known. Some ligands do not require a dedicated system for its induction: In healthy cells, BAT3 is located in the nucleus. Its presence on outer cell membrane indicates that the cell has suffered a heat shock and this is detected by NKp30.[11] This receptor can also bind certain heparan sulfate structural motifs [12] that are typically found on tumor cells.[13]

Structurally, a transmembrane region anchors NKp30 to the cell membrane, while the outer domain is composed of eight  $\beta$ -strands and two short  $\alpha$ -loops, forming two antiparallel  $\beta$ -sheets. *In vivo*, a stalk domain extends toward the membrane, that was not expressed in the truncated protein used for crystallography. Interestingly, this data hints at a possible dimeric structure on the membrane.[14] Structural data is also available for NKp30-bound to its ligand B7-H6 [15] and recent work has confirmed that NKp30 does oligomerize in an *N*-glycosylation dependent manner in an artificial system.[16] Whether this occurs *in vivo* is not known. B7-H6 shares little sequential or structural homology to the other NKp30 ligands. Binding of B7-H6 triggers translocation of Arg143 from the membrane interface into the membrane. This then allows assembly of the TCR $\zeta$ -chain – signaling complex on the cytosolic side. This is notably the same complex established on the TCR after its ligation.[17]

How and how well NK cells can detect viral infection is less well documented than their response to transformed cells. During influenza infection, the receptors NKp30, NKp44 and NKp46 are able to bind viral haemagglutinin.[18] Antibody-dependent cytotoxicity (ADCC) and elimination of “missing self” cells also contribute to viral immunity. How significant this contribution is, is not entirely clear but has become the subject of current research. SARS-CoV-19 infection induces changes in expression profiles of NK cells, with certain activating receptors being induced. Inhibitory receptors are also being induced concomitantly. How these receptors are able to recognize viral infection or viral structural motifs is not known for the majority of receptors.[19]

### **Adhesion and inhibitory receptors**

Apart from an indication of stress, an NK cell requires binding of adhesion receptors to facilitate induction of apoptosis. In this, the receptor integrin  $\beta$ -2 (also referred to as LFA1) serves two functions. It can facilitate adhesion between the NK cell and a target cell or other immune cells, allowing it to maintain contact even if mechanical forces are exerted. It can do this either by homodimerization or by forming a heterodimer with one of its 40 known ligands. Due to the immunological importance of this, ample structural data is available, which has been reviewed by others.[20] This adhesion molecule is not limited to

holding on tightly, however. Particularly, binding integrin  $\beta$ -2 on the NK cell to ICAM-1 on the target cell has been shown to be a key coactivatory signal for a cytotoxic response, with NK cell subsets highly expressing integrin  $\beta$ -2 exhibiting the strongest response.[21] On a mechanistic level, evidence shows that its heterodimer formation with ICAM-1 is key to trigger the actin rearrangement necessary for lytic granule exocytosis in a WASp – dependent manner.[22]

While sensitive recognition of a cell's troubles is desirable for effective immunosurveillance, false recognition of a healthy cell must be prevented to avoid autoimmunity. For this purpose, NK cells express several inhibitory receptors. Receptors of the Killer-cell immunoglobulin-like family bind 'self' HLA-I class receptors HLA-A through HLA-C on other cells. This ligation inhibits cytotoxic effector functions. The non-canonical HLA-E is similarly associated with peptides as its classical counterparts, although through a different system. It is recognized by the NKG2A receptor in the healthy state and this association prevents cell lysis.[23] There is some evidence for a dual function: If the HLA complex is associated with viral peptides from the cellular interior after cytomegalovirus infection, it is instead bound by the NKG2C receptor, resulting in expansion of the NKG2C-positive subset of NK-cells.[24] The finding that deletion of KLRC2, the gene coding for NKG2C, and low expression of HLA-E is associated with more severe progression of SARS-CoV-2 infection suggests that this system may not be limited to detecting cytomegalovirus infection [25], but no mechanistic link has been demonstrated so far.

The sialic acid-binding immunoglobulin-type lectins receptor (Siglec) family is capable of binding sialic acids on the contacted cell. This allows it to distinguish normal and aberrant glycan patterns with the respective functional consequences.[26] Recent data for the Siglec-7 receptor suggest a mechanism that involves modulation of the glycans on the target cell surface by the NK-cell.[27]

The function of the many NK cell receptors and their cognate ligands is beyond the scope of this introduction and reviews can be found at[28-30]. In addition to the specific examples outlined above, further receptor-ligand pairs can communicate DNA damage, heat shock and viral infection. Other ligands are induced upon triggering p53 or after the cell enters a senescent state.[31] It must be noted that while detailed information regarding mechanism and signaling is available for some of these pairs significant to clinical medicine, for others the information available is limited to the fact that binding occurs, and functional consequences may have been observed. The available Natural Killer cell lines, being derived from lymphomas, often only express a subset of the receptors found in primary cells. Expression profiling data for the NK-92 line used in this study are available.[32]

### **Cytokines and the adipocytokine leptin**

A wide variety of small soluble mediators, collectively called cytokines, influence all aspects of leukocyte functions, from maturation and development to migratory behavior and effector functions in both innate and adaptive immunity.

The interleukins IL-2, IL-15, IL-18, IL-21 and IFN- $\alpha$ , *in vivo* secreted by other immune cells, have been shown to augment NK cell cytotoxic response. Their presence at a site of infection indicate that other immune cells have perceived an insult. A lot of these relay their signal via the Jak/STAT signaling pathway.[33] The influence of TNF- $\alpha$  on NK cell cytotoxic behavior was among the first to be discovered in this regard [34] and since more details of the influence of TNF- $\alpha$  is relayed intracellularly via the NF $\kappa$ B and P38 mitogen activated protein kinase (MAPK)-pathway have been found.[35] TNF- $\alpha$  and IFN- $\gamma$  have also been shown to induce killing behavior [36] in an ICAM-1 dependent manner.

It is key to note that while NK cell functions are augmented by some cytokines, they also secrete some of them in turn. The most important of which is IFN- $\gamma$ . Activation of NK cells through its receptors leads not only to initialization of cytolytic functions, but also to secretion of IFN- $\gamma$ , which is a key regulator of T-cell, B-cell and dendritic cell activity. As opposed to lytic granule exocytosis, this secretion is nondirectional and facilitated by a different pathway.[37]

Adipocytokines are cell-signaling proteins secreted primarily from adipocytes in white adipose tissue in relation to metabolic status. As metabolic regulatory systems they modulate energy expenditure, either by directly binding their receptors on cells, or indirectly by acting on neurons that are e.g., part of the hypothalamus. This in turn changes the secretion of further hormones. Adipocytokine secretion, followed by a self-propagating cycle of immune cell invasion and inflammation have led to an understanding of adipose tissue as an endocrine organ.[38]

Leptin is the adipocytokine that was discovered first through work with obese mice.[39] This 16 kDa protein, can bind to six receptors, dubbed LepR<sub>a-f</sub> (also called Ob-R), although only the transmembrane LepR<sub>b</sub> receptor is capable of intracellular signaling through the JAK/STAT and MAPK pathways.[40] Leptin acts on a wide variety of systems in the mammalian organism and consequentially, its dysregulation is associated with a multitude of diseases. The most important of these, through sheer prevalence, is hyperleptinemia and leptin resistance induced by obesity.[41] Reviewing this is beyond the scope of this introduction, that will focus on its effect on NK-cells. A review on the matter can be found at.[42]

A number of clinical studies and animal models have conclusively shown the association between obesity, hyperleptinemia with concomitant leptin resistance and diminished NK cell functionality.[43] As described by Bähr and colleagues, the multifactorial nature of obesity has several contributing factors. Alterations of NK cell receptor expression and shift of NK cell population is one, see [43] (Table 4), but metabolic dysregulation and lipid uptake have also been shown to be sufficient to induce functional defects.[44] However, in isolated systems of either primary NK cells or NK-92 stimulated *in vitro* and directed against a tumor cell line, leptin has been shown to influence NK cell cytotoxic capacity, although the data is paradoxical at first glance: When directed against the K562 cell line in a killing assay, leptin stimulation appears to increase cytolytic function in short timeframes, see Table 2 in [43] and [45, 46], but continued long term exposure results in lowered cytotoxicity.[47] From a signaling perspective, data shows an influence of leptin on the JAK/STAT pathway.[43]

### **Interest in NK cell biology for immunotherapy**

During an infection, innate immune cells, such as NK-cells, mitigate the spread of viral infection, while an adaptive response is mounted. They similarly perform immunosurveillance, being able to identify signs of malignant transformation. Consequently, a wealth of clinical evidence links diminished NK cell functionality to increased incidence of tumors and susceptibility to infectious disease.

A biochemically rather straightforward example is its capacity to perform F<sub>C</sub> $\gamma$ RIIIa - mediated ADCC. When an infected cell has been opsonized with antibodies, the F<sub>V</sub>-domain of IgG1 binds its antigen on the cellular surface. The distal F<sub>C</sub> domain can be bound by the NK-cell receptor F<sub>C</sub> $\gamma$ RIIIa. The decision whether to perform cytolytic effector functions is again straightforward, because opsonization indicates that an antigen has been previously determined as disease-associated. In this manner, NK cells assist phagocytic cells in



performing ADCC. The fact that ADCC provides a way to ‘flag’ certain cellular structures as diseased for the innate immune system has been artificially exploited to great effect by monoclonal antibody therapies.[8]

Cell transfer with irradiated but otherwise unmodified NK-92 cells has been successfully used to treat hematological malignancies [48] and NK-92 cells transfected with  $F_C\gamma RIII A$  have been successfully used to enhance a monoclonal antibody (mAB) treatment directed against the interleukin-3 receptor in a mice xenograft model. The authors show that killing occurs primarily through lytic granule exocytosis.[49]

Although mAB-based immunotherapies have been a boon in cancer therapy, the technology has inherent limitations. Tissue penetration is often limited, with most recombinant mABs remaining in the blood. The  $F_C\gamma RIII A$  receptor is expressed in a low affinity variant by the majority of immune cells, and the  $F_C$  domain of the recombinant mAB competes for binding with all other antibodies.[50]

The use of chimeric antigen receptors (CAR) may provide an alternative with greater efficacy in removing tumor cells. For the CAR-T-Cell technique, T-cells are removed from a patient to be virally transduced *in vitro* with an artificial T-cell receptor. The single chain variable fragment (scF<sub>v</sub>) antigen binding domain of the TCR, is naturally composed of a V<sub>H</sub> and V<sub>L</sub> region. In CARs these regions are engineered to bind the epitope of interest. After successful recognition, the CAR-T-cell engages its cytolytic functions. Binding affinity of the resulting engineered scF<sub>v</sub> domain is only one aspect that determines binding specificity and sensitivity in practical application. Interaction between V<sub>H</sub> and V<sub>L</sub> regions, length of the hinge domain connecting it to the transmembrane domain and the nature of the signaling complex that assembles intracellularly upon binding have all been shown to influence outcomes. The challenge in protein engineering lies in finding the ideal compromise between efficient recognition of the desired epitope and as little off-target binding resulting in toxicity as possible.[51]

Limitations of this technique stem from the fact that CAR-T cells can also only imperfectly infiltrate solid tumors, where they are then subject to an immunosuppressive microenvironment created by the tumor itself,[51] although efforts are being made to overcome this by modulating inhibitory signaling, i.e. via artificially blocking the PD1/PD1L axis.[52] The targeting of one epitope has resulted in the development of resistant tumors in some patients through either lowered expression or complete loss of target antigen recognition.[53] Erroneous binding of the engineered scF<sub>v</sub> can lead to mass activation of CAR-T cells, resulting in excessive T-cell expansion and cytokine secretion. The resulting cytokine release syndrome with possibly grave systemic consequences has been observed in several CAR-T-cell studies.[51]

A number of recent studies have employed CAR- transfected natural killer cells to the same end as CAR-T-cells. While there is currently far more experience with CAR-T-cells, through 500 studies as opposed to 17, the initial data obtained for CAR-NK cells shows potential to overcome some of these limitations. The receptor system that is proving challenging to understand is advantageous in this application, as the activating receptors allow recognition of disease-associated structures independent of the CAR. Additionally, most human tumors are HLA-deficient. The activating receptors, combined with their propensity to eliminate HLA-deficient cells give CAR-NK-cells an inherent ability to recognize tumor cells that CAR-T-cells lack.[54] The preparation of syngeneic CAR-NK cells from primary cells still comes with significant logistical problems. Patients often have low leukocyte counts. These cells must be extracted, purified, lentivirally transduced with the CAR, expanded and then transplanted, all under good manufacturing practice conditions (GMP). Utilization of NK-cell lines, such as the NK-92 line could mitigate some of these issues. Because they can be grown in cell culture, this eliminates the need to obtain

primary cells. This mainly affects safety, as a cell line is genetically homogenous and the CAR-NK-cell can be produced in a standardized manner, that is not subject to the variance encountered in working with primary cells. This solution has the potential to streamline biotechnological manufacturing and thus broaden accessibility. It nevertheless introduces another issue: The NK-92 line is derived from a lymphoma and must be irradiated before transduction. This stops its proliferation, but also lessens its cytotoxic capacity.[55] That origin has also resulted in the fact that it lacks most inhibitory receptors, making it less susceptible to tumor immune escape.[32, 54] Clinical trials using CAR-NK-92 cells have shown their feasibility in the treatment of acute myeloid leukemia by targeting Siglec-3 [56], or treatment of glioblastoma targeting EGFR through intracranial injection and have shown promise and markedly few side effects. For the latter, a summary of the preclinical data needed and an evaluation of Phase I is available.[57] Refinement of these techniques could be helped by improved understanding of the NK cell immune synapse (IS) and lytic granule exocytosis.

### **How does a kill through degranulation work?**

Upon cell-cell contact between an NK cell and another cell of the body, an initial contact patch is formed. Integrins on each membrane form strand-swapped dimers, allowing adhesion. NK-cell receptors can search for their cognate ligands.[58] Briefly, if the signal from binding of activating receptors or HLA-deficiency is stronger than that from inhibitory receptors, the cell proceeds with lytic granule exocytosis. Otherwise, the contact is disbanded, and the NK cells keep migrating. How this decision is made will be discussed later.

The contact patch is also called an immune synapse. Upon activation, a branched f-actin network is formed on the NK-cell side of this membrane contact. The binding of integrin  $\beta$ -2 to ICAM-1 has been demonstrated to initiate this.[59] How the signal is precisely relayed is unclear, but Src, LAT, SLP76, ZAP70, Vav-1, protein kinase C (PKC) and Erk1/2 have all been shown to activate upon ICAM1 binding.[60] Activation of Erk1/2 is also a common consequence of ligand binding for many activating receptors, including NKp30.[59] The highly conserved Rho signaling pathway also regulates cytoskeletal dynamics in NK cells. VAV proteins are Rho-GEFs for Rac1, ROCKs and CDC42 with several publications demonstrating that the rearrangements needed for granule exocytosis are regulated by this pathway and how their artificial modulation changes the coordination at the immune synapse.[61]

These in turn control the activity of proteins that directly shape the actin network: To facilitate actin rearrangement the proteins WASp, WAVE, Arp 2/3 [62, 63], ezrin, moesin, and radixin [64] accumulate at the immune synapse. A microtubule-organizing center (MTOC) is established on the distal side, polarizing the microtubule network. Lytic granules, a specialized form of lysosomes, are then moved toward the MTOC by the dynein/dynactin complex. The MTOC in turn converges onto the immune synapse. This appears to be an early event in the process, and the rearrangement of actin and convergence of lytic granules is independent of MTOC polarization.[65]

To allow fusion with the cell membrane and exocytosis of their contents, granules must first pass through the tight actin network. This is facilitated by the formation of small, sufficiently sized clearances in the network at the sites of granule convergence. These clearances are of minimal size and only slightly larger than the granules of around 200 nm diameter.[66, 67] Only the target is killed, with bystander casualties being rare occasions, which suggests tight control over this complicated motion of cellular components.[68] Formation of these clearances is dependent on the actin-modifying proteins mentioned earlier, as well as further proteins that disassemble f-actin. Coronin 1A has been shown to

be vital to the process, as its deficiency leads to fewer clearances and in the actin mesh at sites of exocytosis and consequently reduced ability to degranulate, while conjugate formation and granule convergence is unaffected.[69]

Exocytosis by fusion of the lytic granule with the cell membrane is an endergonic process and does not happen spontaneously. It requires the action of SNARE proteins.[60] More recent work has shown that other proteins not classically considered SNAREs also perform similar functions: Septins are a family of cytoskeletal proteins that self-assemble into filaments, with a documented role in the establishment of cell polarity and barrier formation at membranes. They have also been shown to associate to f-actin filaments and microtubules.[70] Stabilizing them by pharmacological intervention, hence preventing their dynamic reorganization, impairs conjugate formation. Their siRNA-mediated depletion impairs cytotoxic capacity, but not conjugate formation, MTOC polarization or granule convergence. Co-purification experiments and light scanning microscopy revealed, that septins localize to sites of granule exocytosis, where they interact with SNARE proteins. They thus appear to play a crucial role for NK cell degranulation.[71] Defects in LYST-1 lead to an impermeable actin network preventing granule exocytosis with deleterious consequences for NK-cell immune functions.[65]

After exocytosis, perforin and granzymes, as the main components of the granules, are trapped in the space between the two cells. The perforin monomers self-assemble on the membrane of the target cell, forming the membrane attack complex/perforin, essentially a channel through the membrane: It complicates homeostasis, mainly because its contents can now exit the cell. Granzymes can also enter the target cell through them. These serine proteases then cleave and activate initiator caspases 8 and 10, as well as executioner caspases 3 and 7, inducing the apoptosis cascade.[72] Why this leaves the NK-cell unharmed is remarkable, but not understood. Early data suggests a role for LAMP-1, but current research suggests multiple involved factors in how NK cells avoid their own death, such as cathepsin B, or the granzyme B inhibitor serpin B9 present in cytotoxic cells in high concentrations.[72]

### **NK cell functional assays**

What methods are available to measure NK-cell functions? A chromium release assay was among the first to be employed to judge the strength of the cytotoxic response. A target cell line, representing the diseased cells, is cultivated in a growth medium containing  $^{51}\text{Cr}$ , allowing this radioactive isotope to enter the cytosol. The target cell line is then co-cultivated with the NK cell. The amount of radioactivity detectable in the supernatant is indicative of the strength of the cytotoxic response.[73] For a modern protocol, see Chapter 6.2.4 in.[74] Another method makes use of the protease/esterase activity of granzymes, by using it to cleave a synthetic peptide with a thioester. The product of this cleavage can be detected through a change in color and the rate of change is indicative of the amount of granzyme enzymatic activity.[75] Because these assays are laborious and time-consuming, they are currently mainly used for the purpose of validation.

The flow cytometry-based LAMP1 assay represents a reasonably precise and facile alternative that allows high throughputs. The protein LAMP1, often also referred to as CD107a, is present only in the membrane of lytic granules. For this assay, NK cells and the target cells are similarly co-cultured for a defined amount of time. When the lytic granules fuse with the cell membrane, LAMP1 is moved to the cell membrane as well. The culture medium contains a fluorophore-conjugated antibody directed against LAMP1. This binding can naturally only happen with LAMP1 present in the cell membrane. The intensity of the fluorescent staining thus achieved can then be measured by flow cytometry. Since a single cell suspension is required for this measurement, suspension media containing chelating

agents are used to disassociate cells by removing divalent cations from strand-swapped integrin dimers that allow cell adhesion. Furthermore, fluorophore-conjugated antibodies, commonly against NCAM1 (CD56) are employed for staining to distinguish NK-cells from target cells. For a detailed protocol and related considerations, see Chapter 7 in [74].

Because modern flow cytometers allow the acquisition of roughly 14 fluorescent signals in parallel, this allows great flexibility. For example, expression strength of a ligand on the target cell or a receptor on the NK-cell can be altered by a knock-down. The effect of the knock-down on protein abundance can then be measured in parallel with the LAMP1-signal after degranulation. When analyzing primary cells, the expression level of surface proteins can be acquired in parallel with a measure for the cytotoxic response, and these can then related to one another. Cells can also be pre-treated before the assay with cytokines, small molecule drugs or biological compounds. The evaluation of how strongly NK cells secrete cytokines can be done by performing an analogous co-culture experiment. The amount of cytokines secreted to the culture medium can be determined by an enzyme-linked immunosorbent assay (ELISA).[76] Alternatively, systems based on antibody-bound beads measured via flow cytometry or array plates can be used to determine multiple cytokine concentrations at once.[77] While more complex, they allow the parallel detection of several cytokines with high specificity. For an overview of the permutations possible with the aforementioned techniques, see Chapters 6-8 in [74].

These assays however share a common downside. The contributing factors to the cytotoxic response are, primarily, the expression strength of all NK-cell receptors and target-cell bound ligands taken together, as well as the type and concentration of cytokines in the surrounding medium. While the inputs are thus manifold, the output received is commonly a single value: the amount of LAMP1 on the cell surface or the amount of a cytokine in the supernatant.

### **Influence of differential protein expression due to external stimuli**

Their importance in therapeutic applications has yielded much data that details how various factors affect the decision of whether to induce cytolysis or not. As outlined earlier, which activating or inhibitory ligands are present on the target cell membrane is important, combined with the abundance of said receptors. Altered expression levels of receptors change an NK cells ability to detect the cognate ligands on target cells. The combination of IL-2 and IL-21 has been shown to change expression levels of several surface receptors and to improve the NK cell capacity to kill the K562 tumor cell line.[78] IL-2 acts on NK-cells via their IL2-R $\alpha$  receptor and enhances their cytotoxic capacity: Tumor cells normally resistant to NK cells are killed by them after being exposed to IL-2. This is partially due to an upregulation of perforin expression.[33]

While the data is conflicting due to different methodologies and *in vitro* models, leptin has been shown to affect the expression of several receptors, FasL, TRAIL, granzymes, and perforin.[43] A multitude of factors can influence the differential regulation of the NK cell receptors and a review of their influence can be found at [79].

The case of IFN- $\gamma$  illustrates that, in order to work, a cytokine does not have to be limited to acting on the immune cell directly. For some tumor cells, binding of IFN- $\gamma$  to its receptor results in upregulation of ICAM-1, allowing more of the integrin  $\beta$ -2 on the NK cell to be bound. This leads to enhanced cytotoxicity.[80]

### **Confluence of activating and inhibitory signals**

A convergence of stimuli the NK cell is sensing is in part orchestrated by the signaling triggered upon ligand binding. A receptor can bind a variety of ligands but always undergoes a conformational change after binding. As alluded to earlier, ligand binding of

NKp30 exposes a stalk domain to the cytosol. The mechanism for NKp44 and NKp46 is similar. A positively charged arginine residue interacts with three aspartic acid residues found on either the adaptor proteins DAP-12 for NKp44 or FcεRI-γ and TCRζ for NKp30 and NKp46.[81] From this point onward, signaling is remarkably similar to that initiated by the TCR-complex.[82]

These adaptors in turn contain immunoreceptor tyrosine-based activation motifs (ITAM), with three on TCRζ and one on the other two. An ITAM is an amino acid structural motif, generally YxxI/Lx(6–12)YxxI/L [83], which is conserved between several further receptors and adapter proteins.[29, 84] The ITAM is now phosphorylated by an Src family kinase, which in turn allow SYK and ZAP70 to bind. This recruits phosphoinositide-3-kinase (PI3K) to the membrane, resulting in phosphorylation of phosphatidylinositol 4,5-bisphosphate (PIP<sub>2</sub>). From this point, the signaling cascade widens, and our understanding of the involved mechanisms is less complete. Phospholipase C (PLC) cleaves phosphatidylinositol-3,4,5-trisphosphat (PIP<sub>3</sub>) and release of inositol trisphosphate (IP<sub>3</sub>) and diacylglycerol (DAG) as secondary messengers into the cytosol. But PLCγ itself contains SH1- and SH2-domains as docking sites for other signaling proteins. For one, the guanine exchange factor (GEF) Vav1 can bind the SH2 domain, activating guanosine triphosphate (GTP)-dependent proteins at the site.[85]

While this mechanism is common, it is not exclusive. The receptor NKG2D does not contain an ITAM, neither does it recruit one from an adaptor. Instead, it recruits DAP10 after ligand binding. This adaptor is phosphorylated at its YINM motif, which then allows recruitment of PI3K by binding its p85 subunit.[81] The complex is made up of an NKG2D homodimer and is associated with two DAP10 homodimers.[86] For most receptors the stoichiometry and nature of the complex is less well known and the same is true for their localization at the immune synapse. In this fashion, a signal can simultaneously be relayed throughout the cytosol as a whole and localized signaling complexes can be established at the site of ligand binding.

Inhibitory receptors bind their respective ligands simultaneously and dampen the mechanisms described above. The well-researched PD1 / PD1-L axis provides an example: Binding of the PD1-L on the target cell by the PD1- receptor on the NK cell similarly results in a previously occluded protein domain extending into the cytosol. This exposes an immunoreceptor tyrosine-based inhibitory motif (ITIM) and an immunoreceptor tyrosine-based switch motif (ITSM). They are similar to ITAMs in mechanism, but their (degenerate) consensus motifs are: S/I/V/LxYxxI/V/L and TxYxxV/I respectively.[83] After subsequent phosphorylation by an Src family kinase, they are a binding site for SHP2 and other SH2-domain containing phosphatases, bringing them in close proximity to ITAM-bearing receptors and their signaling complexes. This protein has been shown to negatively affect PI3K activity, as well as dampening signaling through Ras/MEK/Erk and STAT. It thus counteracts the activity of ITAM-bearing receptors in some ways.[87] PD1 is expressed by primary NK cells as well as the NK-92 line,[88] but other authors suggest that this expression is minimal and possibly without functional consequence in NK cells. For T-cells, a crucial role for this PD-1 axis has been demonstrated.[89]

The Killer cell immunoglobuline-like (KIR) family of inhibitory receptor binds a wide variety of ligands, but commonalities can be found in how the signal is relayed: Ligand binding results in a conformational change that extends a receptor domain containing an ITIM into the cellular interior or brings its into close proximity of its kinase. The now phosphorylated ITIM is then bound by one of the SH2-domain containing phosphatases SHP1/2 or SHIP1/2, rendering them active. SHP1/2 appear to act on the ZAP70/TCRζ axis.[90] SHIP1/2 hydrolyze PIP<sub>3</sub>, antagonizing the PI3K that has been recruited to

neighbouring ITAMs. It influences protein binding at the membrane and affects multiple signaling pathways.[91] The accessory proteins and PIPs involved in this process for each inhibitory receptor remain to be discovered in many cases. It remains to be said that many tumors overexpress inhibitory ligands to escape immunosurveillance in a behavior dubbed tumor immune escape.[30]

Cytokines can influence NK cell activity altering the expression of their receptors or perforin and granzymes. They can also influence the signal proteins activated after receptor ligation and some cytokines do both in parallel. IL-2 acts on NK-cells via their IL2-R $\alpha$  receptor and enhances their cytotoxic capacity: Tumor cells normally resistant to NK cells are killed by them after being exposed to IL-2. This is partially due to its influence on Jak/STAT. Interpretation of the available data is complicated by the different biological models used, but a summary that extends to IL-12, IL-15, IL-18, and IL-21, is available in Tables 1+2 of [33].

### **Manifold influences can only result in a binary outcome**

The nature and amount of ligands present on the target cell and the expression strength of the receptors result in functional consequence: If less activating ligand-receptor pairs are formed, fewer signaling complexes are established resulting in an overall weaker signal. This could be a mechanism of integrating multiple signal inputs into a common intracellular pathway, that can simultaneously be antagonized by the inhibitory components. Cytokines and hormones can act on these same pathways through their own receptor and transduction pathways. Evidence and models to understand this coordination quantitatively are still lacking.

It is known that if the activating signaling described above prevails, the actin-modifying proteins localized to the IS during establishment facilitate the opening of minimal clearances to allow passage of lytic granules. For some cases, like the one of WASp-dependent induction of Arp2/3 activity after integrin  $\beta$ -2 engagement outlined earlier, the mode of signal transduction is better explored than for others. How this process is coordinated by the actin modifying proteins involved in space and time has been less well explored.

### **Minimal models**

This complexity makes it difficult to understand the role of individual systems. Minimal models of immune synapses are an attempt at recreating only parts of the immune synapse in a controllable system, to study the contribution of its components separately. For this purpose, a glass coverslip can be coated in a mixture of two monoclonal antibodies. One is directed against an activating receptor, while the other is directed at an integrin. When an NK-cell is placed on this surface, the antibodies bind their antigen on the NK-cell receptor. Immune synapse establishment and subsequent degranulation is triggered.[66] Recombinantly expressed ligand proteins can be used in the same manner.[92]

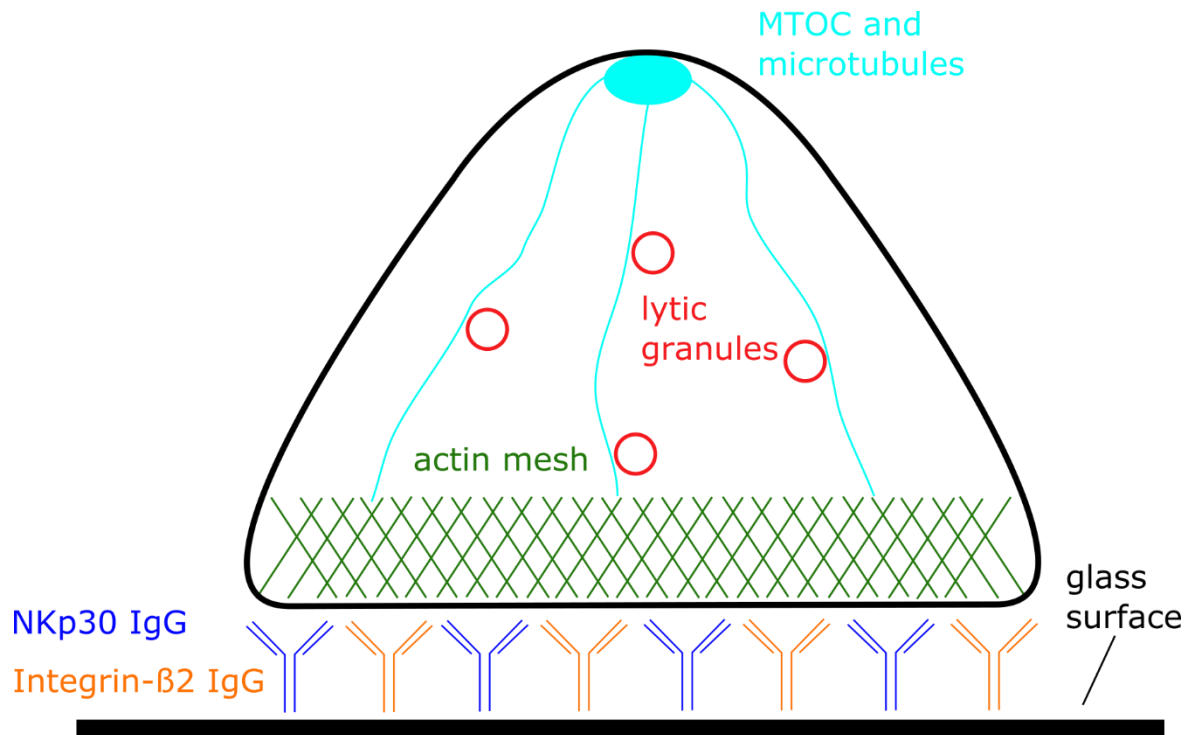


**Figure 1** Sketch of the minimal model for an immune synapse

**Fig. 1** illustrates an NK cell degranulating on such a surface. In order to examine the same issue with a lipid component, supported lipid bilayers can be employed. As an addition, it is possible to include lipids with nitrilotriacetic acid (NTA) chelators binding  $\text{Ni}^{2+}$ .  $\text{His}_6$  tagged proteins can then be introduced to the surface of the bilayer. This has so far been done only with T-cells and care must be taken with the approach, because even ligand free lipids can induce some signaling in Jurkat T-cells.[93] Supported lipid bilayers offer great potential, but they always are an entirely homogenous surface. Efforts using microfabrication have yielded systems, that allow some control over the spatial arrangement of ligands. Nanoscale graphene oxides have been used as templates to create clusters of antibodies directed against the ADCC-receptor  $\text{Fc}\gamma\text{RIIIA}$ . This system triggers NK-cell degranulation and  $\text{IFN-}\gamma$  secretion of primary NK-cells in suspension.[94] Recent advances in nanolithography have yielded systems with precisely functionalized surfaces. In this method, a Ni-NTA chelate and a biotin molecule can be spaced between 0 – 40 nm apart. Two different ligands can then be conjugated to them. The distance has functional consequences for NK-cell cytotoxicity. The authors propose a model to explain how membrane dynamics and flexibility shape the protein organization of the NK-cell degranulating on such a chip.[95]

Coated glass surfaces do not allow such spatial control and they similarly yield a homogenous surface. For the application of super-resolved microscopy, they have the crucial advantage of being made of glass. In this way, an immune synapse can be established on a glass coverslip, where it can be observed with techniques such as total internal reflection structured illumination microscopy (TIRF-SIM), stimulated emission depletion (STED) microscopy, stochastic optical reconstruction microscopy (STORM), that offer good resolution, but only shallow penetration depths.

### Microscopy techniques

Confocal light microscopy combined with immunostaining allows visualization of several components in tandem. That affords an opportunity to examine their spatial coordination. Work with confocal microscopy observing cell lines showed activating receptors and

perforin migrate toward the contact surface after establishment of an immune synapse. A ring of f-actin appears to surround this space. Accordingly, the model of a central supermolecular activating cluster (cSMAC) was proposed as the site of coordination of exocytosis.[96] The same authors later hazarded, that their observations might be shaped by the imaging method. Lytic granules are the largest component involved. Their diameter is commonly around 200 nm, but can range up to 400 nm, so even their dimensions are at the border of the diffraction limit of visible light. Hence, they performed stimulated emission depletion microscopy (STED) and cryo-electron microscopy to obtain further insights. With STED, the excitation laser beam is overlaid with a doughnut-shaped depletion laser. All fluorophores hit by the excitation beam absorb photons and convert into an excited state. Those also hit by the depletion beam immediately undergo stimulated emission. Only the fluorophores in the minimum at the center of the doughnut are free to first undergo vibrational relaxation (Stokes-shift) and to then emit photons when reverting to ground state, and only that signal is detected. This allows an increase in resolution up to 35 nm in ideal circumstances.[97] In practice, resolution depends on multiple factors and is typically around 80 nm in biological applications. The convergence of the MTOC and the perforin-containing lytic granules to the f-actin mesh occur in tandem, with most lytic granules in close proximity to the MTOC. It also became apparent, that there is no central, homogenous f-actin hypodense region, but that rather every granule is allowed to pass the f-actin mesh through a clearance not much larger than the granule before it fuses with the membrane. Manipulation of actin dynamics with inhibitors also influenced this process. In this case, activation was done by using antibody-coated glass, directed against integrin  $\beta$ -2 and NKp30.[66, 67] Using ICAM-1 as a ligand for integrin  $\beta$ -2 and MIC-A as a ligand for NKG2D also leads to activation. The authors show that the mean hole area per granule varies depending on what insult the NK cell perceives and that engagement of an integrin and an activating receptor in tandem is necessary for a robust response.[92]

STED microscopy allows greater resolution, but its long acquisition time results in framerates unsuitable for observation of live cells in this process. Live-cell confocal- and TIRF microscopy have shown that lytic granules are highly motile for up to 10 min after contact of the cell with the activating surface and become stationary afterwards. F-actin disruption with Latrunculin B did not change this. Interestingly, no difference in regard to movement could be observed between the granules that are exocytosed and those that are not.[98] Work similar in methodology was performed activating through the  $F_C\gamma$ RIIIa receptor that is crucial to performing ADCC. In part, styrene beads functionalized with the insulting proteins were used to activate NK cells in suspension. Coligation of  $F_C\gamma$ RIIIa and integrin  $\beta$ -2 induces more targeted degranulation than engagement of  $F_C\gamma$ RIIIa alone, thereby minimizing the amount of bystander cells erroneously killed. They did not observe differences in the structure of the IS.[68]

With this data suggesting a central role for the actin network, the observation of LifeAct-GFP in NK-92 cells with TIRF-SIM microscopy allowed further understanding of the dynamics involved. Using TIRF allows imaging of only a roughly 200 nm thin layer at the interface of the cell with the glass, reducing background noise from fluorophores outside this layer.[99] For SIM, the sample is repeatedly illuminated with a grate or lattice pattern. The super-resolved image is then reconstructed from the individual images.[100] TIRF-SIM allows imaging beyond the diffraction limit, but its resolution is inferior to that of STED. Nevertheless, the high framerate allowed acquisition of kymographs showing actin remodeling needed to allow lytic granule passage. The same publication also showed the key role for the Arp2/3 complex that allows actin branching in this process, by observing changes in actin dynamics after its inhibition.[101]



Photoactivated localization microscopy (PALM) has been used to consider the spatial organization of the receptors engaged during activation. The inhibitory receptor KIR2DL1 is not distributed homogeneously across the membrane but organized in clusters. This organization is changed when KIR2DL1 is ligated by a monoclonal antibody directly, but interestingly it is also affected when the activating NKG2D receptor is engaged, hinting at crosstalk between these events. Concomitant treatment with Latrunculin A was able to abolish the effect of NKG2D engagement on KIR2DL1 organization, showing that this phenomenon is dependent on actin dynamics. Engagement of CD28 contrarily had no effects on KIR2DL1 organization.[102] Later work homed in on this: KIR2DS1 is the short-tailed counterpart to KIR2DL1 and it has an activating function. Its adaptor DAP12 coalesces with it only upon activation. Site-directed mutagenesis of Lys233 in KIR2DS1 affected nanocluster size, meaning the sequence of the transmembrane domain influences cluster size. In the same publication, a set of elegant experiments showed that cluster size has an influence on downstream signaling: Phosphorylation of the KIR2Ds adaptor ZAP-70 is favored in larger clusters, and the same is true for KIR2DL1 and its adaptor SHP1.[103] An earlier publication using a microfabricated immune synapse partially relates to this, as it shows that the organization of the membrane at the immune synapse is subject to biomechanical constraints.[95] However, neither the chip nor a coated glass surface reflect the *in vivo* state well for this investigation, as the target cell also generates forces through its cytoskeleton. Methods to record the biomechanical forces with high temporal resolution are being pioneered, but most are currently being applied to investigate adaptive immune cells, hence there is no information regarding this for NK cells.[104, 105]

Like PALM, STORM microscopy relies on stochastic activation of fluorophores. The sample is continuously imaged, while fluorophores transition randomly between activated, resting, and dark states. The resulting series of images allows a super-resolved reconstruction of the position of the fluorophores. For detection of membrane-associated proteins, the combination of STORM with TIRF is often beneficial. This requires the fluorophores be able to transition to dark states with the aid of blinking buffers. They must also be sufficiently sparse on the sample so they can be detected individually.[106] Contrarily, STED relies on the depletion of excited fluorophore states and requires a high density of photostable fluorophores. Alone or in combination, these techniques allow imaging beyond the diffraction barrier and the detection of the described protein nanoclusters.

### **Choice of in vitro model**

First, a cellular model must be selected to obtain Natural Killer cells in the same cellular state to examine with several different methods. Due to their nature, this is somewhat nontrivial. Primary NK cells, that have differentiated in humans are not one homogeneous population but comprised of subpopulations that specialize in their function. Cytotoxic NK cells, with the function that the present study focuses on, are one subpopulation. Cytokine-secreting NK cells are another, activated in the same manner but they react mainly with cytokine secretion and not degranulation. Other subpopulations such as NKT cells have regulatory functions and are similar to adaptive immune cells in some aspects. All these subpopulations can be identified through distinct markers.[107]

Primary cytotoxic NK cells can be obtained from blood donations. For this, the blood is collected, centrifuged and the immune fraction, often called a 'buffy coat', is separated. This fraction now contains all immune cells and NK cells can be purified from it mainly by two methods: First, identifying protein surface markers can be stained with fluorophore-conjugated antibodies, so that the target cell population is distinguishable by their

fluorescent signal from other immune cells. Cell sorting allows them to be separated with high fidelity using fluorescence assisted cell sorting. This technique separates cells into droplets after flow cytometry and sorts them into different reservoirs. While this yields reasonably pure populations, it comes with an important complication for NK cell functional assays[108]: Most of the distinctive markers are NK cell receptors and their ligation with an mAB can come with functional consequences, such as giving them a proclivity to degranulate as discussed before.

The use of a bead-based cell separation system is an alternative. In this method, styrene beads are coated with antibodies against distinctive cellular markers. The cell suspension of all immune cells is then flushed over a column with these beads, and cells containing these markers are bound to the beads. They can later be eluted from the column. To obtain unactivated cells with this, the technique is inverted for negative selection: Beads with antibodies against cellular markers for all other immune cells are used, and the flow-through of the column containing NK cells is used. This can also give higher fidelity than cell sorting, but most importantly no receptors are ligated in the process, preventing their 'pre-activation' during purification.[109]

Nevertheless, primary NK cells exhibit large variance in functional parameters, both between cells of one donor and regarding the averages between individual donors. This necessitates analysis of enough cells to obtain a statistically meaningful average, which is possible for ELISA-based assays and flow cytometry, assuming an absolute minimum of 10.000 cells per sample and samples from 10 different donors per condition to be examined that is commonly used to ensure statistical meaningfulness of results. It is possible but cost- and time intensive for proteomics, as quantification of low-abundance signaling proteins and their phosphorylation state requires considerable instrument time. For super-resolved imaging, this becomes somewhat unfeasible: Acquisition of a 15  $\mu\text{m}$  x 15  $\mu\text{m}$  field of view (FOV) in two or three colors that encapsulates the NK cell IS takes approximately 20-30 min for STED, depending on the system used and the number of stained epitopes. 3D-STED requires longer imaging times, due to the need to record stacks of images. In part due to the technical limitations of the chosen methods and in part due to the significant recent interest in them for the purpose of immunotherapy, this work was performed with *in vitro* cultivated NK cell lines, primarily the NK-92 line. For a further understanding of the spatial organization of the NK-cell immune synapse, the influence of hyperleptinemia on it and its regulatory pathways, super-resolved imaging was combined with proteomics and immunoassays.

# Results

## Validating the cell model and induction of degranulation

Previous work has shown that antibody-coated glass can be used to induce NK cell degranulation. To ensure that the method used in this study can reliably induce degranulation in the actual cell line used, validation work was performed first. To ligate integrin  $\beta$ -2, the TS1/18 and for later experiments the hu1124 clone were chosen, because comparatively more knowledge on their mode of binding is available. To ligate NKp30, a recombinant IgG1 mAb expressed in mammalian cells was chosen (see **Table 9** in methods section). Compared to antibodies produced by the hybridoma method, this ensures that all

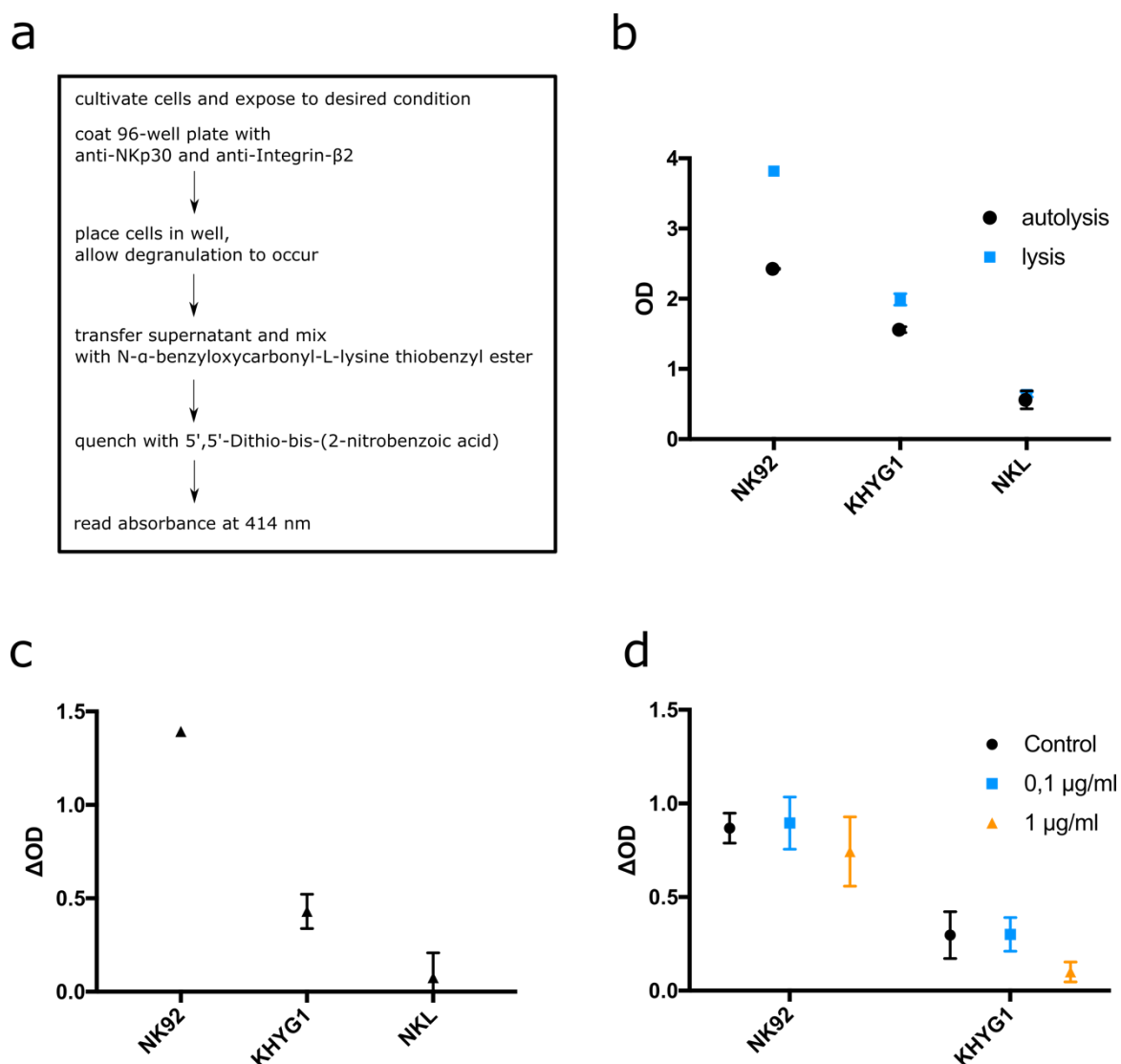


**Figure 2:** The amount of granzymes released after degranulation was measured through their enzymatic activity. **(a)** Flow chart of the assay procedure **(b)** absolute optical density values obtained. 'Autolysis' describes cells values obtained from cells placed in uncoated wells. **(c)** Difference of OD values between autolysis and granzyme release due to receptor ligation. **(d)** Shows the same for cells treated with 0,1  $\mu$ g/ml or 1  $\mu$ g/ml Leptin for 2 h. No statistically significant differences were observed after treatment. Shown is the pooled data from three biological replicates. The bar shows the mean value, whiskers show standard deviation.

mABs share the same isotype and are expressed in the same cell line, thus eliminating possible variance due to different isotypes.

To ascertain whether the cell line used was able to perform cytolytic effector functions in this setting, a granzyme B assay was performed. The bottoms of a 96-well plate were coated with mABs against integrin  $\beta$ -2 and NKp30, washed and NK-92 cells were placed within them. After allowing for degranulation to occur cells were removed and the enzymatic activity of granzyme B was assayed through its cleavage of the artificial N- $\alpha$ -benzyloxycarbonyl-L-lysine thiobenzyl ester substrate. The concentration of the resulting product can be determined colorimetrically in an end-point assay. As can be seen in **Fig. 2**, this ligation of only two receptors is sufficient to induce sequestration of granzyme B. The enzymatic activity in the resulting supernatants is different between cell lines, which is highest for NK-92, while for NK-L the difference between autolysis and induced lysis is negligible. Due to the nature of the assay, this could be either due to different frequency of degranulation events or due to different expression of granzyme B between cell lines. However, the low sensitivity of the assay, as is evident from the small difference between uncoated control and the coated wells, is unsuitable for more detailed analysis.

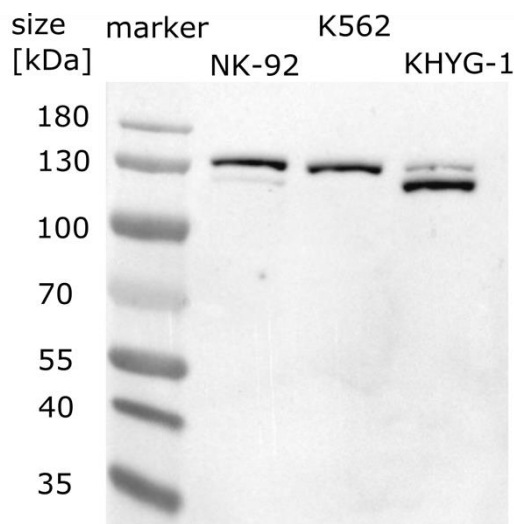


**Figure 3** Expression of the leptin receptor on the indicated NK cell lines was determined by western blotting. NK-92 and KHYG-1 cells express both the long and short isoform of LepR, but with different relative abundance. The antibody binds both isoforms.

To examine the influence of leptin on NK-92 cells, it was first necessary to verify that this cell line expresses the receptor. It is reported that these cells express the LepR, but in low abundance. Detection of LepR through flow cytometry was unsuccessful (data not shown), likely due to the signal being too weak. Western blotting confirmed the expression of LepR on NK-92 cells (**Fig 3**). It is also detectable on the K562 target cell line and the KHYG1- NK cell line.

With previous reports that leptin influences the expression of several NK cell receptors, whether the receptors considered here are also affected by leptin. If differential regulation occurs, this would mean that any systemic consequence could be due either to the altered abundance of receptors and consequently the number of signaling complexes after ligation. Alternatively, it could also be due to the direct influence of leptin on signaling pathways like the Jak/STAT system. NK-92 cells were thus

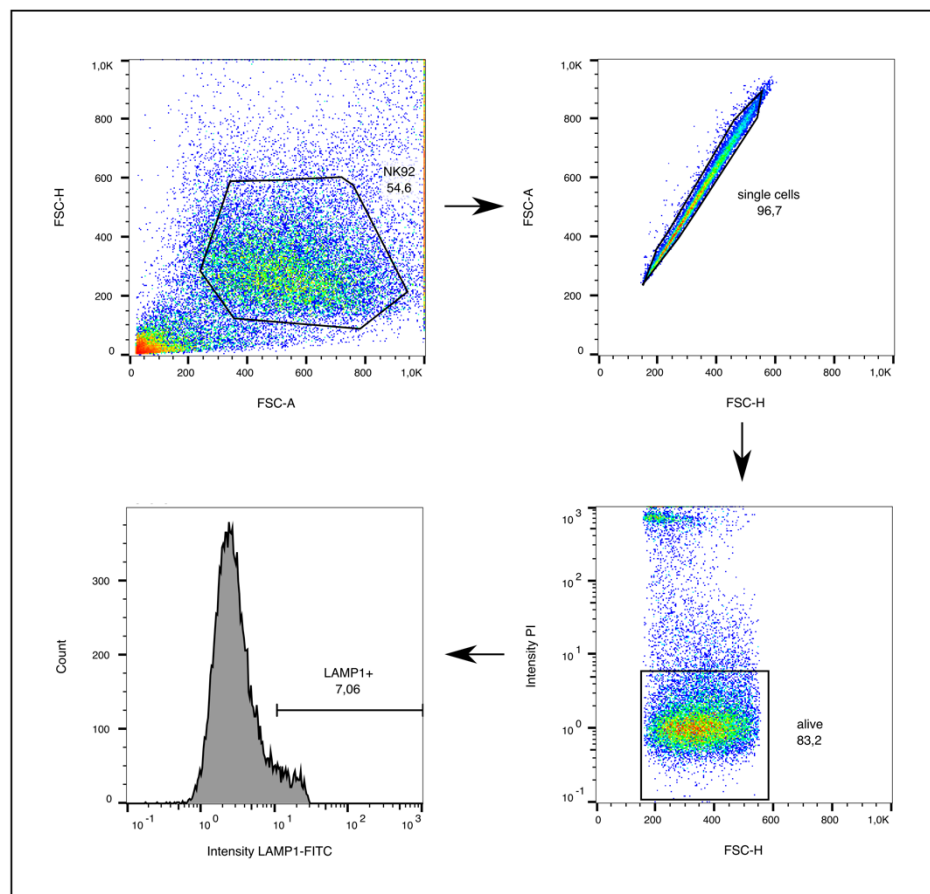
exposed to 100 ng/ml leptin for the relevant durations, then stained for the receptors of interest and measured through flow cytometry. The results seen in **Fig. 4 (c)** demonstrate that no noteworthy differential regulation for the receptors NKp30 and integrin  $\beta$ -2 was observed. These receptors were then selected for further experiments.

## Modifying the LAMP1 degranulation assay for the minimal model

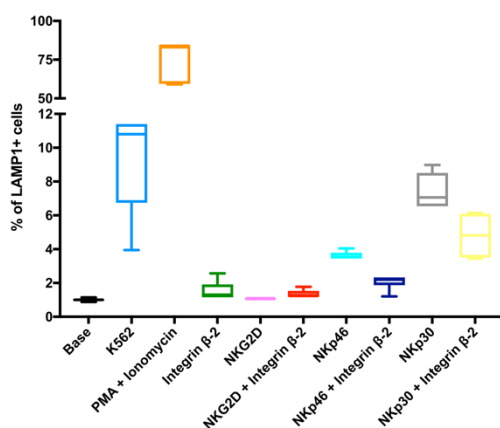
Consequently, LAMP1-degranulation assays were performed next. The method is derived from the one described by Lorenzo-Herrero et al. with numerous modifications, as this protocol uses K562 cells and not coated glass to induce degranulation.[74]

In a similar fashion, 96-well plates were coated with mABs against the same epitopes as for the granzyme B assay and then placed in cell culture wells. NK-92 cells were then added to the wells, together with anti-LAMP1 mABs and the inhibitor monensin. In resting NK cells, LAMP1 is localized on the membrane of lytic granules. During degranulation, these vesicles fuse with the cell membrane, its contents are exocytosed and LAMP1 is moved to

a



b



c

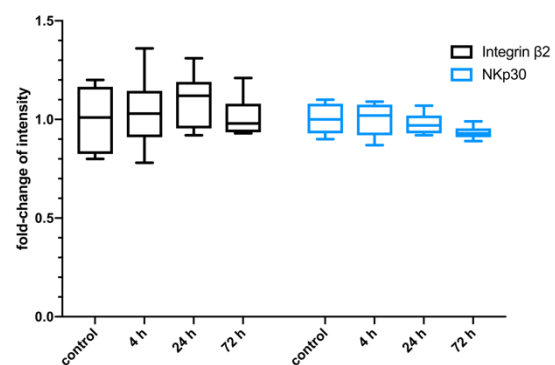


**Figure 4:** LAMP1 degranulation assay to determine degree of lytic granule exocytosis. **(a)** gating strategy used to obtain the LAMP1-FITC signal, with data from one representative sample. Numbers below gate name indicate the percentage of the data points that are included in the gate. Arrows indicate the sequence of gates. Cells were first gated according to size (forward scatter, FSC-A) and granularity (side scatter, SSC-A) to exclude cellular debris. Plotting the height of FSC peak (FSC-H) versus its area (FSC-A, path integral of signal intensity over its duration) allows the exclusion of instances where two adhering cells are in the optical chamber at the same time (doublet exclusion). Cells positive for propidium iodide, indicating a perforated cell membrane, were excluded as dead cells. Histogram of the LAMP1-FITC signal. Cutoff value for the LAMP1+ gate was selected so that a maximum of 0.1 % of cells were included in this gate in the “Base” control without receptor ligation. **(b)** Percentage of LAMP1 positive cells, shown as box plots. Note the break and different scaling of the y-axis segments. **(c)** Fold-change of receptor expression after treatment of cells with 100 ng/ml leptin for the indicated time points. No statistically significant change in expression was detected for any time point. For **(b)** and **(c)** the bar of the boxplots indicates median values, the box indicates 25<sup>th</sup> to 75<sup>th</sup> percentile and the whiskers show minima and maxima, data shown is from three biological replicates.

the cell membrane. Only LAMP1 on the cell membrane is accessible to the antibody and stained by it. Monensin is used here to prevent Golgi trafficking. This is needed, as otherwise the LAMP1 protein would be removed from the cell membrane, and either be degraded through the proteasome or re-shuffled back to nascent lytic granules.[110] In the former case, the fluorescent signal is lost and in the latter it is attenuated by exposure of the fluorophore to the acidic pH range of the lytic granule. Both processes distort results.

The cells could be observed adhering tightly to the glass surface during the assay. Using flow cytometry buffer with slightly increased EDTA concentration, to remove divalent cations needed for integrin-mediated adhesion combined with light agitation through a cell scraper was used to resuspend cells. These cells were then stained with propidium iodide to distinguish living and dead cells and measured via flow cytometry. The gating strategy to obtain this signal is shown in **Fig 4 (a)**. As a baseline value, the fluorescence intensity of cells exposed to uncoated glass was used. One selected control was the combined treatment of cells in uncultured wells with ionomycin, artificially triggering Ca<sup>2+</sup> signaling and phorbol 12-myristate 13-acetate, which artificially induces PKC activity. This allows a reference of the maximum amount of LAMP1 that can be mobilized to the cell surface, as it essentially sidesteps the normal activation pathway. Degranulation against K562 target cells to compare with the LAMP-1 assay commonly used was also performed. **Fig 4 (b)** shows that the NK-92 cell line performs degranulation when encountering K562 cells and that activation with PMA/ionomycin results in a LAMP1 signal that is an order of magnitude larger. This implies that only part of the lytic granules are mobilized, which is in line with previous observations that NK cells are capable of serial killing. [111] Ligation of integrin  $\beta$ -2 alone is insufficient to induce degranulation, and so is ligation of the NKG2D receptor, either alone or in combination with integrin  $\beta$ -2. Ligation of NKp46 alone did significantly induce degranulation, but not in combination with the integrin. For NKp30, single ligation or the combination with integrin  $\beta$ -2 lead to significant degranulation. It appears paradoxical, that the addition of integrin  $\beta$ -2 leads to less degranulation, as ligation of this protein has been reported as a strong induction signal for it. In this case, it can be explained by a practical limitation of the assay: Ligation of this integrin leads to stronger adhesion to the glass compared to ligating an activating receptor, like the C-type lectins or NKG2D. This leads to incomplete retrieval of cells. Further increasing the EDTA concentration in the buffer or more vigorous mechanical detachment were attempted but resulted in cell death (data not shown). It is further noteworthy, that the

standard deviation of the LAMP1 signal is much smaller for antibody-exposed cells than those exposed to K562 cells. Although the absolute value is higher, the standard deviation of the PMA/Ionomycin sample is similar to the former. These results confirm that receptor ligation on a glass surface is sufficient to induce robust degranulation only when certain receptors are ligated. It also yields cell population that degranulate more homogeneously compared to using K562 cells.

### **STED imaging of leptin-simulated NK-92 cells**

To examine whether leptin exposure influenced the density of the actin mesh at sites of lytic granule exocytosis, STED imaging was employed.

NK-92 cells were exposed to 100 ng/ml leptin for 4 h, 24 h and 72 h, degranulation was induced as previously described, and samples subsequently stained for STED imaging. Filamentous actin was phalloidin-stained, while lytic granules were stained through secondary immunostaining of the perforin that they contain. An example of the images obtained can be seen in **Fig. 5 (a)** with the inset **(b)** magnifying the section within the white frame. It is noteworthy that in the case of f-actin, recording three line averages with comparatively lower depletion power yielded a higher level of detail than no averaging with higher depletion power, although the latter theoretically gives a narrower point-spread-function (PSF) resulting in higher resolution in the *xy*-plane. This was mainly due to bleaching observed when using higher depletion laser power. In the interest of brevity, the optimization of sample preparation and titrations of each staining reagent needed to find optimal staining conditions, as well as the optimization of image acquisition parameters is not described here. The resulting method used is described in detail in the method section, together with image acquisition and data analysis.

The aim was to determine whether leptin treatment affected the density of the actin mesh at the sites where lytic granules are approaching the immune synapse. With the calculated PSF suggesting a resolution of 60 nm at the STED-laser powers used, an individual f-actin filament with a diameter of 9.5 nm cannot be resolved. The obtained image is essentially density map, although a more accurate one: A 200 nm diameter spot would be at the resolution limit of conventional imaging and show no detail below that scale.

First, maxima in the perforin channel were automatically detected to obtain the position of lytic granules. They were found to have an average diameter as determined by perforin staining of 200 nm. Note, that this staining method only stains their insides, while the membrane is not visible. This size is similar to, but slightly smaller, than that reported by others [66]. Circular regions of interest of 200 nm diameter were then placed over these maxima. An example of this is shown in **Fig. 5 (c)** and inset **(d)**. The average intensity of the actin signal of all pixels in the ROI was then calculated. Note, that the intensity value is stored on a scale from 0 – 256. **Fig. 5 (e)** shows this exemplarily for 10 control cells in the first replicate. Each dot represents the average actin intensity at one granule location. There is notable variance within one cell, but the clustering of data points between cells is similar, with only some cells presenting with lytic granules at sites where the actin mesh is very dense. These values were then averaged to obtain a value for one entire cell and one such value is represented by one data point in **Fig 5 (f)**. After 4 h of leptin treatment, the average density of the actin mesh was higher compared to control. Treatment for 24 h and 72 h did not result in changes from control.

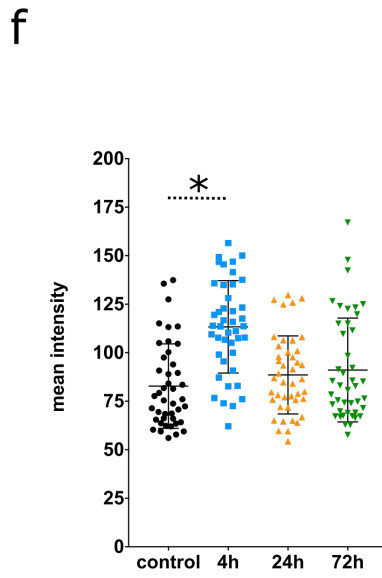
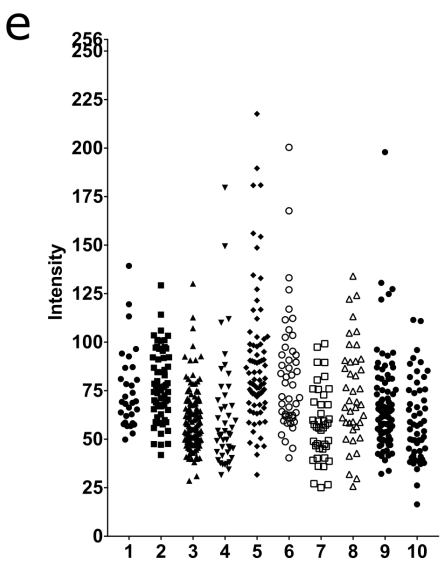
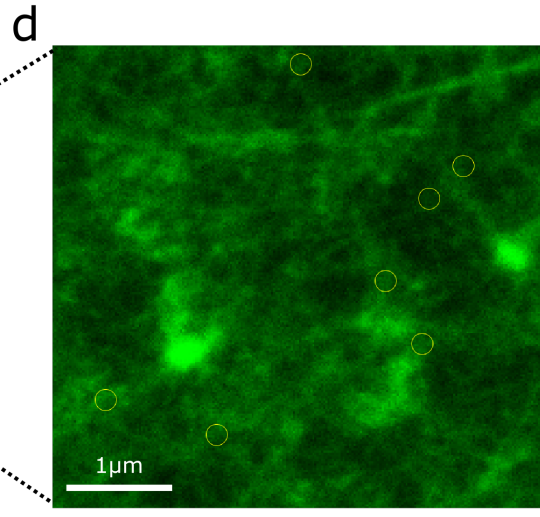
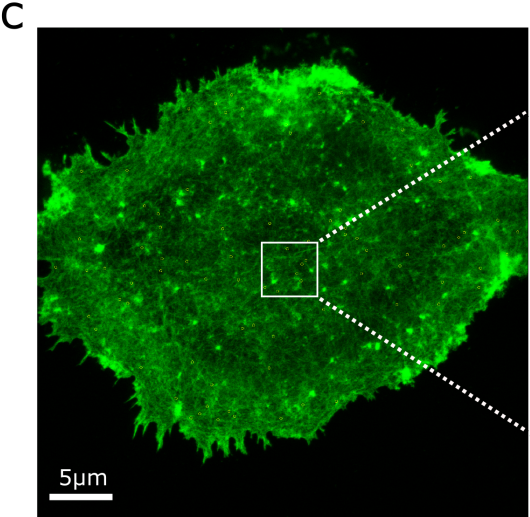
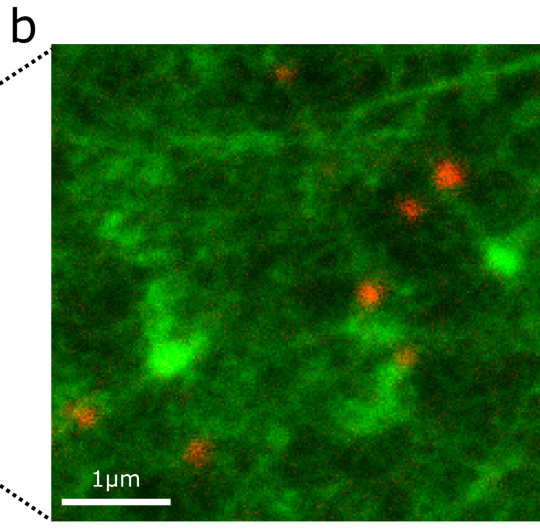
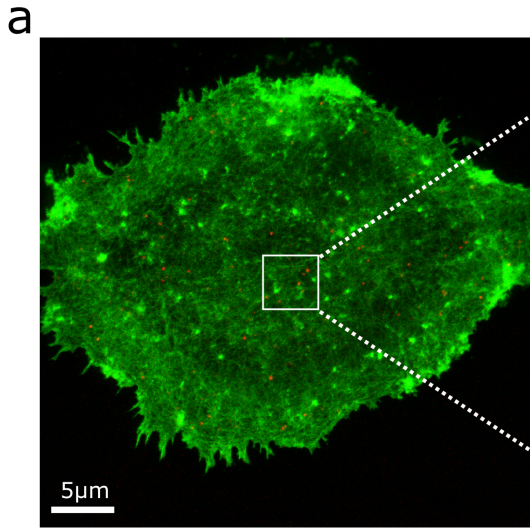




**Figure 5** STED imaging of NK-92 cells degranulating on the minimal immune synapse. **(a)** representative image with f-actin shown in green and perforin in red. One pixel is 20 nm<sup>2</sup>. Inset **(b)** gives an enhanced view of the white-framed area, note the difference in length of the scale bar. **(c)** with inset **(d)** shows the regions of interest defined by automated image analysis detecting maxima in the perforin channel. **(e)** Statistical analysis of imaging data. Each dot represents the average intensity in the actin channel at one site of exocytosis. Exemplary data shown is from 10 cells of one replicate. **(f)** Pooled data from three independent replicates. Each dot represents the average intensity of the actin channels across all ROIs for one cell. The bar shows the mean value across all cells, while whiskers indicate the standard deviation. Average intensity was significantly higher ( $p < 0.0001$ ) in a Mann-Whitney-U test after 4 h of treatment with 100 ng/ml leptin, while no difference was found for the 24 h and 72 h time points in any comparison. Done in cooperation with Katharina Reglinski, Silvia Galiani, Ulrike Schulze and the Wolfson Imaging Facility at the Weatherall Institute for Molecular Medicine.

### Colocalization of NKp30 receptor clusters and lytic granules

During preliminary experiments to further study the coordination of lytic granule exocytosis, it became apparent, that the NKp30 receptor forms clusters roughly at the center of the immune synapse **Fig. 6 (a)-(c)**. This happens in spite of the mAB binding to it homogeneously coating the glass surface **Fig 6 (d)**. Previous publications reported that ligand binding of this receptor exposes an intracellular docking site and that the establishment of signaling complexes here induce the cytotoxic response. This protein complex is known to have binding sites for SH-domain containing proteins, some of which have downstream effectors that mediate actin remodeling (see introduction). In this context, three questions emerged: First, is this local signaling relevant to the establishment of clearances that allow the passage of lytic granules through the mesh, thus allowing the granule to fuse with the cell membrane? Second, is there interplay between the actin network and these receptor clusters, or are they independent of one another? Third, if there is interplay, is leptin capable of influencing this?

A literature search performed to approach the first question revealed, that the immediate effectors binding to the exposed NKp30 stalk domain are well researched. However, almost no information directly relating to NK cells is available which actin-modifying proteins are relevant here. Contrarily, a multitude of actin-modifying proteins could potentially be relevant and each of these have several upstream regulators. To obtain a first indication whether there is a local coordination, observable with imaging, the first question was rephrased to: Do lytic granules, that are immediately above the actin meshwork preferentially locate to sites of NKp30 clusters?

The biological model used to perform this experiment is analogous to that shown in **Fig. 5**, but with the staining reworked: Secondary immunostaining of perforin yielded poor signal-to-noise ratios, necessitating extensive optimization of parameters during imaging. Here, lytic granules are stained with LysoTracker dye instead. This dye can pass through the cell and lysosomal membranes into lytic granules and is then trapped here. The mechanism allowing this is incompletely understood but suspected to be due to protonation in the acidic lysosome (see introduction of [112]). The aforementioned modification also made secondary immunostaining of NKp30 possible. An exemplary resulting image is shown in **Fig. 6 (a)-(c)**.



**Figure 6** STED imaging of NK-92 cells during degranulation. **(a)** Maximum Intensity projection of the z-stack of an exemplary cell. The viewpoint is perpendicular to the glass surface. F-actin is shown in blue, lytic granules are shown in red and NKp30 in green. Locations where the signals from lytic granules and NKp30 overlap appear yellow. **(b)** Projection rotated by 90° **(c)** relevant z-plane above the actin mesh used for analysis. **(d)** Glass surface coated with monoclonal antibodies to induce degranulation, stained by directing fluorophore-conjugated secondary antibodies against them. The dynamic range of this image is low, around 10% when compared to previous images. Contrast is enhanced accordingly to show what differences there are. **(e)** Sum of the NKp30 signal in ROIs placed over maxima in the lytic granule channel ('valid') plotted against the same calculation for randomly placed ROIs ('random'). Shown is the pooled data from three independent replicates. For the outliers, each dot represents a ROI. The differences between the dataset for 'valid' and 'random' for all conditions and the difference between the 'valid' datasets for each condition compared to control are statistically significant in a Mann-Whitney-U-test with all  $p < 0.03$ . Inhibitor/cytokine concentrations: 100  $\mu\text{M}$  CK666, 100 nm Latrunculin B, 1.35 ng/ml IFN- $\gamma$ , 100 ng/ml Leptin **(f)** Comparison of different threshold values of the lytic granule signal to determine maxima, where ROIs are placed. The legend shows, what general threshold value applied to all images corresponds to which plot. For all multiple comparisons, the Kruskal-Wallis test was used to compare different parameters for each condition. No significant differences were observed for using different threshold values, with all  $p > 0.9$ . **(g)** Comparison whether different diameters of circular ROIs placed above the detected lytic granule positions influences the mean NKp30 signal within them. No significant differences were observed, with all  $p > 0.9$ , except for IFN- $\gamma$  ( $p = 0.708$ ). **(h)** Comparison, what influence the number of randomly placed ROI has on the sum of the NKp30 signal within them. No significant differences are observable, with all  $p > 0.7$ . **(i)** Comparison, whether the minimal distance randomly placed ROIs must have to detected ROIs influences the mean NKp30 signal within random ROIs. All differences are non-significant, with  $p > 0.1$ . For all boxplots, the bar indicates median values, the box indicates 25<sup>th</sup> to 75<sup>th</sup> percentile and whiskers show 5<sup>th</sup> to 95<sup>th</sup> percentile. Done in cooperation with Felix Hildebrandt, Katharina Reglinski and Francesco Reina at the Institut für angewandte Optik und Biophysik, Friedrich-Schiller-Universität Jena and the Leibniz-Institut für photonische Technologien.

Asking whether lytic granules localize to clusters of NKp30 is, in essence, a colocalization study. Most data analysis methods used to study colocalization, such as Pearson's, Spearman's or Mander's coefficients are designed to examine whether two proteins colocalize and are based on the assumption of a stoichiometric relation between each protein-fluorophore combination. In this case, the question is rather if a microtubule-bound vesicle is localizing to a cluster of membrane proteins. The amount of LysoTracker dye trapped in a lytic granule is not stoichiometric to its contents, but arbitrary. Additionally, the thresholding of the aforementioned techniques was optimized for diffraction-limited confocal imaging using photomultiplier tube detectors. This experiment uses STED and avalanche photodiodes as detectors.

When approaching this question, a data analysis strategy previously employed to study peroxisomal import was adapted [113]: To obtain the positions of lytic granules directly above the actin meshwork, the signal of the LysoTracker dye was thresholded and a 200 nm diameter region of interest was defined around the center of these maxima. The intensity of the NKp30 signal in this region was then summed. To determine whether a preferential localization is observable, random regions of interest were defined within the cell and the NKp30 signal intensity in them was equally summed. The result of this analysis can be seen in **Fig. 6 (e)** "control", which shows a significant difference in NKp30 intensity between valid lytic granule ROIs and randomly defined ROIs. The validity of this analysis rests on the assumptions made through the defined parameters. It was thus necessary to examine whether these parameters introduce bias. Maxima in the lytic granule channel were

found using a single threshold value across all images examined (n.b. this is only possible, if laser power is calibrated before and during each imaging session, procedure not shown to preserve brevity). Varying this value did not result in statistically significant differences **Fig 6 (f)**. The size of lytic granules varies, with 200 nm being the most common diameter as outlined before. It is thus necessary to check whether the size of the ROI has an influence on the outcome of the analysis. Varying the ROI did not change the result of the analysis in a statistically significant fashion **Fig. 6 (g)**.

When determining where to place random ROIs, it was first attempted to define a mask over the entire outline of the cell and then place ROIs anywhere within them. This however significantly skewed results toward low values for the sum of the NKp30 signal in random ROIs. An explanation for this can be found when considering, that the furthest outlines of the cell are thin lamellipodia **Fig 6 (b)** and that most valid lytic granule positions are found near the center of the cell. Instead, random ROIs were placed so that they are a minimal distance away from valid ROIs. With this approach, neither the number of randomly defined ROIs **Fig. 6 (h)** nor their minimal distance to valid ROIs **Fig. 6 (g)** influenced outcomes.

With these validations, the experiment provides evidence for the hypothesis that lytic granules preferentially localize to clusters of NKp30 during exocytosis.

In order to answer the second question, NK-92 cells were treated with actin inhibitors. CK666 inhibits actin branching by binding to the Arp2/3 complex and inhibiting the change into its short-pitch conformation, that would provide a nucleation point for a branching actin filament.[114] Latrunculin B inhibits the binding of monomeric g-actin to ATP, hindering the polymerization to f-actin [115]. Both inhibitors thus alter actin dynamism, albeit with distinct mechanisms. For the method to determine the concentration of the inhibitors used, see the methods section. **Figure 6 (e)** shows that treatment with 100  $\mu$ M CK666 or 100 nM Latrunculin B resulted in lower absolute amounts of NKp30 being present at the sites of granule exocytosis. When comparing the difference between ‘valid’ and ‘random’ ROIs, a reduced preference of NKp30 to localize to these sites is also noticeable. These tendencies are more pronounced for CK666 at the chosen inhibitor concentrations. This suggests that altering actin dynamism leads to either less pronounced clustering of NKp30 or less preferential localization of lytic granules to these clusters. In either case, inhibiting actin polymerization or branching appears to impair this colocalization of lytic granules toward NKp30.

As a point of comparison, for which Natural Killer cell cytotoxicity is known to be enhanced, treatment with interferon- $\gamma$  was included. IFN- $\gamma$  directly influences NK cell cytotoxicity through JAK/STAT and MAPK signaling, but crucially for this experiment it also upregulates PKC activity via PI3K signaling [116]. (n.b: An abundance of research focuses on the indirect effect of IFN- $\gamma$  on cytotoxicity, mediated through upregulating the abundance of NK-cell ligands on target cells or through interplay with other immune cells. Due to the nature of the model system, these effects are not pertinent here)

This treatment reduced the absolute amount of NKp30 present at exocytosis sites, as well as slightly reducing the localization preference when comparing ‘valid’ and ‘random’ positions. It also increased the variance of the summed intensities detected in ROIs, contrary to all other conditions where this variance is reduced compared to untreated cells. In leptin-treated NK-92 cells a reduction of the absolute amount of NKp30 present at lytic granule sites was observable when comparing to control samples. However, the difference of NKp30 abundance at ‘valid’ compared to ‘random’ ROIs is similar to that of untreated cells. While this provides evidence for the notion, that leptin alters the coordination of lytic granule exocytosis, it also suggests that this alteration is more complex than the inhibition of actin branching or lowering actin polymerization.

## Rac1 and CDC42 pulldown assay

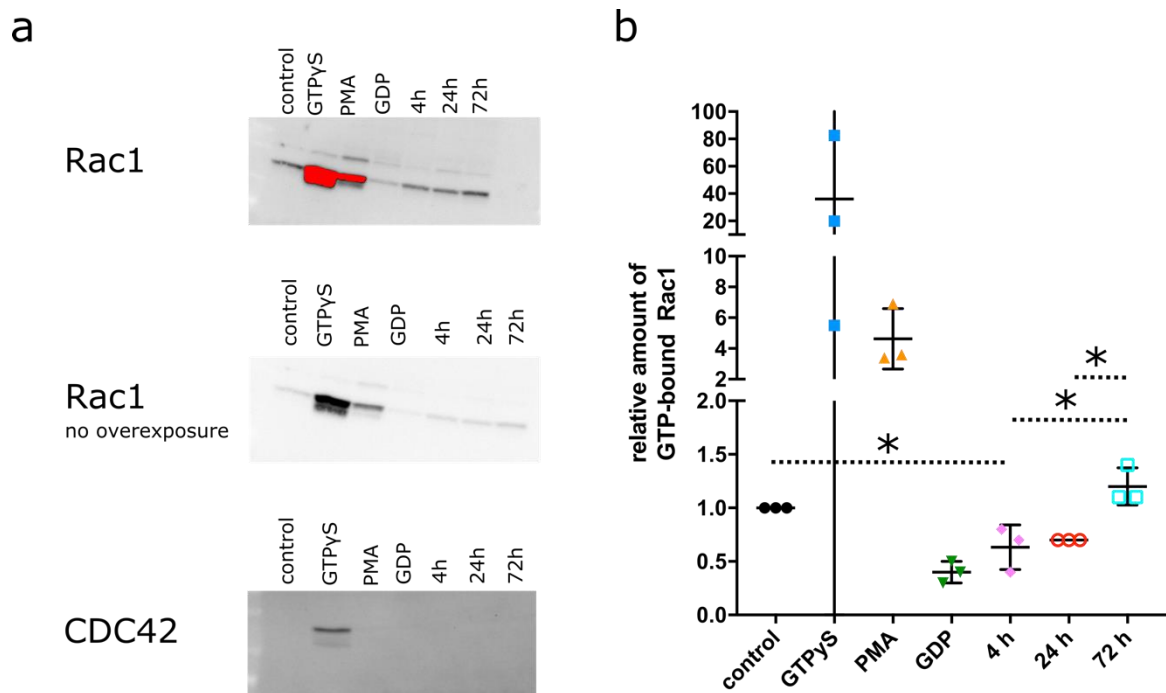


**Figure 7** Rac1 and CDC42 activation assay. Only GTP-bound and thus enzymatically active Rac1 or CDC42 in NK-92 protein cell lysates were bound via their active centers to an artificial substrate anchored on beads. GDP-bound inactive proteins are unable to bind. Bound protein was then eluted from the beads and quantified. **(a)** The top western blot shows an exemplary blot for Rac1 with detection optimized for the biological samples. In the middle the same blot is shown with no overexposure. Bottom blot shows the analogous experiment for CDC42. The amount of GTP-bound CDC42 for all samples was below the detection limit of the assay for all examined conditions. **(b)** shows the fold-change in GTP-bound Rac1, with the untreated control averaged across all replicates normalized to 1. For biological conditions, statistically significant differences ( $p < 0.05$ ) were observed in a Tukey's test for all pairs marked with an asterisk. Each dot represents the value of one of the three independent replicates, the bar their average and the whiskers the 95 % CI.

To further investigate whether exposure to leptin affects actin dynamism, it was investigated if leptin treatment affects known upstream regulators of actin-modifying proteins. The small Rho-GTPases Rac1 and CDC42 regulate multiple proteins that in turn shape the actin cytoskeleton. Only GTP-bound Rac1 and CDC2 are enzymatically active, while hydrolysis of  $\text{PO}_4^{3-}$  renders them inactive. For an overview, see introduction of [117]. The p21 binding domain of their common downstream target PAK is used as bait. It is expressed as a glutathione-S-transferase fusion protein and bound to glutathione agarose beads. These beads were added to NK-92 whole cell protein lysate, allowing only the GTP-bound proteins to bind. Bound protein eluted from the beads was then detected by two separate western blots for Rac1 and CDC42. **Fig. 7 (a)** shows exemplary western blots. **Fig. 7 (b)** shows the relative amount of GTP-bound Rac1 with values normalized to the untreated control. Since hydrolysis of GTP occurs spontaneously and its kinetics is temperature dependent, carefully selected controls were needed. GTPγS is a GTP-analogue, in which one oxygen atom in the  $\gamma$ -phosphate group is substituted by a sulfur atom (resulting in the terminal group being dihydroxyphosphinothioyl). This hydrolyzes much slower than GTP and can thus be used to forcibly activate some protein to determine whether the pull-down is working. The large variance (n.b. breaks in axis and scaling)

shows that the amount is outside the feasible detection range of the assay and the control is not able to accurately determine the total amount of protein present in the cell. It is however sufficient to estimate that it is roughly an order of magnitude larger than what is present in an untreated resting NK cell ('control'). PMA is again used to artificially induce PKC activity, whose downstream targets facilitate GDP/GTP exchange of Rac1/CDC42. This can be used to determine the amount of active protein in an extreme cellular state, which is around 10 % for most cells and NK-92 cells deviate only slightly from this. 'GDP' represents a control to determine the lower detection boundary of the assay: GDP is added to the protein lysate and the mixture is then heated. This results in all proteins being GDP-bound. Any protein that still binds to the glutathione agarose does so unspecifically. This is around 40 % of the amount detected for the untreated control. The three time points shown in **Fig. 7 (b)** represent treatment with 100 ng/ml leptin. Interestingly, the amount of GTP-bound Rac1 after 4 h of treatment is only 63 % compared control. This is notably the same time point where a difference in actin density at sites of granule exocytosis during degranulation was observed **Fig. 5 (f)**. But after 24 h, activity remains at 70 % compared to control, while no changes in actin density were observed at this time point. At the 72 h time point, 20 % more Rac1 is GTP-bound compared to untreated control.

### Rho-family kinase activity

The Rho-family kinases (ROCK) are central to coordination of cellular motility and, in relation to the question at hand, cellular contractility. Whether leptin influences their activity was examined in an enzymatic immunoassay. The two isoforms ROCK-I and ROCK-II are commonly reported to only be active if bound to GTP-bound RhoA. See introduction of [118]. The assay procedure is shown in **Fig. 8 (a)**.

MYPT1 is a downstream target of ROCK-I/II and phosphorylated by it at Thr696. It is noteworthy, that myotonic dystrophy protein kinase (DMPK) performs the same phosphorylation and the assay cannot distinguish between them. The amount of phospho-MYPT1 was then detected through an ELISA. **Fig. 8 (b)** shows the fold-change in kinase activity normalized to the untreated control. No statistically significant changes occurred between the examined time points.

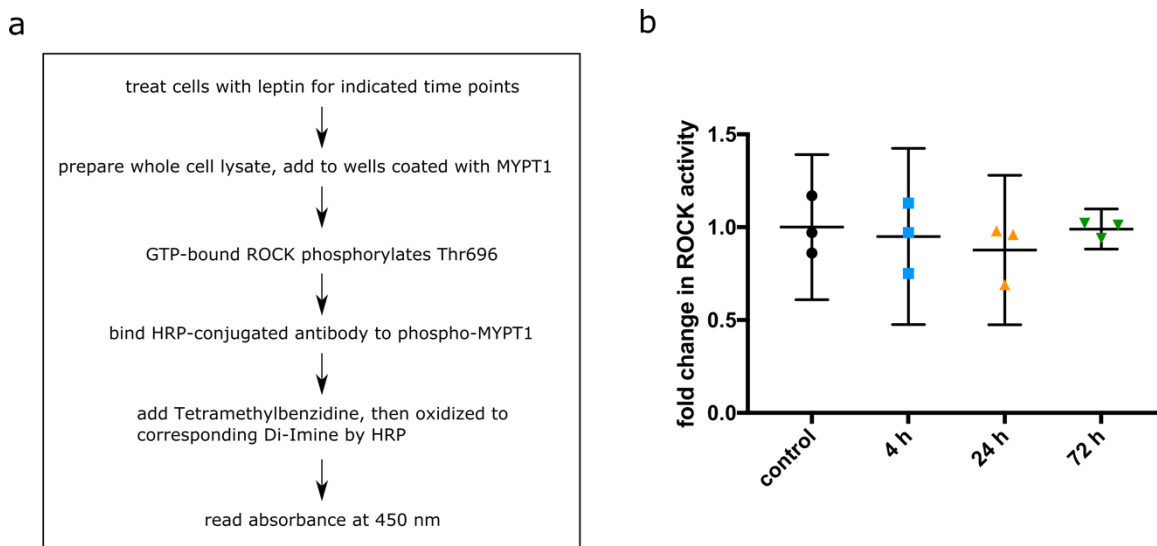


**Figure 8** Secondary enzyme immunoassay to determine change in activity of Rho-family kinases ROCK-I, ROCK-II and DMPK. **(a)** flow chart of experimental procedure **(b)** fold-change of kinase activity normalized to control after exposure to 100 ng/ml leptin for the indicated time points. No statistically significant differences were observed. Bar shows the mean, while whiskers indicate 95 % confidence interval

### Bottom-up proteomics approach for target identification

While pull-down assays and enzymatic immunoassays allow the detection of active, labile GTP-bound states of signaling proteins, they detect only the protein they were designed for. Thus, examining all related signaling pathways for changes upon hormonal stimulation is both prohibitively time consuming and liable to selection bias, as a change can only be detected in the specific proteins that were selected at the outset. While several publications describe the importance of actin dynamics for the NK cell immune synapse, almost no information is available on how leptin stimulation could change actin dynamics and related signaling to explain the changes observed in microscopy. A bottom-up proteomics approach with label-free quantification was thus chosen to obtain an indication of what changes in cell homeostasis follow leptin stimulation at the examined time points. This approach is unable to differentiate GTP- and GDP-bound states, as the labile ternary phosphate group is split off during ionization. It however allows an unbiased approach that can quantify a multitude of proteins in parallel. As opposed to guanosine binding, the phosphorylation of a protein can be differentiated with mass spectrometry. As this regulates activity for many proteins, it permits conclusions about what effect leptin stimulation might have on the cellular state.

For sample preparation, whole cell protein was obtained from NK-92 cells exposed to leptin for the same durations. In analogy to the microscopy sample preparation, lysates of NK-92 cells degranulating on a mAB coated surface were obtained by following the same protocol for microscopy, but adding lysis buffer instead of formaldehyde 15 min after beginning of degranulation. With this, quantitative, label-free proteomics analysis of resting and leptin-exposed NK-92 cells was performed, detecting 6869 master proteins. To reveal phosphorylation events in response to this exposure, phosphopeptide enrichment was also performed, revealing 1910 phosphopeptides. A precise description of the technique and data analysis used can be found in the methods section. Additionally, only proteins or phosphopeptides with a fold-change in abundance of at least 2 and a  $p$ -value  $< 0.0005$  were considered in the subsequent evaluation. For a phosphopeptide to be considered here, the protein it is derived from must also be detected with sufficient confidence.

When considering the resulting data, the role of leptin as a master energy regulator has to be considered.[38] It reportedly increases the metabolic activity of NK-92 cells without changing proliferation when exposed to 100 ng/ml leptin for the durations used here.[45] When using a bottom-up approach it is thus expected that the majority of impacted pathways relate to this increase in metabolic activity. To identify changes with potential relevance to the changes observed in microscopy, a set of Gene Ontology (GO) terms [119, 120] was defined as relevant functions for closer examination shown in **Table 1**. To identify targets for further study, only hits with at least one of these terms are being more closely examined.

Biological process	Cellular Component
Conjugation	Cell surface
Defense Response	Cytoskeleton
Response to Stimulus	Membrane

**Table 1** List of Gene Ontology terms with relevance to either receptor-ligand binding or potential influence of leptin on regulating actin dynamics.



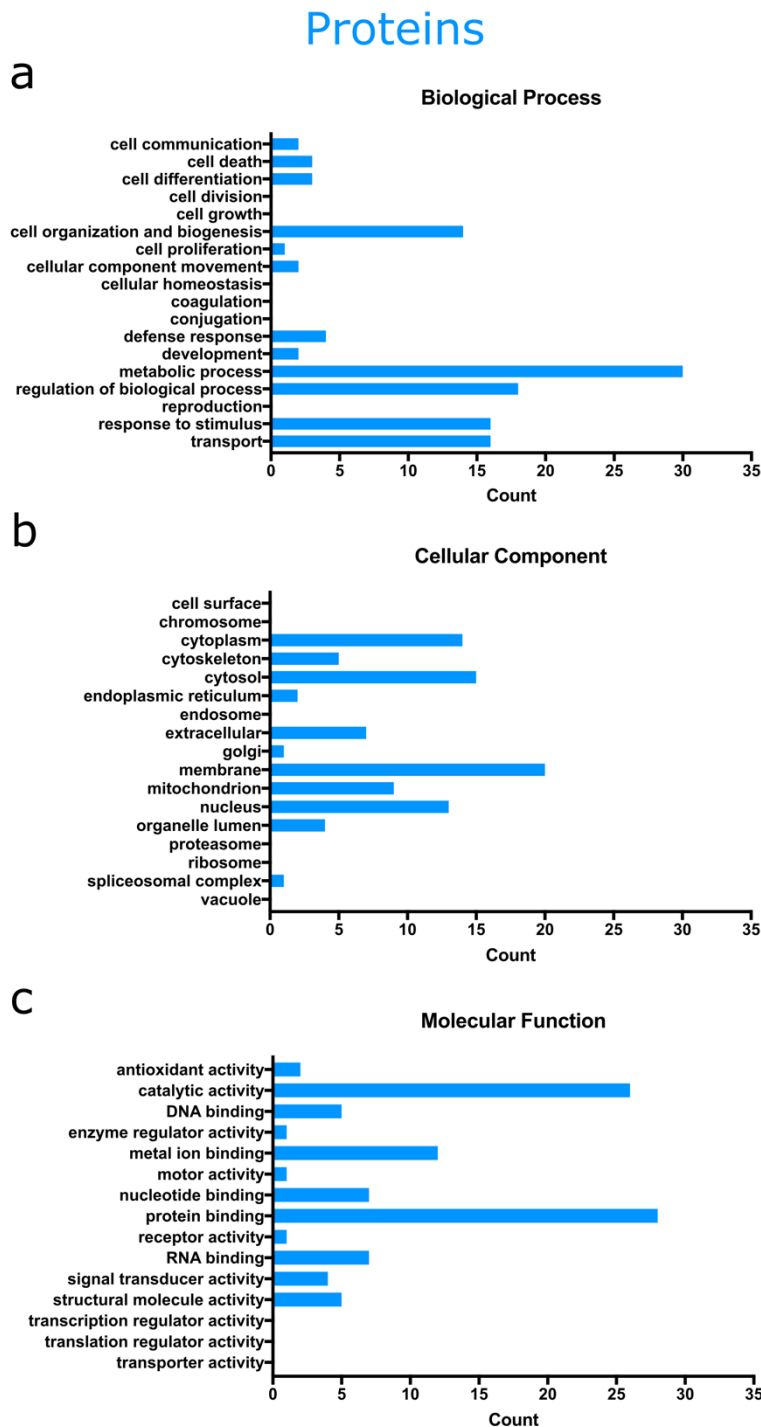


**Figure 9** Visualization of bottom up-proteomics data with leptin-stimulated NK-92 cells. Number of differentially abundant proteins with the GO term indicated in the bar chart. Gene Ontology term enrichment from differential protein abundance following leptin stimulation regarding **(a)** biological process **(b)** cellular component **(c)** molecular function. Performed in cooperation with Matthew Fuszard and the core facility proteomics at the Proteinzentrum Charles Tanford.

### Changes in protein expression

The first consideration was what proteins differ in abundance after leptin stimulation. Each comparison is made between untreated control and the indicated time point. **Fig. 9 (a)** shows a bar chart of GO terms among proteins with different abundance after leptin stimulation. From **(b)** no preference for a specific cellular compartment is evident. As outlined above, the majority is associated with metabolic processes and most of these **(c)** show catalytic activity or bind proteins. A list of the individual proteins with abundance difference and adjusted *p*-value can be found in **Tables 2-4**. Entries printed in bold have at least one of the GO terms defined in **Table 1** associated with them. Their observed differential regulation is visualized in the heatmap **Fig 11 (a)**.

Some affected proteins regulate actin dynamics and exocytosis. Two proteins with differing abundance can modify the cytoskeleton. LSP1 is an f-actin-binding protein that is differentially regulated 4 h and 24 h after leptin stimulation, returning to baseline after 72 h. Its role in coordinating actomyosin contractility has been shown to be key to macrophage migration.[121] Whether it serves the same function in NK cells or any function



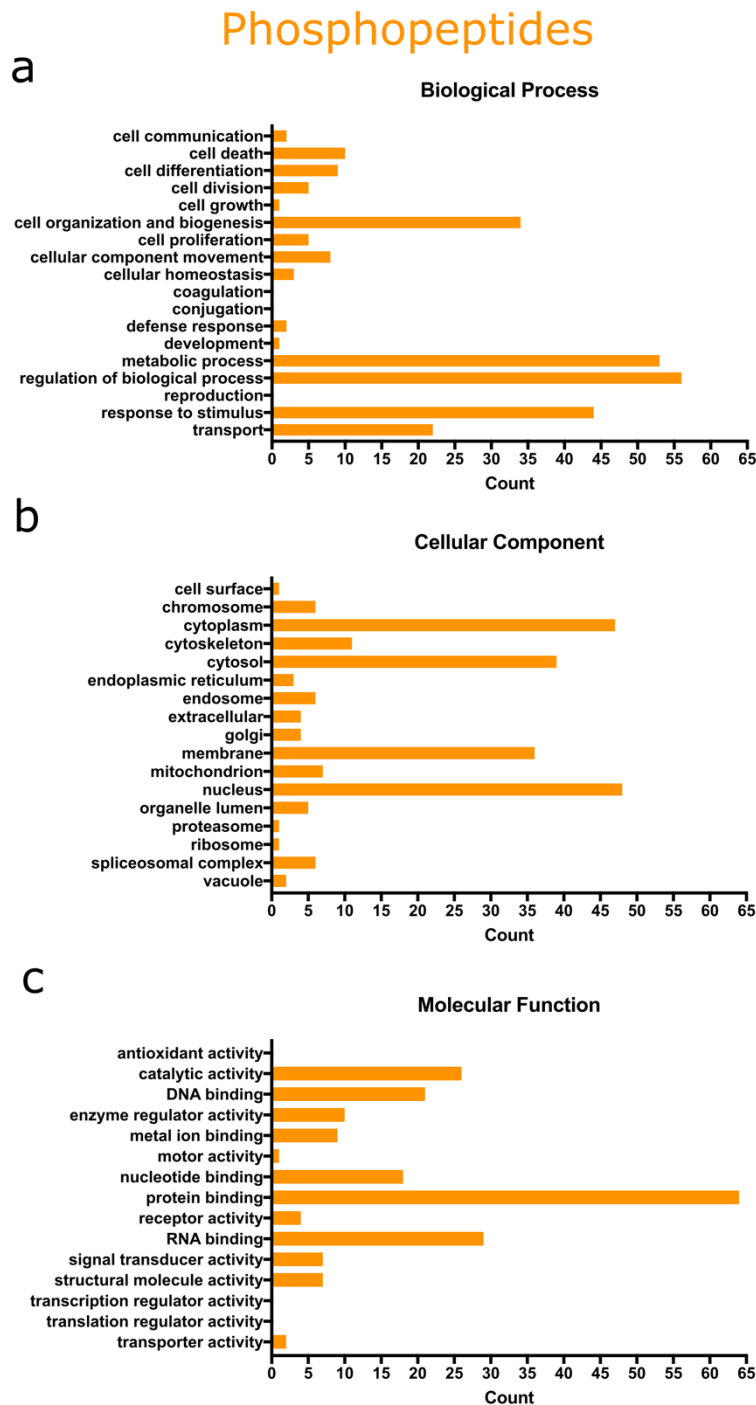


**Figure 10** Visualization of bottom up-proteomics data with leptin-stimulated NK-92 cells. Number of differentially abundant phosphopeptides with the GO term of the master protein indicated in the bar chart. GO term enrichment from differential phosphorylation stimulation regarding (a) biological process (b) cellular component (c) molecular function. Results shown in bar charts are summed for all time points. Performed in cooperation with Matthew Fuszard and the core facility proteomics at the Proteinzentrum Charles Tanford.

regarding the immune synapse is unknown. With PLS1, also known as Fimbrin, a member of the calponin homology domain superfamily is found downregulated roughly 2.5-fold for the 4 h and 72 h time point, and 2-fold for 24 h time point. Its main function is cross-linking of f-actin in orthogonal orientation, but it can also bind signaling proteins to the actin network. During degranulation, it reportedly localizes to the immune synapse of NK cells. The authors further demonstrate that its siRNA knockdown increases actin density at the immune synapse, while negatively affecting the cytotoxic capacity through degranulation. Meanwhile, granule polarization or secretion of cytokines after contact are unaffected.[122]

Two proteins with a known role in exocytosis were expressed in lower abundance following stimulation: RAB15 is downregulated only for the 4 h time point by 3.06 -fold. It is a binding partner of Munc13-4, which is crucial for lytic granule exocytosis, and has itself been shown to be relevant to exocytosis in HUVEC cells. No such studies for the role of RAB15 in immune cells exists to date.[123] RABIF is a chaperone holdase that stabilizes RAB, which is downregulated in the 4 h samples 2.3 -fold. It has been demonstrated to participate in exocytosis of GLUT4 in HeLa cells, but whether it also involved in lytic granule exocytosis has not been investigated.[124]

## Phosphorylation in response to leptin

Exposure to leptin resulted in a number of phosphorylation events being observed for each of the individual time points. Comparisons are being made, as before, between the untreated control with the individual, indicated time point. The phosphopeptides with their difference in abundance and adjusted *p*-value are listed in **Tables 5-7**. If the peptide's master protein is associated with one of the GO-terms in **Table 1**, the entry is printed in bold. As can be seen in **Fig. 10** the majority of the differentially phosphorylated proteins are associated with anabolic processes and metabolism. The contents of **Tables 5-7** are visualized in the heatmap **Fig. 11 (b)**. Each row represents a phosphopeptide and is annotated with the gene name of the associated master protein. However, several of the differentially phosphorylated proteins have functions that are of interest to elucidate how leptin stimulation leads to the changes in actin dynamics observed, meriting their individual examination.

## Jak/STAT, MAPK/Erk- pathways and signaling proteins regulating actin-modifying proteins

Regarding signaling, STAT5 shows an increase in phosphorylation by ~2.5x for each time point. Interestingly, an induction of phosphorylation in the Jak/STAT pathway has previously been observed when comparing primary NK-cells obtained from the blood of obese rats [46] and study participants [125] when compared to their lean counterparts. Leptin alone is also able to induce phosphorylation of STAT5 via Jak.[126]

Several components of the MAPK/Erk pathway exhibit differential phosphorylation: The Ras-GEF SOS1 is induced >6.64 fold at the 4 h time point, and 4.21 fold at the 72 h time point. It should be noted, that an indicated log<sub>2</sub>-fold change of 6.64 is the upper limit of the dynamic range of the quantification technique employed and the actual value might be higher. Phosphorylation of MAP3K20 (also known as ZAK) is also increased threefold in the 24 h sample, however no information is available whether its phosphorylation has any bearing on actin-modifying proteins. An increase in BRAF phosphorylation for the 4 h time point further suggests an alteration of the MAPK/Erk pathway.

Of note is also the ~5.5 -fold induction of PI4KB for all three observed time points. This enzyme itself phosphorylates phosphatidylinositol at the D4 position to yield phosphatidylinositol 4-phosphate (PI4P). For the present case, this is of particular interest as the ligation of the NKp30 receptor is relayed into the cytosol by phosphatidylinositol signaling. It alone however cannot sufficiently explain the changes in the formation of actin clearances for the 4 h time point, as this induction was observed for all three time points. It could suggest a possible pre-activation of this signaling system due to leptin exposure.

Multiple parts of the Rho signaling pathway were altered after stimulation. For PAK2 in the 4 h sample, one phosphopeptide was detected in 2.7 -fold lower abundance, while another was increased by 2.1-fold. This provides a possible link to actin-modifying proteins and their respective control systems, as it is a target of CDC42 and Rac1 and is involved in Rho-associated signaling.

ARHGEF6 can bind to PAK1, PAK2 or PAK3 via its SH3 domain theoretically allowing them to localize to the site of ligand-bound receptors and their associated protein complexes. Through its RhoGEF domain, it is also capable of exchanging GDP for GTP in Rac1 and CDC42.[127] In their GTP-bound active state, Rac1 and CDC42 are then capable of binding to the PAKs. When bound to these active Rho-family GTPases, the PAKs are then capable of kinase activity. It thus fulfills a dual role both as a scaffold signaling protein and as a GEF. The associated phosphopeptide was found with an increase of 6.64-fold (see

above, likely higher) in the 4 h and 24 h time points, suggesting that leptin induces signaling through this system. While no information is available regarding its function in NK-cells, loss of function has been associated with decrease of migratory capability in T-cells, but not with defects in TCR-signaling.[127]

Two further proteins with SH domains but opposing function were also found to be differentially phosphorylated: Phosphopeptides for SH3BP1 were more abundant in the 4 h and 24 h leptin-treated samples. It is a GTPase for Rho-family proteins including CDC42 and Rac1, dampening their activity by converting them to their GDP-bound form. In turn this allows actin remodeling after an external stimulus in a PI3K-dependent fashion. This has been demonstrated to be key to facilitate phagocytosis [128], but its role in exocytosis or in NK cells is unknown. For SH3GL1, differentially phosphorylated at the same time points, a similar role in endocytosis has been shown. It is associated with the Rho-pathway and is capable of binding to WASp and WAVE, thus modifying the actin cytoskeleton. While it is known for facilitating fast-endophilin mediated endocytosis, its role in exocytosis in neurons has been demonstrated.[129] No such knowledge exists for NK cells, however its deficiency has been shown to influence TCR-related signaling.[130]

Phosphorylation of TNIK was increased 5.29 -fold only in the 4 h time point. This kinase is an activator in the Wnt-signaling pathway. It is capable of autophosphorylation induced by Rap2 and itself has several phosphorylation targets, one of which is gelsolin. It furthermore is capable of binding SH3 domains, allowing it to localize to the immune synapse.[131] While no knowledge exists about its role in lytic granule exocytosis, or how its autophosphorylation is induced following leptin stimulation, circumstantial evidence suggests a possible role in the clearance of the f-actin mesh required for exocytosis: Gelsolin is a part of the actin-severing gelsolin/vilin superfamily and either its [132] or TNIK overexpression disrupts actin filaments.[131] For the former case, a role in actin dynamics in Jurkat T-cells has been shown. For gelsolin, phosphorylation removes its need to bind  $Ca^{2+}$  to become active.[133] Unfortunately, while gelsolin itself was detected with high confidence in this dataset, the peptides containing the sequence phosphorylated by TNIK was not detected. It is hence not possible to determine, whether this phosphorylation actually took place.

### **Leptin alters phosphorylation of actin-modifying proteins and proteins coordinating exocytosis**

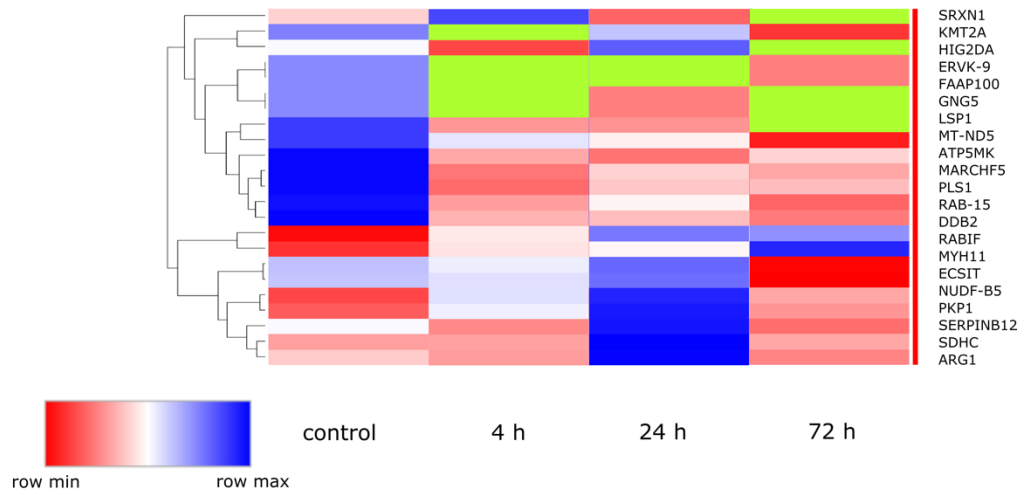
While the previously described proteins all relate to signaling, two of the differentially phosphorylated proteins directly modify the actin cytoskeleton.

ARPC1B, with a 5.64-fold increase in phosphorylation only in the 4 h time point, is a part of the Arp2/3 complex. The establishment of the actin meshwork at the immune synapse is crucially dependent on the function of this complex to mediate f-actin branching. Phosphorylation of the Arp-complex is known to alter its function, but the consequence of the phosphorylation at the site detected here (S310, S311, T315) are unknown.

ADD1 is a membrane-cytoskeleton associated protein that promotes the assembly of spectrin-actin networks. It is a target of PLC and is further capable of binding  $Ca^{2+}$  bound Calmodulin. The 2.64-fold increase in phosphorylation of the detected peptide is of interest here, as control of actin organization at the membrane is paramount for lytic granule exocytosis.

With SEC22B, a SNARE protein is phosphorylated 4 h after leptin stimulation. While it has a reported function in vesicle trafficking, no information is available whether it has a role in the transport of secretory granules for exocytosis in T or NK cells.[134]

a



b

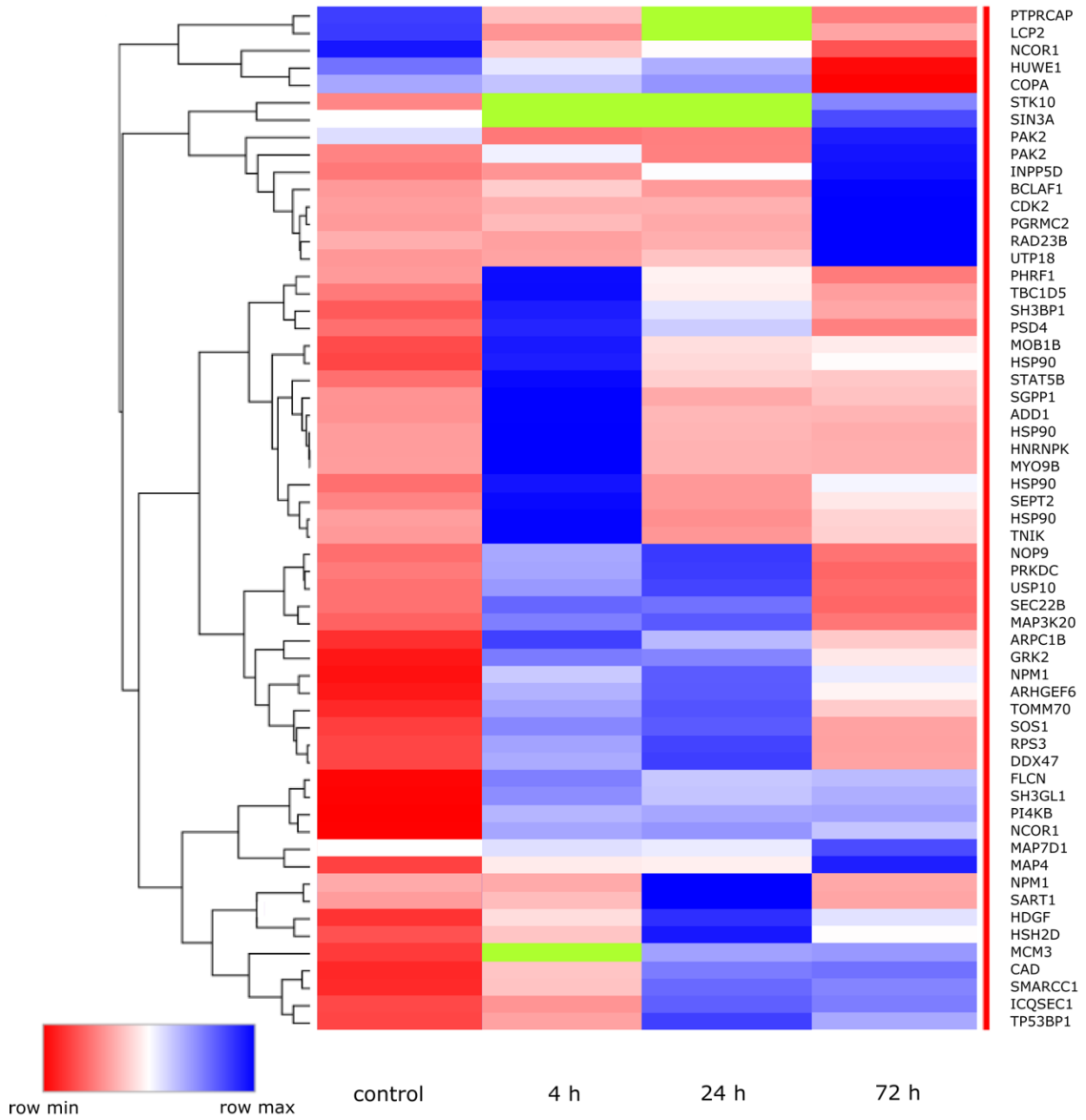


**Figure 11 (a)** Heatmap of differentially abundant proteins with relevant GO-terms annotated by corresponding gene name of master protein and **(b)** Heatmap of differentially abundant phosphopeptides with master proteins associated with relevant GO-terms. Each row represents one phosphopeptide group, with the row label showing the gene name of the associated master protein. In both heatmaps, a green square indicates that this protein/peptide was not found with sufficient confidence in the sample. The red to blue colour grading is scaled to the row minima and maxima. Performed in cooperation with Matthew Fuszard and the core facility proteomics at the Proteinzentrum Charles Tanford.

The phosphopeptide for NBEAL2 was detected with a 6.06-fold increase in abundance in the 4 h time point. The clinical observation that patients with NBEAL2-defects presented with increased susceptibility to infection led to the discovery of its role in immune function: NK cells and neutrophils of NBEAL2<sup>-/-</sup> mice exhibit defects in degranulation, but its precise role in coordination lytic granule formation and exocytosis is not known.[135] SEPTIN2 shows a roughly 3.3-fold increase in phosphorylation for all observed time points. The crucial role of septins for NK-cell degranulation has been introduced before. When considering the publications referenced in the introduction, it is however valuable to keep in mind, that these experiments were performed with primary cells and the cell lines KHYG1 and NKL, but not with NK-92 cells. For SEPTIN7 in dendritic cells it has been demonstrated that phosphorylation regulates activity, but no such data is available for SEPTIN2.[131]

Gene Name	Protein Accession	Description	Abundance Ratio [log <sub>2</sub> ]	Adj. p-Value
CHAF1A	Q13111	Chromatin assembly factor 1 subunit A	2.15	1.0528E-11
<b>ECSIT</b>	<b>Q9BQ95</b>	<b>Evolutionarily conserved signaling intermediate in Toll pathway, mitochondrial</b>	<b>2.38</b>	<b>7.1958E-05</b>
EDF1	O60869	Endothelial differentiation-related factor 1	2.03	1.5439E-16
<b>ERVK-9</b>	<b>P63128</b>	<b>Endogenous retrovirus group K member 9 Pol protein</b>	<b>-6.64</b>	<b>1.5439E-16</b>
<b>FAAP100</b>	<b>E7EVV8</b>	<b>Fanconi anemia core complex-associated protein 100</b>	<b>-6.64</b>	<b>1.5439E-16</b>
<b>GNG5</b>	<b>P63218</b>	<b>Guanine nucleotide-binding protein G(I)/G(S)/G(O) subunit gamma-5</b>	<b>-6.64</b>	<b>1.5439E-16</b>
GSPT2	Q8IYD1	Eukaryotic peptide chain release factor GTP-binding subunit ERF3B	-6.64	1.5439E-16
<b>HIGD2A</b>	<b>Q9BW72</b>	<b>HIG1 domain family member 2A, mitochondrial</b>	<b>-2.53</b>	<b>4.5014E-10</b>
<b>KMT2A</b>	<b>Q03164</b>	<b>Histone-lysine N-methyltransferase 2A</b>	<b>-6.64</b>	<b>1.5439E-16</b>
LSM8	O95777	U6 snRNA-associated Sm-like protein LSm8	-2.33	1.5439E-16
<b>LSP1</b>	<b>E9PBD8</b>	<b>Lymphocyte-specific protein 1 (Fragment)</b>	<b>-6.64</b>	<b>1.5439E-16</b>
<b>MARCHF5</b>	<b>Q9NX47</b>	<b>E3 ubiquitin-protein ligase MARCHF5</b>	<b>-2.52</b>	<b>1.3785E-10</b>
<b>MT-ND5</b>	<b>P03915</b>	<b>NADH-ubiquinone oxidoreductase chain 5</b>	<b>-2.69</b>	<b>1.5439E-16</b>
MTAP	F8WES2	S-methyl-5'-thioadenosine phosphorylase	-3.67	1.5439E-16
PDSS1	Q5T2R2	Decaprenyl-diphosphate synthase subunit 1	2.16	5.663E-09
PDXK	O00764	Pyridoxal kinase	-3.24	1.5439E-16
<b>PLS1</b>	<b>Q14651</b>	<b>Plastin-1</b>	<b>-2.44</b>	<b>3.3215E-09</b>
PUM1	H0YDQ6	Pumilio homolog 1 (Fragment)	2.11	0.00047542
<b>RAB15</b>	<b>P59190</b>	<b>Ras-related protein Rab-15</b>	<b>-3.06</b>	<b>1.5439E-16</b>
<b>RABIF</b>	<b>P47224</b>	<b>Guanine nucleotide exchange factor MSS4</b>	<b>-2.32</b>	<b>2.4919E-08</b>
SMPD4	C9J647	Sphingomyelin phosphodiesterase 4 (Fragment)	3.7	9.3288E-12

**Table 2** Proteins of resting NK-92 cells after 4 h of exposure to 100 ng/ml of leptin with a log<sub>2</sub> -fold abundance change >2. Listed in alphabetical order of the associated Gene Name. Entries printed in **bold** are associated with the GO-terms defined in Table 1

Gene Name	Protein Accession	Description	Abundance Ratio [log <sub>2</sub> ]	Adj. P-Value
<b>ARG1</b>	<b>P05089</b>	<b>Arginase-1</b>	<b>3.28</b>	<b>7-2747E-15</b>
C18orf25	K7EQH1	Uncharacterized protein C18orf25 (Fragment)	5.75	1.6467E-16
CBR3	O75828	Carbonyl reductase [NADPH] 3	-6.64	1.6467E-16
CD151	K4DIA7	Tetraspanin (Fragment)	-2.8	7.2202E-14
<b>ECSIT</b>	<b>Q9BQ95</b>	<b>Evolutionarily conserved signaling intermediate in Toll pathway, mitochondrial</b>	<b>2.91</b>	<b>0.00010794</b>
<b>FAAP100</b>	<b>E7EVV8</b>	<b>Fanconi anemia core complex-associated protein 100</b>	<b>-6.64</b>	<b>1.6467E-16</b>
FBXW2	Q9UKT8	F-box/WD repeat-containing protein 2	2.46	2.3399E-05
FLG2	Q5D862	Filaggrin-2	2.62	1.6467E-16
GAMT	A0A1W2PR36	Guanidinoacetate N-methyltransferase	-6.64	1.6467E-16
<b>IGHA1</b>	<b>P01876</b>	<b>Immunoglobulin heavy constant alpha 1</b>	<b>2.06</b>	<b>1.2735E-05</b>
MARCHF5	Q9NX47	E3 ubiquitin-protein ligase MARCHF5	-2.32	3.8844E-07
<b>MT-ND5</b>	<b>P03915</b>	<b>NADH-ubiquinone oxidoreductase chain 5</b>	<b>-2.89</b>	<b>1.6467E-16</b>
MTAP	F8WES2	S-methyl-5'-thioadenosine phosphorylase	-3.66	1.6467E-16
<b>MYH11</b>	<b>P35749</b>	<b>Myosin-11</b>	<b>3.63</b>	<b>1.6467E-16</b>
<b>NDUFB5</b>	<b>O43674</b>	<b>NADH dehydrogenase [ubiquinone] 1 beta subcomplex subunit 5, mitochondrial</b>	<b>2.63</b>	<b>1.1883E-06</b>
PDSS1	Q5T2R2	Decaprenyl-diphosphate synthase subunit 1	2.95	1.8124E-14
PDXK	O00764	Pyridoxal kinase	-3.15	1.6467E-16
<b>PKP1</b>	<b>Q13835</b>	<b>Plakophilin-1</b>	<b>2.06</b>	<b>1.6467E-16</b>
S100A9	P06702	Protein S100-A9	3.35	1.6467E-16
<b>SERPINB12</b>	<b>Q96P63</b>	<b>Serpin B12</b>	<b>2.91</b>	<b>0.00010901</b>
SMPD4	C9J647	Sphingomyelin phosphodiesterase 4 (Fragment)	3.76	7.4107E-09
TRANK1	A0A2R8YEM9	TPR and ankyrin repeat-containing protein 1	2.41	1.0887E-14
TSFM	C9JT21	Elongation factor Ts, mitochondrial (Fragment)	-6.64	1.6467E-16

**Table 3** Proteins of resting NK-92 cells after 24 h of exposure to 100 ng/ml of leptin with a log<sub>2</sub> -fold abundance change >2. Entries printed in **bold** are associated with the GO-terms defined in Table 1

Gene Name	Accession	Description	Abundance Ratio [log <sub>2</sub> ]	Adj. P-Value
<b>ATP5MD</b>	<b>Q96IX5</b>	<b>ATP synthase membrane subunit DAPIT, mitochondrial</b>	<b>-2.03</b>	<b>1.5514E-14</b>
C19orf47	Q8N9M1	Uncharacterized protein C19orf47	-2.97	1.86816E-08
C1orf167	H0Y5F2	Uncharacterized protein C1orf167 (Fragment)	2.02	4.43817E-05
<b>DDB2</b>	<b>Q92466</b>	<b>DNA damage-binding protein 2</b>	<b>-3.07</b>	<b>2.05492E-13</b>
<b>GNG5</b>	<b>P63218</b>	<b>Guanine nucleotide-binding protein G(I)/G(S)/G(O) subunit gamma-5</b>	<b>-6.64</b>	<b>1.75214E-16</b>
GTF3C2	Q8WUA4	General transcription factor 3C polypeptide 2	3.14	8.86103E-10
HAS1	M0QXH4	Hyaluronan synthase 1	3.82	1.75214E-16
<b>HIGD2A</b>	<b>Q9BW72</b>	<b>HIG1 domain family member 2A, mitochondrial</b>	<b>-6.64</b>	<b>1.75214E-16</b>
KIR3DX1	Q9H7L2	Putative killer cell immunoglobulin-like receptor-like protein KIR3DX1	-2.31	2.97269E-12
<b>LSP1</b>	<b>E9PBD8</b>	<b>Lymphocyte-specific protein 1 (Fragment)</b>	<b>-6.64</b>	<b>1.75214E-16</b>
<b>MYH11</b>	<b>P35749</b>	<b>Myosin-11</b>	<b>3.55</b>	<b>1.75214E-16</b>
NUDT3	O95989	Diphosphoinositol polyphosphate phosphohydrolase	-2.76	2.39449E-13
PDXK	O00764	Pyridoxal kinase	-2.92	1.75214E-16
<b>PLS1</b>	<b>Q14651</b>	<b>Plastin-1</b>	<b>-2.45</b>	<b>2.12498E-05</b>
<b>SDHC</b>	<b>Q99643</b>	<b>Succinate dehydrogenase cytochrome b560 subunit, mitochondrial</b>	<b>-3.35</b>	<b>1.75214E-16</b>
SMPD4	C9J647	Sphingomyelin phosphodiesterase 4 (Fragment)	3.99	2.33466E-10
<b>SRXN1</b>	<b>Q9BYN0</b>	<b>Sulfiredoxin-1</b>	<b>-6.64</b>	<b>1.75214E-16</b>
TSFM	C9JT21	Elongation factor Ts, mitochondrial (Fragment)	-2.3	8.44194E-05

**Table 4** Proteins of resting NK-92 cells after 72 h of exposure to 100 ng/ml of leptin with a log<sub>2</sub> -fold abundance change >2. Entries printed in **bold** are associated with the GO-terms defined in Table 1



Gene Name	Master Protein Accessions	Annotated Sequence	Master Protein Descriptions	Abundance Ratio [log2]	Adj. P-Value
<b>ADD1</b>	<b>P35611</b>	<b>[R].SPGSPVGGGTGSPPK.[W]</b>	<b>Alpha-adducin</b>	<b>2.34</b>	<b>6.05218E-06</b>
AKAP2	Q9Y2D5	[K].SPGALETPSAAGSQGNTASQGK.[E]	A-kinase anchor protein 2	-2.57	3.3046E-05
<b>ARHGEF6</b>	<b>Q15052</b>	<b>[R].KPSEEEYVIR.[K]</b>	<b>Rho guanine nucleotide exchange factor 6</b>	<b>6.64</b>	<b>8.83698E-17</b>
<b>ARPC1B</b>	<b>O15143</b>	<b>[K].KASSEGGTAAGAGLDSLHK.[N]</b>	<b>Actin-related protein 2/3 complex subunit 1B</b>	<b>5.64</b>	<b>8.83698E-17</b>
<b>BCLAF1</b>	<b>Q9NYF8</b>	<b>[K].KAEGEPQEESPLK.[S]</b>	<b>Bcl-2-associated transcription factor 1</b>	<b>4.91</b>	<b>8.83698E-17</b>
BRAF	A0A2R8Y8E0	[R].RDSSDDWEIPDGQITVGQR.[I]	Serine/threonine-protein kinase B-raf	2.45	2.66616E-05
<b>CAD</b>	<b>P27708</b>	<b>[R].ASDPGLPAEEP.[E]</b>	<b>CAD protein</b>	<b>2.26</b>	<b>7.46352E-06</b>
<b>DDX51</b>	<b>Q8N8A6</b>	<b>[R].VNDAEPGSPEAPQGK.[R]</b>	<b>ATP-dependent RNA helicase DDX51</b>	<b>4.95</b>	<b>1.75545E-14</b>
DKC1	O60832	[R].KRESESEDETTPPAAPQLIK.[K]	H/ACA ribonucleoprotein complex subunit DKC1	5.09	8.83698E-17
EEF1D	E9PL71; E9PRY8; E9PK06	[R].ATAPQQTQHVSPMR.[Q]	Elongation factor 1-delta	4	8.83698E-17
EIF4B	E7EX17	[K].EEDCHSPTSKPPKPDQLK.[V]	Eukaryotic translation initiation factor 4B	5.65	8.83698E-17
FIP1L1	Q6UN15	[R].DHSPTPSVFNSEER.[Y]	Pre-mRNA 3'-end-processing factor FIP1	2.93	1.94977E-07
<b>FLCN</b>	<b>Q8NFG4</b>	<b>[R].AHSPAEGASVESSSPGPK.[K]</b>	<b>Folliculin</b>	<b>4</b>	<b>2.22396E-08</b>
GPATCH8	Q9UKJ3	[R].KPSVSEEVQATPNK.[A]	G patch domain-containing protein 8	6.64	8.83698E-17
<b>HNRNPK</b>	<b>P61978; Q5T6W2</b>	<b>[R].DYDDMSPR.[R]</b>	<b>Heterogeneous nuclear ribonucleoprotein K</b>	<b>2.24</b>	<b>5.95774E-05</b>
<b>HSP90AB1</b>	<b>P08238; Q58FF7</b>	<b>[K].EISDDEAEEEEK.[G]</b>	<b>Heat shock protein HSP 90-beta</b>	<b>3.08</b>	<b>6.65538E-11</b>
<b>HSP90AB1</b>	<b>P08238; Q58FF7</b>	<b>[K].EISDDEAEEEEKGEKEEEDK.[D]</b>	<b>Heat shock protein HSP 90-beta</b>	<b>4.17</b>	<b>8.83698E-17</b>
<b>HSP90AB1</b>	<b>P08238</b>	<b>[K].IEDVGSDEEDDSGK.[D]</b>	<b>Heat shock protein HSP 90-beta</b>	<b>2.33</b>	<b>6.87339E-12</b>
<b>HSP90AB1</b>	<b>P08238</b>	<b>[K].IEDVGSDEEDDSGKDK.[K]</b>	<b>Heat shock protein HSP 90-beta</b>	<b>4.19</b>	<b>8.83698E-17</b>
<b>MAP7D1</b>	<b>Q3KQU3</b>	<b>[R].RSSQPSPTAVPASDSPPTK.[Q]</b>	<b>MAP7 domain-containing protein 1</b>	<b>6.64</b>	<b>8.83698E-17</b>

**Table 5** Phosphopeptides of resting NK-92 cells with log<sub>2</sub>-fold difference in abundance >2 after 4 h of exposure to 100 ng/ml of leptin. Entries printed in **bold** are associated with the GO-terms defined in Table 1

<b>MCM3</b>	<b>P25205</b>	<b>[R].RYSDLTTLVAFPSSSVYPTKDEENNP LETEYGLSVYK.[D]</b>	<b>DNA replication licensing factor MCM3</b>	<b>-6.64</b>	<b>8.83698E-17</b>
<b>MOB1</b>	<b>Q7L9L4; Q9H8S9</b>	<b>[K].HAEATLGSGLNR.[MQ]</b>	<b>MOB kinase activator 1A/B</b>	<b>2.04</b>	<b>6.56419E-05</b>
<b>MYO9B</b>	<b>M0R300</b>	<b>[R].VQEKPDSPPGGSTQIQR.[Y]</b>	<b>Unconventional myosin-IXb (Fragment)</b>	<b>3.76</b>	<b>5.86385E-15</b>
NBEAL2	A0A494C1V1	[R].RISQVSSGETEYNPTPEAR.[-]	Neurobeachin-like protein 2	6.06	8.83698E-17
<b>NCOR1</b>	<b>O75376</b>	<b>[R].VSPENLVDK.[S]</b>	<b>Nuclear receptor corepressor 1</b>	<b>6.38</b>	<b>8.83698E-17</b>
<b>PAK2</b>	<b>Q13177</b>	<b>[K].YLSFTPPEKDGFPSPGTPALNAK.[G]</b>	<b>Serine/threonine-protein kinase PAK 2</b>	<b>-2.68</b>	<b>5.5802E-07</b>
<b>PAK2</b>	<b>Q13177</b>	<b>[R].SVIDPVPAPVGDSDHVDGAAK.[S]</b>	<b>Serine/threonine-protein kinase PAK 2</b>	<b>2.13</b>	<b>1.97403E-05</b>
PANK2	Q9BZ23	[R].ASSASVPAVGASAEGR.[R]	Pantothenate kinase 2, mitochondrial	3.27	2.71672E-08
<b>PI4KB</b>	<b>A0A0B4J1S8</b>	<b>[R].SVENLPECGITHEQR.[A]</b>	<b>Phosphatidylinositol 4-kinase beta</b>	<b>5.62</b>	<b>8.83698E-17</b>
<b>PRKAR2B</b>	<b>P31323</b>	<b>[R].RASVCAEAYNPDEEEDDAESR.[I]</b>	<b>cAMP-dependent protein kinase type II-beta regulatory subunit</b>	<b>5.47</b>	<b>8.83698E-17</b>
<b>PSD4</b>	<b>Q8NDX1</b>	<b>[K].SHSSPSLHQDEAPTTAK.[V]</b>	<b>PH and SEC7 domain-containing protein 4</b>	<b>5.03</b>	<b>1.56095E-14</b>
<b>RPS3</b>	<b>P23396</b>	<b>[K].DEILPTTPISEQK.[G]</b>	<b>40S ribosomal protein S3</b>	<b>3.06</b>	<b>6.74302E-10</b>
<b>SEC22B</b>	<b>O75396</b>	<b>[R].NLGSIINTELQDVQR.[I]</b>	<b>Vesicle-trafficking protein SEC22b</b>	<b>3.62</b>	<b>1.1198E-10</b>
<b>SEPTIN2</b>	<b>Q15019; B5MCX3</b>	<b>[K].IYHLPDAESDEDEDFK.[E]</b>	<b>Septin-2</b>	<b>3.52</b>	<b>3.3116E-14</b>
<b>SGPP1</b>	<b>Q9BX95</b>	<b>[R].RNSLTGEEQLAR.[V]</b>	<b>Sphingosine-1-phosphate phosphatase 1</b>	<b>2.52</b>	<b>1.38485E-08</b>
<b>SH3BP1</b>	<b>Q9Y3L3</b>	<b>[R].ENHGQADHSPSMTATHFPR.[V]</b>	<b>SH3 domain-binding protein 1</b>	<b>2.77</b>	<b>0.000129532</b>
<b>SH3BP1</b>	<b>Q9Y3L3</b>	<b>[K].ERTESEVPPRPASP.[V]</b>	<b>SH3 domain-binding protein 1</b>	<b>5.67</b>	<b>8.83698E-17</b>
<b>SH3GL1</b>	<b>Q99961</b>	<b>[K].IAASSSFR.[S]</b>	<b>Endophilin-A2</b>	<b>6.19</b>	<b>8.83698E-17</b>
<b>SOS1</b>	<b>Q07889</b>	<b>[R].SASVSSISLTK.[G]</b>	<b>Son of sevenless homolog 1</b>	<b>6.64</b>	<b>8.83698E-17</b>
SRRM1	A9Z1X7	[K].VPKPEPIPEPKEPSPEK.[N]	Serine/arginine repetitive matrix protein 1	2.41	1.14923E-06
SRRM1	A9Z1X7	[R].RLSPSASPPR.[R]	Serine/arginine repetitive matrix protein 1	6.64	8.83698E-17
SRRM2	Q9UQ35	[R].RGEGDAPFSEPGTTSTQRPSSPETA TK.[Q]	Serine/arginine repetitive matrix protein 2	2.69	6.73655E-11
SRRM2	Q9UQ35	[R].HGGSPQPLATTPLSQEPVNPSEASP TR.[D]	Serine/arginine repetitive matrix protein 2	2.99	4.7543E-09
SRRM2	Q9UQ35	[K].THTTALAGRSPSPASGR.[R]	Serine/arginine repetitive matrix protein 2	3.11	5.11121E-10

**Table 5 continued**

<b>STAT5A/B</b>	<b>P51692; P42229</b>	<b>[K].AVDGYVKPQIK.[Q]</b>	<b>Signal transducer and activator of transcription 5A/B</b>	<b>2.83</b>	<b>8.89627E-12</b>
<b>TBC1D5</b>	<b>Q92609</b>	<b>[R].GSFSGQAQPLR.[T]</b>	<b>TBC1 domain family member 5</b>	<b>3.29</b>	<b>1.16414E-09</b>
<b>TNIK</b>	<b>Q9UKE5</b>	<b>[K].SEGSPVLPHEPAK.[V]</b>	<b>TRAF2 and NCK-interacting protein kinase</b>	<b>5.29</b>	<b>8.83698E-17</b>
USP10	Q14694	[K].NHSVNEEEQEEQEGESEDWEQVG PR.[N]	Ubiquitin carboxyl-terminal hydrolase 10	3.34	1.39681E-12
WDHD1	O75717	[R].SHILEDDENSVDISMLK.[T]	WD repeat and HMG-box DNA-binding protein 1	3.07	2.76459E-06

**Table 5 continued**

Gene Name	Master Protein Accessions	Annotated Sequence	Master Protein Descriptions	Abundance Ratio [log2]	Adj. P-Value
<b>ARHGEF6</b>	<b>Q15052</b>	<b>[R].KPSEEEYVIR.[K]</b>	<b>Rho guanine nucleotide exchange factor 6</b>	<b>6.64</b>	<b>9.86379E-17</b>
C18orf25	K7EQH1	[R].RDSSSQLASTESDKPTTGR.[V]	Uncharacterized protein C18orf25 (Fragment)	5.75	1.00682E-08
<b>CAD</b>	<b>P27708</b>	<b>[R].ASDPGLPAEPPK.[E]</b>	<b>CAD protein</b>	<b>6.64</b>	<b>9.86379E-17</b>
CWC25	Q9NXE8	[K].MANSSPVLSK.[V]	Pre-mRNA-splicing factor CWC25 homolog	3.33	2.05947E-08
<b>DDX47</b>	<b>Q9H0S4</b>	<b>[-].MAAPEEHDSPTASQPIVEEETK.[T]</b>	<b>Probable ATP-dependent RNA helicase DDX47</b>	<b>2.61</b>	<b>3.30288E-06</b>
GPATCH8	Q9UKJ3	[R].KPSVSEEVQATPNK.[A]	G patch domain-containing protein 8	6.64	9.86379E-17
<b>HDGF</b>	<b>P51858</b>	<b>[R].AGDLLEDSPK.[R]</b>	<b>Hepatoma-derived growth factor</b>	<b>3.41</b>	<b>6.84548E-06</b>
HIRIP3	Q9BW71	[R].EVSDSEAGGGPQGER.[K]	HIRA-interacting protein 3	3.85	1.11861E-05
HSH2D	Q96JZ2	[R].SVSCIEVTPGDR.[S]	Hematopoietic SH2 domain-containing protein	2.6	0.000132213
<b>IQSEC1</b>	<b>Q6DN90; A0A0C4DGT3</b>	<b>[R].SALSSSLR.[D]</b>	<b>IQ motif and SEC7 domain-containing protein 1</b>	<b>3.78</b>	<b>1.42609E-13</b>
LCP2	Q13094	[R].NFPLPLPNKPRPPSPAEEENSLNEEW YVSYITRPEAEAALR.[K]	Lymphocyte cytosolic protein 2	-6.64	9.86379E-17
<b>MAP3K20</b>	<b>Q9NYL2</b>	<b>[R].SSSPTQYGLTK.[N]</b>	<b>Mitogen-activated protein kinase kinase kinase 20</b>	<b>3</b>	<b>2.28015E-07</b>
<b>NCOR1</b>	<b>O75376</b>	<b>[R].VSPENLVDK.[S]</b>	<b>Nuclear receptor corepressor 1</b>	<b>6.45</b>	<b>9.86379E-17</b>
NOP9	Q86U38	[R].GSSVDGSPLLLFLR.[D]	Nucleolar protein 9	3.37	4.10547E-10
<b>NPM1</b>	<b>P06748</b>	<b>[K].DELHIVEAEAMNYEGSPIK.[V]</b>	<b>Nucleophosmin</b>	<b>3.8</b>	<b>8.82409E-12</b>
<b>NPM1</b>	<b>P06748</b>	<b>[K].CGSGPVHISGQHLVAVEEDAEESEDE EEEDVK.[L]</b>	<b>Nucleophosmin</b>	<b>6.4</b>	<b>9.86379E-17</b>
<b>PI4KB</b>	<b>A0A0B4J1S8</b>	<b>[R].SVENLPECGITHEQR.[A]</b>	<b>Phosphatidylinositol 4-kinase beta</b>	<b>5.74</b>	<b>9.86379E-17</b>
PPA2	Q9H2U2	[R].SLVESVSSSPNK.[E]	Inorganic pyrophosphatase 2, mitochondrial	6.64	9.86379E-17
<b>PRKAR2B</b>	<b>P31323</b>	<b>[R].RASVCAEAYNPDEEEDDAESR.[I]</b>	<b>cAMP-dependent protein kinase type II-beta regulatory subunit</b>	<b>6.64</b>	<b>9.86379E-17</b>
<b>PRKDC</b>	<b>P78527</b>	<b>[R].ATQQQHDFTLTQTADGR.[S]</b>	<b>DNA-dependent protein kinase catalytic subunit</b>	<b>3.66</b>	<b>8.08476E-10</b>

**Table 6** Phosphopeptides of resting NK-92 cells with log<sub>2</sub>-fold difference in abundance >2 after 24 h of exposure to 100 ng/ml of leptin. Entries printed in **bold** are associated with the GO-terms defined in Table 1

<b>PTPRCAP</b>	<b>Q14761</b>	<b>[R].AEEARDSDTEGDLVLGSPGPASAG GSAEALLSDLHAFAGSAAWDDSAR.[A]</b>	<b>Protein tyrosine phosphatase receptor type C-associated protein</b>	<b>-6.64</b>	<b>9.86379E-17</b>
<b>RPS3</b>	<b>P23396</b>	<b>[K].DEILPTTPISEQK.[G]</b>	<b>40S ribosomal protein S3</b>	<b>3.15</b>	<b>8.04332E-08</b>
<b>SART1</b>	<b>O43290</b>	<b>[R].RVSEVEEEEKEPVPQPLPSDDTR.[V]</b>	<b>U4/U6.U5 tri-snRNP-associated protein 1</b>	<b>2.79</b>	<b>3.27884E-07</b>
<b>SCAF8</b>	<b>Q9UPN6</b>	<b>[K].ETVQTTQSPTPVEK.[E]</b>	<b>SR-related and CTD-associated factor 8</b>	<b>-4.02</b>	<b>9.86379E-17</b>
<b>SEPTIN2</b>	<b>Q15019; B5MCX3</b>	<b>[K].IYHLPDAESDEDEDFK.[E]</b>	<b>Septin-2</b>	<b>3.32</b>	<b>6.89203E-07</b>
<b>SH3BP1</b>	<b>Q9Y3L3</b>	<b>[K].ERTESEVPPRPASP.[V]</b>	<b>SH3 domain-binding protein 1</b>	<b>2.15</b>	<b>0.000380703</b>
<b>SH3BP1</b>	<b>Q9Y3L3</b>	<b>[R].ENHGQADHSPSMTATHFPR.[V]</b>	<b>SH3 domain-binding protein 1</b>	<b>2.34</b>	<b>0.000269714</b>
<b>SRRM1</b>	<b>A9Z1X7</b>	<b>[K].VPKPEPIPEPKEPSPEK.[N]</b>	<b>Serine/arginine repetitive matrix protein 1</b>	<b>2.35</b>	<b>2.68792E-05</b>
<b>SRRM1</b>	<b>A9Z1X7</b>	<b>[R].SPSPAPPPR.[R]</b>	<b>Serine/arginine repetitive matrix protein 1</b>	<b>6.64</b>	<b>9.86379E-17</b>
<b>SRRM2</b>	<b>Q9UQ35</b>	<b>[R].RGECDAPFSEPGTTSTQRPSSPETA TK.[Q]</b>	<b>Serine/arginine repetitive matrix protein 2</b>	<b>2.6</b>	<b>1.48582E-07</b>
<b>STAT5A/B</b>	<b>P51692; P42229</b>	<b>[K].AVDGYVKPQIK.[Q]</b>	<b>Signal transducer and activator of transcription 5B GN=STAT5A/B</b>	<b>2.61</b>	<b>9.74666E-08</b>
<b>STK10</b>	<b>O94804</b>	<b>[K].RDSFIGTPYWMapeVVMCETMK.[D]</b>	<b>Serine/threonine-protein kinase 10</b>	<b>-6.64</b>	<b>9.86379E-17</b>
<b>TCEA1</b>	<b>A0A1W2PPZ5</b>	<b>[K].EPAITSQNSPEAR.[E]</b>	<b>Transcription elongation factor A protein 1</b>	<b>4.96</b>	<b>9.86379E-17</b>
<b>TOMM70</b>	<b>O94826</b>	<b>[R].ASPAPGSGHPEGPGAHLDMNSLDR. [A]</b>	<b>Mitochondrial import receptor subunit TOM70</b>	<b>2.76</b>	<b>9.03399E-07</b>
<b>TRANK1</b>	<b>A0A2R8YEM9</b>	<b>[K].IIATEQNTCAMEKSGR.[I]</b>	<b>TPR and ankyrin repeat-containing protein 1</b>	<b>2.41</b>	<b>1.25289E-05</b>
<b>USP10</b>	<b>Q14694</b>	<b>[K].NHSVNEEEQEEQGEGSEDEWEQVG PR.[N]</b>	<b>Ubiquitin carboxyl-terminal hydrolase 10</b>	<b>2.4</b>	<b>0.000134262</b>
<b>WDHD1</b>	<b>O75717</b>	<b>[R].SHILEDDENSVDISMLK.[T]</b>	<b>WD repeat and HMG-box DNA-binding protein 1</b>	<b>2.81</b>	<b>1.31795E-05</b>
<b>ZRANB2</b>	<b>O95218</b>	<b>[R].ENVEYIEREESDGEYDEFGR.[K]</b>	<b>Zinc finger Ran-binding domain-containing protein 2</b>	<b>2.39</b>	<b>0.000364574</b>

Table 6 continued

Gene Name	Master Protein Accessions	Annotated Sequence	Master Protein Descriptions	Abundance Ratio [log2]	Adj. P-Value
<b>BCLAF1</b>	<b>Q9NYF8</b>	<b>[K].KAEGEPQEESPLK.[S]</b>	<b>Bcl-2-associated transcription factor 1</b>	<b>6.64</b>	<b>1.06429E-16</b>
CCDC97	Q96F63	[R].TPTHQPPKPGSPGRPACPLSNLLLQSYEER.[E]	Coiled-coil domain-containing protein 97	-6.64	1.06429E-16
CCNL1	Q9UK58	[K].SPISINVK.[T]	Cyclin-L1	3.53	1.70255E-13
<b>CDK1/2</b>	<b>P24941; P06493</b>	<b>[K].IGEGTYGVVYK.[AG]</b>	<b>Cyclin-dependent kinase 1/2</b>	<b>4.42</b>	<b>9.29588E-10</b>
<b>COPA</b>	<b>P53621</b>	<b>[K].NLSPGAVESDVR.[G]</b>	<b>Coatomer subunit alpha</b>	<b>-2.7</b>	<b>8.60576E-07</b>
DUT	H0YNJ9	[-].MPCSEETPAISPSK.[R]	Deoxyuridine 5'-triphosphate nucleotidohydrolase	-6.64	1.06429E-16
GPATCH8	Q9UKJ3	[R].KPSVSEEVQATPNK.[A]	G patch domain-containing protein 8	6.64	1.06429E-16
<b>GRK2</b>	<b>P25098</b>	<b>[R].SPVVELSK.[V]</b>	<b>Beta-adrenergic receptor kinase 1</b>	<b>2.62</b>	<b>8.92135E-08</b>
<b>HSP90AB1</b>	<b>P08238</b>	<b>[K].IEDVGSDEEDDSGKDK.[K]</b>	<b>Heat shock protein HSP 90-beta</b>	<b>2.38</b>	<b>8.52004E-09</b>
<b>HUWE1</b>	<b>Q7Z6Z7</b>	<b>[R].AGSSTPGDAPPAVAEVQGR.[S]</b>	<b>E3 ubiquitin-protein ligase HUWE1</b>	<b>-4.39</b>	<b>1.70255E-13</b>
<b>INPP5D</b>	<b>Q92835</b>	<b>[R].GESPTPPGQPPISPK.[K]</b>	<b>Phosphatidylinositol 3,4,5-trisphosphate 5-phosphatase 1</b>	<b>2.75</b>	<b>2.08904E-05</b>
<b>IQSEC1</b>	<b>Q6DN90; A0A0C4DGT3</b>	<b>[R].SALSSSLR.[D]</b>	<b>IQ motif and SEC7 domain-containing protein 1</b>	<b>3.37</b>	<b>1.35362E-12</b>
KPNA3	O00505	[R].NVPQEESELESDVDADFK.[A]	Importin subunit alpha-4	2.57	5.93788E-06
<b>MAP4</b>	<b>E7EVA0</b>	<b>[R].SPSTLLPK.[K]</b>	<b>Microtubule-associated protein</b>	<b>4.71</b>	<b>1.06429E-16</b>
<b>MAP7D1</b>	<b>Q3KQU3</b>	<b>[R].RSSQPSPTAVPASDSPPTK.[Q]</b>	<b>MAP7 domain-containing protein 1</b>	<b>6.64</b>	<b>1.06429E-16</b>
<b>NCOR1</b>	<b>O75376</b>	<b>[K].HEAPSSPISGQPCGDDQNASPSK.[L]</b>	<b>Nuclear receptor corepressor 1</b>	<b>-2.51</b>	<b>3.24552E-05</b>
<b>NCOR1</b>	<b>O75376</b>	<b>[R].VSPENLVDK.[S]</b>	<b>Nuclear receptor corepressor 1</b>	<b>6.25</b>	<b>1.06429E-16</b>
<b>NPM1</b>	<b>P06748</b>	<b>[K].DELHIVEAEAMNYEGSPIK.[V]</b>	<b>Nucleophosmin</b>	<b>3.82</b>	<b>9.81462E-14</b>
<b>PAK2</b>	<b>Q13177</b>	<b>[R].SVIDPVPAPVGDSDHVDGAAK.[S]</b>	<b>Serine/threonine-protein kinase PAK 2</b>	<b>3.04</b>	<b>1.55376E-09</b>
PANK2	Q9BZ23	[R].ASSASVPAVGASAEGTR.[R]	Pantothenate kinase 2, mitochondrial	2.73	0.000116813
<b>PGRMC2</b>	<b>O15173</b>	<b>[R].LLKPGEEPSEYTDEEDTK.[D]</b>	<b>Membrane-associated progesterone receptor component 2</b>	<b>3.76</b>	<b>1.06429E-16</b>

**Table 7** Phosphopeptides of resting NK-92 cells with log<sub>2</sub>-fold difference in abundance >2 after 72 h of exposure to 100 ng/ml of leptin. Entries printed in **bold** are associated with the GO-terms defined in Table 1

<b>PHRF1</b>	<b>F8WEF5</b>	<b>[R].EASPAPLAQGEPGR.[E]</b>	<b>PHD and RING finger domain-containing protein 1</b>	<b>-2.4</b>	<b>0.000191123</b>
<b>PI4KB</b>	<b>A0A0B4J1S8</b>	<b>[R].SVENLPECGITHEQR.[A]</b>	<b>Phosphatidylinositol 4-kinase beta</b>	<b>5.58</b>	<b>1.06429E-16</b>
RAD23A	A0A494C0B4	[R].EDKSPSEESAPTTSPESVSGSVPSSGSSGR.[E]	UV excision repair protein RAD23 homolog A	2.16	6.3503E-05
<b>RAD23B</b>	<b>P54727</b>	<b>[K].QEKPAEKPAETPVATSPTATDSTGDSSR.[S]</b>	<b>UV excision repair protein RAD23 homolog B</b>	<b>2.71</b>	<b>4.56513E-05</b>
RNF20	Q5VTR2	[K].ALVVPEPEPDSDSNQER.[K]	E3 ubiquitin-protein ligase BRE1A	3.7	2.23752E-12
<b>SEPTIN2</b>	<b>Q15019; B5MCX3</b>	<b>[K].IYHLPDAESDEDEDFK.[E]</b>	<b>Septin-2</b>	<b>3.28</b>	<b>1.38763E-11</b>
<b>SH3GL1</b>	<b>Q99961</b>	<b>[K].IAASSFR.[S]</b>	<b>Endophilin-A2</b>	<b>6.06</b>	<b>1.06429E-16</b>
<b>SIN3A</b>	<b>Q96ST3</b>	<b>[R].SPPVQPHTPVITISLGTAPSLQNNQPV EFNHAINVVK.[I]</b>	<b>Paired amphipathic helix protein Sin3a</b>	<b>6.64</b>	<b>1.06429E-16</b>
<b>SLTM</b>	<b>Q9NWH9</b>	<b>[K].DGQDAIAQSPEK.[E]</b>	<b>SAFB-like transcription modulator</b>	<b>-2.14</b>	<b>4.77653E-05</b>
<b>SMARCC1</b>	<b>Q92922</b>	<b>[R].KHSPPPPPTPTESR.[K]</b>	<b>SWI/SNF complex subunit SMARCC1</b>	<b>4.54</b>	<b>1.06429E-16</b>
<b>SOS1</b>	<b>Q07889</b>	<b>[R].SASVSSISLTK.[G]</b>	<b>Son of sevenless homolog 1</b>	<b>4.21</b>	<b>1.06429E-16</b>
SRRM1	A9Z1X7	[K].AASPSPQSVR.[R]	Serine/arginine repetitive matrix protein 1	-2.66	1.31329E-07
SRRM1	A9Z1X7	[R].SPSPAPPPR.[R]	Serine/arginine repetitive matrix protein 1	6.64	1.06429E-16
SRRM2	Q9UQ35	[R].TPPVALNSSR.[M]	Serine/arginine repetitive matrix protein 2	2.21	0.000108853
SRSF10	O75494	[R].SFDYNYR.[R]	Serine/arginine-rich splicing factor 10	-5.25	1.06429E-16
<b>STAT5A/B</b>	<b>P51692; P42229</b>	<b>[K].AVDGYVKPQIK.[Q]</b>	<b>Signal transducer and activator of transcription 5A/B</b>	<b>2.24</b>	<b>1.23377E-06</b>
<b>TP53BP1</b>	<b>Q12888</b>	<b>[K].SPEPEVLSTQEDLFDQSNK.[T]</b>	<b>TP53-binding protein 1</b>	<b>2.6</b>	<b>9.36612E-05</b>
<b>UTP18</b>	<b>Q9Y5J1</b>	<b>[R].VQEHEDSGDSEVENEAK.[G]</b>	<b>U3 small nucleolar RNA-associated protein 18 homolog</b>	<b>3.72</b>	<b>2.40773E-12</b>

Table 7 continued

## Discussion

The protein machinery of NK-92 cells required for exocytosis appears to be affected by short-term exposure to leptin. Changes in the density of the actin meshwork at sites of granule exocytosis were observable, as well as a reduced amount of NKp30 being present at these sites. The relative degree of colocalization between NKp30 clusters and granules however remained unaffected, while inhibiting actin polymerization or branching reduced this tendency to colocalize.

Rac1 is activated in response to leptin treatment, along with further components of Rho-related signal transduction being affected. The phosphorylation state or abundance of proteins that modify the f-actin network or proteins coordinating exocytosis are altered by it. Several of these proteins contain SH-domains that would allow them to localize to the membrane in response to receptor ligation and mediate local signaling.

### Validity of the model system

The granzyme B and LAMP1 assays demonstrate that NK-92 cells can be induced to degranulate in this manner, which has also been confirmed by others.[66] The amount of granzyme B released, varied between cell lines which is in line with previous reports comparing cytotoxicity between NK cell lines.[32] NK-92 cells treated with very high leptin concentrations released less granzymes, but the standard deviation makes this result somewhat unreliable. This is likely high due to the small difference between lysis and autolysis, compressing the dynamic range. The same assay with primary NK cells and HLA-deficient target cells would likely allow more precision. The detection in culture supernatant through an enzymatic assays however allows to qualitatively show that the release of granzyme B is occurring on a coated coverslip.

Regarding the leptin treatment, it must be noted that the chosen concentration of 100 ng/ml is relatively high. For non-obese humans, it is typically around 12 ng/mL. The concentration is higher for females than for males and this difference is exacerbated in obesity, with women averaging at 65 ng/ml and men at 40 ng/ml. Higher serum concentration does not necessarily equal a proportionately higher cellular response, as most obese patients are leptin-resistant to some degree. The serum level is also not constant but varies diurnally: During periods of fasting, it decreases and rises again after energy uptake.[136, 137]

These assays can also not distinguish between the frequency of degranulation events and the expression strength of granzyme B and granzyme A, which both cleave the peptide. Leptin has been reported to differentially regulate granzyme B expression,[45] but the proteomics data in this study is unsuitable to determine this. Sequence homologies between granzymes A, B, K, M and H makes assignment of detected peptides to master proteins difficult, resulting in high *p*-values and uncertainty in abundance. In sum, these complications prohibit obtaining precise quantitative data with these methods.

There are also marked differences between cell lines, implying that ligation of one set of receptors leads to different strength of response, up to no induction of degranulation (e.g. NK-L). Since NK-92 cells showed the highest cytotoxicity and because most applications for immunotherapy are focusing on it, this cell line was chosen for further experiments.

The LAMP1 assay partially solves this issue, as its output depends only on the frequency of the degranulation events, assuming homogenous distribution of LAMP1. It also allows greater replicability and yields a comparatively smaller spread of data points between



individual cells. Indeed, usage of antibody-coated glass gives a smaller spread of LAMP1 values per replicate and smaller deviation between replicates than with K562 cells. This is likely due to the reasons leading to biological variance discussed before. Low variance is especially desirable for applications with super-resolved microscopy, as the long acquisition time limits the number of cells that can be imaged.

The finding that the degranulation response depends on the ligated receptor is consistent with previous observations.[66] The expression strength of the chosen NKp30 receptor also does not change with leptin stimulation, hence any observed change must be independent of differential receptor expression. It is however paradoxical at first glance, that ligation of NKp30 gave a stronger LAMP1 signal than NKp30 and integrin  $\beta$ -2 combined. However, some degranulating cells of the latter were lost during assay preparation, as their strong adhesion to the coverslip made it impossible to resuspend them. This skews the assay in artificially decreasing high values and could not be solved by increasing EDTA concentrations. An enzymatic detachment is also not possible, as that would also cleave LAMP1 located on the membrane.

### Utility of the model

While degranulation can be induced in this way in a very reproducible manner, it is important to bear in mind that this is an artificial system: The binding strength and mode of the mAB to the receptor is not the same as to a ligand. Its density is also likely not the same as that of a ligand on a cell surface. This could be resolved by using supported lipid bilayers with nickelated phospholipids and attached His<sub>6</sub>-tagged ligands, that would also be laterally mobile on the SLB, which is more comparable to a cell membrane. However, it is more difficult to produce SLBs of comparable homogeneity and additionally fixation then becomes an issue, as the cell rests on a non-fixable SLB. Chip-like surfaces [95] provide an alternative, but the nanolithography used requires the substrate to be made from monocrystalline silicon, which makes observation from below impossible. Imaging through the entire cell instead would result in tissue penetration between 10 – 15  $\mu$ m in depth, distorting the PSF and markedly decreasing resolution.

The abovementioned model surfaces are stiff and the forces generated by the NK cell is negligibly small, which also does not reflect the *in vivo* state. Functionalized gels encounter similar problems regarding ligand distribution because the polymerization reaction does not produce a homogenous gel. But such gels, e.g. made out of polyacrylamide, offer the advantage that their rigidity can be tuned by the amount of crosslinks in them, which can be easily adjusted through the amount of N,N'-Methylenebisacrylamide added.[138] Their use in combination with traction force microscopy [139] would thus afford the opportunity to observe the forces generated at the immune synapse and determine if they change if actin dynamics are altered.

One issue is not resolved by any of these systems: When an NK cell encounters a target cell *in vivo*, it usually sits on epithelium surrounded by other cells. Killing of healthy bystander cells is known to be very rare.[68] This means that *in vivo* the spread of an NK cell is limited by the dimensions of the target cell, which is not true for the glass surface.

Using plates with microwells of a size comparable to a target cell is a solution, but they are commonly manufactured from silicone or polydimethylsiloxane, again making microscopy impractical. Recently however, a laser-etching method was demonstrated that can manufacture wells in glass, which could be a potential solution, if the microfluidics of reproducibly coating them can be managed.[140] Retrieving an attached cell from the bottom of a well to purify proteins or perform flow cytometry would be more difficult, however.

As the object of a minimal model is to recapitulate only parts of the *in vivo* reality to study them in isolation, the use of multiple systems in comparison is needed to understand the spatiotemporal coordination of proteins needed for granule exocytosis and how and when a cell commits to it. This is especially helpful when considering multifactorial diseases such as obesity, where a multitude of parameters is different between the non-obese and the obese condition.

### **STED-Imaging shows differences in actin density**

STED-Imaging allowed acquisition of the actin mesh with very high spatial precision. It is important to bear in mind though, that an f-actin filament has a diameter of 9.5 nm which is well below the STED resolution. The resulting image is thus more akin to a density map, which explains why more averaging with lower STED powers resulted in better image quality than less averages with higher power; fluorophore bleaching being the limiting factor for both.

At first glance, it is paradoxical that a higher density of the actin mesh was observed after 4 h of stimulation: Formation of a hole is necessary for exocytosis, but other data suggests that this short-term leptin exposure results in an increase in cytotoxic capacity (see introduction). One possible explanation is that the action of SNAREs is required for exocytosis and that these use f-actin as an anchoring point. This contradiction is however difficult to resolve without dynamic data from live-cell imaging. Among super-resolution techniques STED allows for the best spatial resolution. With an acquisition time of around 30 min per cell and the degranulation event taking only 15 min, these images can only be snapshots of a dynamic process.[98] Specialized adoptions of TIRF-SIM are alternative and powerful tools to observe the actin meshwork.[141] Another explanation could be the influence of leptin on the exocytosis machinery that the proteomics data hints at. This will be discussed later. Nevertheless, this data demonstrates that actin dynamics in NK-92 cells are affected by leptin exposure.

### **Lytic granules preferentially localize to NKp30 protein clusters**

In this model system, lytic granules localized preferentially to clusters of the NKp30 receptor during degranulation. First, this raises the question whether NKp30 is also clustered in resting NK-cells or rather homogeneously distributed across the cell membrane, with clusters forming only upon ligation or activation. In theory, this would be solvable by placing NK cells on a non-activating surface, fixing them, immunostaining the receptor of interest and recording z-stacks. In practice, this would be fraught with confounding factors. NK cells have a wide variety of different receptors and their abundance is relatively low. If the receptors are distributed across the entire cell surface, this would give poor signal to noise ratios. It is also conceivable, that clusters form and disassociate in resting cells. The temporal scale is also entirely unknown: How much time elapses between receptor ligation and alteration of its diffusion dynamics? No current microscopy system exists that can monitor a 15-20  $\mu\text{m}$  diameter cell at appropriate speeds, if the signal is weak. To obtain reliable results, it would thus be necessary to first establish a knock-out line of the receptor of interest. This could then be transduced with a fluorophore-receptor fusion protein, that must still have the same docking sites for adaptor proteins as the wild-type receptor. Then, fluorescence correlation spectroscopy [142] can be performed with resting cells to establish diffusion when no offending agent is present. After receptor ligation with soluble ligands, by antibodies or recombinant ligand proteins, its diffusion constant could then be measured again and corrected for the influence the ligand-binding has on its diffusion speed. If after

this correction, the diffusion constant is still lower, clustering only occurs in response to ligand binding.

Finding a truly non-activating surface is an ongoing concern, that is not limited to NK-cell imaging. Suspension cells do not adhere to glass or plastic. Even coatings widely used for this purpose, such as Poly-L-Lysin, have recently been shown to still activate T-cells.[143] Coatings that recapitulate the extracellular matrix, such as fibronectin are possible, but they come with the complication of inducing non-directed migration of cells.[144] This, or the changes in morphology during IS establishment if the receptors of a surface-bound NK would severely limit the time scale during which FCS measurements can be performed: It is not possible to measure diffusion at a spot of the cell membrane, if that spot is trying to move together with the rest of the cell. Doing away with the surface entirely by capturing the cell in an optical trap instead could however solve these issues in the future.[145]

Inhibiting actin polymerization or branching through inhibitors lowered the relative localization preference of lytic granules to NKp30 clusters. This suggests that there is interplay between the actin meshwork and the membrane receptors, but gives little indication as to its nature. The cluster size may be affected directly through the actin network or indirectly, through the actin network affecting the positioning and recruitment of adapter proteins that mediate signaling through localized feedback loops.

It is possible, that this inhibition resulted in a less dense actin meshwork, thus reducing the need to recruit actin-severing proteins in order to make a hole in the meshwork for exocytosis. It could also be possible that local signaling at NKp30 clusters is required to coordinate other components of the exocytosis machinery. These might not relate directly to actin, but could require actin rearrangement to organize local signal protein complexes. IFN- $\gamma$  induces PKC activity, thereby lowering the 'threshold' of signal to induce degranulation.[116] The observation that IFN- $\gamma$  treatment reduced the absolute amount of NKp30 at sites of exocytosis, but not the localization preference provides some tangential support for the latter hypothesis.

A first avenue of approach would be to determine if the establishment of a hole in the meshwork alone is sufficient to enable exocytosis. This could be done with a somewhat analogous experiment, enabled through the recent development of optically activatable Jaspaklinolide.[146] A glass surface only coated with integrin  $\beta$ 2 leads to IS establishment and lytic granule convergence, but not exocytosis. Photoactivation of opto-Jaspaklinolide at the position of lytic granules could then allow the artificial establishment of clearances in the absence of local NKp30 signaling. Parallel use of a mCherry-LAMP1-pHluorin construct would allow the observation if exocytosis still occurs. Observation of granules and actin through live cells with TIRF-SIM should provide sufficient spatial and temporal resolution [101]. Regarding the choice of imaging method, it must be noted that a recent publication applying ROCS microscopy to the observation of mast cell degranulation has cast some doubt on the established notion, that degranulation happens over the span of minutes. Here, (see Fig. 4 in [147]) the passage of a granule through the actin meshwork and to the cell surface is shown to happen within 2 seconds. Such events would be entirely missed with TIRF-SIM. Mast cell degranulation is certainly not the same as NK cell degranulation. For one, mast cell granules do not fuse with the cell membrane, but are rather extruded as whole vesicles. Additionally, no differential consideration what activating or inhibiting receptors are ligand-bound is necessary for mast cells. If a sufficient amount of IgE is crosslinked through an offending agent and thus able to bind to the mast cell surface through their F<sub>C</sub> part, degranulation is triggered. Crucially, the authors point out that no granule release toward the glass surface was observable, but that vesicles were extruded

laterally. Nevertheless, the common need to pass an actin meshwork (called actin cortex in this publication) and the many commonalities shared in the rest of the exocytosis machinery between the two cells would make it interesting to apply this method to NK cell degranulation.

Short-term exposure to leptin reduced the amount of NKp30 present at sites of granule exocytosis, but did not alter the relative localization preference of lytic granules toward NKp30 clusters. This result must be seen in conjunction with the result that IFN- $\gamma$  treatment produced a similar tendency, and earlier reports, that short-term leptin exposure increases NK cell cytotoxicity (see introduction). The question what precise mechanism mediates this effect cannot be answered conclusively through the data presented in this study. Indeed, leptin appears to simultaneously affect whole-cell signaling through the Jak/STAT pathway, adapter proteins with SH-domains capable of localized signaling at sites where the NKp30 receptor is ligand bound, signaling pathways whose downstream targets affect actin-modifying proteins, as well as some actin modifying proteins directly. These effects are likely related, but answering how they relate to one another requires further experimental data.

Due to the very pleiotropic nature of leptin stimulation and additionally the known effects of immune cell metabolism on their cytotoxic functions, stepping away from using leptin exposure directly might be a sensible way forward. Instead, it would be interesting to recapitulate singular events triggered by it through artificial means: Overexpression or knockdown of relevant proteins; Similarly, forcing phosphorylation or dephosphorylation by modifying corresponding enzymes. This would allow the establishment of mechanistic links, e.g: Is activating Rac1 sufficient to change the activity of proteins needed to remodel the actin mesh for the establishment of clearances? Many combinations are possible and some of these mechanism rely on tight spatio-temporal coordination to exert their influence. This complexity and the time required for imaging capable of detecting these effects, make approaching the issue with imaging alone unfeasible. Instead, it might be more advisable to perform these biochemical manipulations and consider functional consequences first. Doing this with methods capable of higher throughput, such as the LAMP1 assay, would make it possible to establish what effects are most important first, so that they can then be further examined by microscopy.

### **Leptin affects Rho-family proteins and further regulatory pathways**

With these differences observed in imaging, the question arose how the binding of leptin to LepR results in a change in actin dynamics. The signaling events immediately following leptin binding its receptor have however been well explored in some aspects, but a literature search returned almost no data regarding how leptin can change cytoskeletal dynamics.

Some data exists for certain cellular system, but none of them are immune cells.[148-150] Following this, efforts to find relevant signaling events were focused on the pathways that control actin-modifying proteins. Among these, the Rho protein family takes a central role. Leptin exposure indeed reduced the amount of GTP – bound Rac1 and the strongest decrease coincides with the observation of changes in actin density at the 4 h time point. However, the amount of GTP-bound Rac1 was only slightly higher after 24 h – while no difference to control was observed in actin density. After 72 h it returns to baseline and no difference in actin density was evident at this time point. This suggests either a desensitization downstream of Rac1 or that activity of Rac1 is changed by leptin, but this has no bearing on the establishment of clearances for lytic granules.

Unfortunately, a pulldown assay of very similar design to that of the one used for Rac1 was unable to detect any GTP-bound CDC42, even in samples where PMA was used for artificial induction. With GTP $\gamma$ S loading, CDC42 loaded with it was detected and proteomics data confirmed that CDC42 is expressed in NK-92 cells (data not shown). The pulldown assay and detection were working, but no GTP-bound CDC42 was present. This suggests that the GEFs for CDC42 might be defective in NK-92 cells. While this is plausible in a lymphoma line, no direct evidence if this is the case is available.

The isoforms ROCK1 and ROCK2 are major downstream effectors of RhoA, with both commonly reported to only be enzymatically active if bound to GTP-bound RhoA, see introduction of [118]. Their enzymatic activity can thus be used to gauge how much GTP-bound RhoA is present. The finding that leptin exposure leaves this unchanged is paradoxical at first glance, as both it and Rac1 are part of Rho-related signaling. Both indeed share upstream effectors that are set in motion in response to an external stimulus, but no direct cross-talk has been shown so far. The assay cannot distinguish between ROCK1 and ROCK2 activity, but their activity is regulated the same way, rendering this scenario unlikely. The wide 95 % confidence interval, equal to an error of 0,5-fold of baseline activity is the primary concern when considering this data. It stems from an overall low ROCK1 activity in all samples determined. This could have resulted from the fact that lysates were obtained from resting cells, where no cytoskeletal remodelling is happening. In this context, it must be noted that convincing direct evidence exists that contradicts the common notion that ROCK activity is dependent on RhoA-GTP binding. The authors instead suggest that its activity is independent of the latter or phosphorylation. Instead, the enzyme might be constitutively in its active confirmation but can only perform its catalytic function if the substrate is brought into proximity. This would suggest that ROCK activity is regulated by spatial positioning in relation to its substrate [118] and dissecting if its spatiotemporal organization changes in response to hormonal stimuli is necessary to determine their effect.

With indications of changes to the Rho pathway and previous knowledge about the pleiotropic effects of leptin, an unparametrized, bottom-up proteomics approach was chosen to obtain an overview of the effects of leptin on NK-92 cells. The experimental design was chosen to be similar to the samples used in microscopy – with lysates obtained from cells exposed to leptin for the same durations. The nature of the results is also similar, as they provide mainly a snapshot of the proteome.

As expected, most observed changes are related to cellular metabolism, which is in accordance with leptin's role in relaying energy availability. This necessitated the definition of a set of Gene Ontology-terms to filter for hits that can more directly explain the changes observed during microscopy, as metabolic changes are not the subject of the present study. The alteration of their metabolism nevertheless changes their cytotoxic response. Primary NK cells from obese individuals accumulate lipids in a PPAR -dependent manner. These impair the trafficking required for exocytosis and as a consequence their cytotoxic response is blunted.[44] If such grave metabolic consequences can also be induced by hyperleptinemia alone is not known.

The phosphorylation of STAT5 and parts of the MAPK/Erk pathway can serve as validation that the hormonal stimulation was working as intended, as both have been reported previously for NK-cells.[46, 125] For the former, it must be noted that the presence of IL-2 in the medium is needed to cultivate NK-92 cells and it also induces STAT5 phosphorylation, creating a background.[151]

This experiment revealed further alterations of Rho- family proteins. Regarding Rac1 and CDC42, both the GEF ARHGEF6 and the two GAPs SH3BP1 and SH3GL1 were differentially phosphorylated. All three of these contain SH-domains, allowing them to localize to the immune synapse during degranulation. IQSEC1, an ARF6-GEF, is also phosphorylated in response to leptin, but the consequences of that phosphorylation are unknown. The role of ARF6 for the innate immune system has been investigated before: While it has a documented influence on actin polymerization and branching via its influence on Rho-family GTPases and also impacts phosphatidylinositol-signaling, it is doubtful whether this is of relevance for the present question: Most of its functions relate to endocytosis and signaling via Toll-like receptors and both of these cellular functions are not relevant here.[152] Similarly to the three proteins mentioned previously, more data is required to determine if this event is of functional consequence. Downregulation using siRNA interference or small molecule inhibitors with concomitant live-cell imaging of actin dynamics could clarify its influence on the cytoskeleton, while degranulation assays could investigate whether functional differences result from this inhibition.

Since ligand binding of NKp30 is relayed into the cell via phosphoinositide signaling it is of interest that the abundance of PI4KB is increased more than fivefold for all observed time points. While this increases the amount of total PI4KB present, it does not necessarily increase the amount of its enzymatically active form, as activation requires phosphorylation by protein kinase D [153] and no differential phosphorylation was observed in the corresponding peptide. This does not preclude the possibility that the increase in abundance means more PI4KB can be rendered active during ligand binding and degranulation.

With exocytosis crucially dependent on establishment of clearances and its five-fold increase in relative phosphorylation for the 4 h time point only, TNIK is a curious hit. Whether it has any meaning depends on two things that cannot be deduced from the available data. For future experiments it would first be valuable to determine if its phosphorylation results in phosphorylation and activation of gelsolin. Second, it would be interesting if this change in gelsolin activity has an effect on NK cells that is similar to the effects observed when it is overexpressed in Jurkat T-cells.[132]

### **Alterations in the exocytosis machinery**

Apart from signaling, leptin exposure also affected several proteins that directly modify the actin skeleton. For ARPC1B, a difference in phosphorylation was found for the 4 h time point only. That this is of functional consequence appears unlikely though: The Arp2/3 complex is made up of several proteins that change the activity of the complex upon phosphorylation. The detected phosphorylation of ADD1 is not associated with a change in protein activity, and no difference was observed in the proteins where phosphorylation has a known consequence.

The observation that PLS1 is less abundant for all time points is somewhat paradoxical. It also cross-links f-actin strands, but in a 90° orientation as opposed to the 70° of the Arp2/3 complex.[154] Recent reports indicate that it facilitates exocytosis and that its knockdown negatively impacts degranulation. The impact of this could be determined by exposing PLS1-overexpressing cells to leptin, so that the expression level in sum approaches “wild type” levels and performing LAMP1 assays with this setup.[122]

The differential regulation of LSP1 is of similar interest, but whether this is consequential cannot be determined by using coated glass coverslips, as the glass cannot be moved by any contractile force the cell could exert. With knowledge that its knockdown impairs

cytotoxicity[121], LAMP1 assays using a high-expressing variant could determine whether its upregulation increases the capacity to degranulate. Traction force microscopy or atomic force microscopy using leptin-exposed cells and knockdowns as further comparisons could show whether the generated force is affected by this.[139]

In contrast, a multitude of changes were observed regarding the coordination of exocytosis. Both RAB15 and RAB1F are differentially abundant after leptin exposure and both facilitate exocytosis in other cell lines. It has to be kept in mind however, that increase in total protein abundance does not equal change in activity of properly localized protein. In the same vein, lytic granule exocytosis shares many components with other exocytosis functions, but they are not wholly similar. To the finding that SEC22B is differentially phosphorylated, the same caveats apply with one more addition: Currently no known change is associated with phosphorylation at the site observed.

The sixfold increase in phosphorylation of NBEAL2 appears to be more interesting, as its deficiency is known to lead to defects in degranulation of NK cells and neutrophils in mice, as mentioned earlier.[135] It would thus be interesting if its overexpression facilitates degranulation. This would be possible with by an adoption of the imaging methodology used. A cell with artificially induced phosphorylation of NBEAL2 additionally transfected with an mCherry-LAMP1-pHluorin [155] could be induced to degranulate on a glass surface while being observed with TIRF-SIM microscopy. Comparison of the degranulation frequency to cells expressing normal levels of NBEAL2 would provide an answer. The same experiment but with artificially induced phosphorylation of SEPTIN2 could show whether it has crucial role in NK cells similar to that observed of SEPTIN7 in dendritic cells.[131]

With a strong indication that leptin has an effect on Rho-family proteins, the question arises how impactful this is in relation to exocytosis as a process. One way to investigate this would be to modulate activity of Rac1 with an inhibitor [117] and measure either the activity of downstream effectors or degranulation through LAMP1. This would have the shortcoming of implicitly assuming, that the activity of proteins coordinating the actin cytoskeleton are synchronized and homogenous throughout the cell, which is not the case. Work concerning cell migration with photoactivatable effectors of Rac1 and CDC42 has shown that zones of their activity are shaped by the localization of GEFs or GAPs and coordinated over time by them.[156] A similarly complex spatio-temporal coordination of WASp has been shown to be needed to facilitate migration.[157] The f-actin meshwork at the IS with the need to make clearances is not the same as a treadmilling f-actin meshwork during migration, but likely both must be tightly coordinated. In combination with an mCherry-LAMP1-pHluorin construct, this would allow the observation whether the patterns of Rac1 activation change in response to either GEF activation or leptin and if this affects degranulation.

Understanding when and through which mechanisms an NK cells commits to degranulation is paramount to understand how they perform immunosurveillance. The decision-making process occurring at the immune synapse is an intricate, multifactorial process and the use of minimal models allows the reduction of complexity to study individual components. Using super-resolved imaging techniques allows studying the spatial organization of the actin meshwork and membrane receptors. In this case, their application to study the influence of leptin revealed that it appears to alter the shape of the actin meshwork during degranulation. It also allowed the observation that lytic granules preferentially localize to

clusters of the NKp30 receptor, and that this tendency is reduced if actin polymerization or branching is inhibited.

While these imaging techniques are considerable improvements compared to diffraction-limited techniques, they must nevertheless be complimented by other methods for use in cell biological or biochemical questions. The present study underlines that it is crucial to validate that the chosen model system is suitable for the biological question.

Understanding the effects of a hormone on the cell as a whole is greatly aided by techniques such as proteomics. This allows a non-parametrized approach considering all possibly relevant differential regulation and phosphorylation. Here, this showed an influence of leptin on parts of the exocytosis machinery and a differential phosphorylation of actin-regulating proteins. In the case of Rho-family proteins, this was partially validated with pull-down- and enzymatic immunoassays.

Greater knowledge of the involved components, their coordination in space over time and what affects both can possibly allow us to alleviate conditions where they are less vigilant. It could also afford the opportunity to tailor them to activate under well-defined conditions for use in cellular immunotherapy.



# Methods

## Cell culture

The human NK-92 cell line was obtained from the Deutsche Sammlung von Mikroorganismen und Zellkulturen (DSMZ). NK-92 is designated under “ACC488” by the DSMZ and “CRL-2407” by the ATCC.

KHYG-1 cells were also obtained from the DSMZ (ACC725). NK-L cells (CVCL\_0466) and K562 (ACC10, CCL243) cells were a gracious gift from Professor Roland Jacobs, MHH Hannover. All cell lines were cultured in RPMI 1640 (10-040-CV, Corning) supplemented with 10 % fetal calf serum (S0615, Sigma-Aldrich) 100 U/ml Penicillin and 100 mg/ml Streptomycin (both P0781, Sigma-Aldrich) and 1 mM sodium pyruvate (11360070, Thermo Fisher). Human recombinant interleukin-2 (2238131, Novartis) was kept aliquoted and frozen, being added to each cell culture flask containing a natural killer cell line to a final concentration of 160 U/ml. Cells were kept in cell culture at 37° C with 5 % CO<sub>2</sub> and atmospheric oxygen.

## Leptin stimulation

In order to prepare NK-92 cells stimulated for various times simultaneously for sample preparation, NK-92 cells were seeded in one cell culture flask per time point. Recombinant human leptin expressed as a truncated protein in *E. coli* (Val22-Cys167; 398-LP-, R&D Systems) was reconstituted in 20 mM Tris-HCl pH 8.0, at 1 mg/l aliquoted and frozen to prevent freeze-thaw cycles. Working solutions of 10 µg/ml were diluted for each experiment in the same buffer. Leptin was added immediately after seeding cells for the 72 h time points. After 48 h, medium was replenished for all cells, with Leptin added to medium of cells for 72 h and 24 h time points. 4 h before degranulation, Leptin was added for the 4 h time point and cells for all conditions were resuspended by pipetting. Buffer containing no leptin was used for mock treatment where applicable.

## Bicinchoninic acid assay

To determine protein concentration of lysates, the Pierce BCA Protein Assay Kit (23227, Thermo Fisher) was used according to the manufacturer’s instruction. Absorbance of the Cu<sup>1+</sup>/di-BCA chelator-metal complex at 562 nm was read on a Synergy M plate reader (BioTek).

## Western Blotting

Whole cell protein lysates were obtained by lysing 2 \*10<sup>7</sup> cells in 200 µl of MPER buffer (78503, Thermo Fisher) with added protease and phosphatase inhibitors (04906837001, Roche). BCA assay as outlined above was used to determine protein concentration.

SDS-PAGE was run in an electrophoresis chamber (EI0001, Thermo Fisher) using a 4 % to 20 % Tris-Glycin gel (XP04200BOX, Thermo Fisher) and a 10 to 180 kDa protein size marker (26616, Thermo Fisher). 20 µg of total protein were loaded per sample. Proteins were then transferred to a 0,2 µm nitrocellulose membrane (10600080, Amersham), which was then blocked in TBS-T with 5 % milk powder (145.2, Roth). Incubation with the primary antibody anti-LepR clone JA73-01 (MA5-32685, Invitrogen) diluted 1:500 was done in the same solution over night at 4° C. The blot was washed 3x 15 min in TBS-T, washed again for 5 min in TBS and subsequently incubated in TBS-T with 5% milk powder with the secondary HRP-conjugated goat anti-rabbit IgG (7404, Cell Signaling) diluted 1:5000. After washing as before, presence of HRP was detected using chemiluminescent reagent (RPN2232, Amersham) on a ChemiDoc Touch Imaging System (BioTek).

### **Granzyme B assay**

NK-92, NKL and KHYG1- were cultured as described above and resuspended prior to the assay at 250.000 cells/ml in a medium similar to that described above, but without phenol red (17-105-CV, Corning). The assay must be performed in a flow hood under sterile conditions to minimize ingress of contaminants that NK-cells could detect as pathogen-associated molecular patterns. The bottom of 96-well plates were coated with a solution of both anti- integrin  $\beta$ -2 (MA1810, Thermo Fisher) and anti-NKp30 (130-094-272, Miltenyi Biotec) at a final concentration of 5  $\mu$ g/ml in PBS with 1 % (w/v) bovine serum albumin A7906, Sigma-Aldrich) over night at in a cell culture incubator. Control wells for determination of autolysis were incubated with buffer alone. Wells were then washed 3x 5 min with 100  $\mu$ l PBS and 200  $\mu$ l of the cell suspension described above was added. Care must be taken not to let the wells dry out during washing and the addition step. After incubation for 2 h, the plate is agitated on a plate shaker (400 rpm, 3 min) and resuspended by pipetting up and down each well 3x. Cells are then centrifuged down (300g, 5 min, RT) and 100  $\mu$ l of the supernatant is transferred to a new 96 well plate. 100  $\mu$ l of substrate solution composed of 0.1 mM Tris pH 8.1 with 0.4 mM N- $\alpha$ -benzyloxycarbonyl-L-lysine thiobenzyl ester substrate (200274, Sigma-Aldrich) and 0.4 mM 5,5'-Dithio-bis-(2-nitrobenzoic acid) (D8130, Sigma Aldrich) was then added to the supernatant. Absorbance at 410 nm was read after 3 h of incubation at RT.

### **Measurement of integrin $\beta$ -2 and NKp30 surface expression**

NK-92 cells were harvested from cell culture and dispersed into a single cell suspension. Fc receptor blocking (130-059-901, Miltenyi Biotec) was performed and cells were subsequently stained using anti- integrin  $\beta$ -2-FITC and anti-NKp30-PE antibodies (130-120-248 and 130-112-430, both Miltenyi Biotec). Doublets were excluded using side-scatter height to forward-scatter area, while live/dead exclusion was performed with propidium iodide staining (P1304MP, Invitrogen). Gating strategy is shown in **Fig. 3 (a)**. Stained cells were analysed on a MACSQuant10 Flow Cytometer (Miltenyi Biotec).

### **LAMP1 degranulation assay**

PBS containing anti-integrin  $\beta$ -2-antibody (MA1810, Thermo Fisher) and anti-NKp30 (130-094-272, Miltenyi-Biotec) at final concentrations of 3  $\mu$ g/ml were added to a 96-well plate. This coating solution was allowed to incubate in a cell culture incubator overnight. The solution was then removed and the wells washed with 3x PBS 1 % BSA. Leptin stimulation of NK-92 cells was performed as described above. Cells were then added to all wells. K562 cells and medium containing PMA (524400, Merck) were added to appropriate wells. Immediately after, anti- LAMP1-FITC antibody (130-111-620, Miltenyi Biotec) was added to all wells. After incubation for 1 h, monensin (554724, Becton Dickinson) was added and incubation allowed to proceed for another 3 h. Cells were then resuspended by pipetting and transferred to FACS tubes on ice. FACS-Buffer with 10 mM EDTA (PBS; pH 7.2; 10 mM EDTA; 1 % FCS and 0.05 % (w/v) sodium azide) was then added to all wells with antibody-coating. After incubating for 15 min, cells stuck to the well-bottom were dislodged by repeated pipetting and also transferred to FACS-tubes. Cells were then stained with propidium iodide and anti NCAM-1-APC antibody (Miltenyi Biotec, 130-113-310). Each condition was assayed in duplicate. Gating strategy can be seen in **Fig. 3 (a)** and was analysed as described above, but on a MACSQuant16 Flow Cytometer (Miltenyi Biotec).

## **Figure 5: Imaging of Actin density at sites of exocytosis**

### *Preparation of samples for microscopy*

Glass coverslips were pre-cleaned in 70% EtOH with distilled water and washed 3x with PBS. Coating solution was composed of PBS containing anti-integrin  $\beta$ -2-antibody (MA1810, Thermo Fisher) and anti-NKp30 (130-094-272, Miltenyi Biotec) at final concentrations of 3  $\mu$ g/ml. Coating was performed by spotting antibody solution on parafilm in petri dishes, placing coverslips on top of them and incubation proceeded overnight. Similarly, leptin-stimulated NK-92 cells (see above) were harvested from cell culture and their nucleus was stained using Hoechst 3342 stain (R37605, Thermo Fisher). Cells suspension was added to coverslip in 6 well plate and incubated for 15 min. Culture medium was carefully removed and cells were washed once with PBS. Cells were then fixed in PBS containing 4 % *para*-Formaldehyde (158127, Merck Millipore) for 20 min and subsequently permeabilized in 0.1 % Triton-X100 (648463, Merck Millipore) in PBS for 5 min. Blocking was then performed in PBS 2 % BSA (w/v) and 5 % FCS (w/v) for 1 h. Coverslips were incubated with the primary anti-perforin antibody (308102, BioLegend) over night at 4° C. Secondary antibody staining using polyclonal anti-mouse STAR600-conjugated antibody (ST600-1001-500UG, Abberior) was performed in tandem with phalloidin-STAR635-conjugate (ST635-0100-20UG, Abberior) for 1 h. Embedding was then performed using Mowiol containing 1,4-Diazabicyclo[2.2.2]octan (81381 and D27802, both from Merck Millipore). Washing for every step after fixation was done 3x using PBS 1% BSA (w/v).

### *STED microscopy*

Time – gated STED microscopy was performed on a Leica TCS SP8 3X STED using a HCX PL APO 100x 1,40 NA oil immersion objective. Excitation was performed using a pulsed white laser; STAR 600 (lytic granules) was excited at 561 nm and STAR635 (f-actin) was excited at 633 nm, while depletion for both dyes was performed using the 775 nm STED Laser. Hoechst stain (nucleus) was excited using 405 nm diode. Detection for STAR600 and STAR635 was done using a time-gated HyD SMD detector, while Hoechst stain was detected using the PMT detector built into the SP8. Three line-averages were acquired at a pixel size of 20 nm. Images were recorded using the LAS X Software.

### *Image analysis*

Image analysis was performed using a custom script for Fiji [158] written by Ulrike Schulze. Briefly, both STED-channels were aligned according to the nucleus using the “Correct 3D-Drift” – Plugin. Subsequently, maxima in the perforin-channel were detected and within a circle of 200 nm diameter around the maximum, the mean intensity in the actin channel was measured and recorded. For each cell, the average of all regions was calculated. These averages were then treated as single data points and the pooled data from three independent biological replicates was plotted for each condition. To determine if a statistical difference is observable between conditions, the Mann-Whitney-U test was used.

### *Contributions*

This experiment was performed in cooperation with Katharina Reglinksi, Silvia Galiani, both members of the Christian Eggeling group, and Ulrike Schulze at the Weatherall Institute for Molecular Medicine in Oxford.

M.B. designed the experiment, optimized experimental and staining parameters, and prepared all samples. K. R. gave guidance regarding choice and optimization procedure for staining. The microscope is part of the Wolfson Imaging facility. S.G. from the facility assisted in choice of microscope setup and optimization of imaging. Imaging was

performed by M.B. U.S. assisted in choice of analysis method and wrote an ImageJ script for analysis. Image analysis was performed by M.B.

### Figure 6: Imaging for colocalization and clustering analysis

#### Preparation of samples for microscopy

Glass coverslips were coated with antibodies against NKp30 and integrin  $\beta$ -2 as described above, but with different antibodies to allow staining of NKp30 receptor. For ligating integrin  $\beta$ -2, the hu1124 clone (also known as Efalizumab, NBP2-52686-0.2mg, Novus Biologicals) and for NKp30 the REA823 clone (130-112-430, Miltenyi Biotec) were used. NK-92 cells were harvested from cell culture, resuspended at 500.000 cells/ml, and placed in 6-well plates. The hormones or small molecule inhibitors in **Table 8** were added to the indicated final concentrations.

**Table 8** Inhibitors and recombinant cytokines

Final concentration	Name	Compound Source
100 $\mu$ M	CK666	182515, Merck
100 nM	Latrunculin B	428020, Merck
1.35 ng/ml	IFN- $\gamma$	RIFNG100, Thermo Fisher
100 ng/ml	Leptin	398-LP, R&D Systems

All inhibitors were solved in DMSO, while IFN-  $\gamma$  and Leptin were solved in 50 mM Tris-HCl. Equivalent amounts of DMSO and Tris-HCl were added to control and hormone-treated samples respectively. LysoTracker-DND99 was added immediately after to a final concentration of 10  $\mu$ M. After mixing by gentle pipetting, incubation proceeded for 60 min in an incubator. Briefly, the concentrations of small molecule inhibitors were determined by titration: Starting from a higher concentration with the same experimental procedure, inhibitor concentration was reduced stepwise until NK-92 cells were still capable of establishing an immune synapse after 1 h of treatment. Leptin concentration was chosen to be in line with other experiments, and IFN-  $\gamma$  concentration was chosen to be representative of an extreme *in vivo* state.

After incubation, cells were resuspended in growth media containing the abovementioned compounds but not LysoTracker DND-99 at 250.000 cells/ml. Coated coverslips were then washed, and cells pipetted on top of them. Degranulation was allowed to proceed for 15 min, cells were then washed once with PBS and fixed in 4 % (v/v) *para*-Formaldehyde solution for 20 min. Subsequent permeabilization was done with 0,1 % Triton-X100 (648463, Merck Millipore) in PBS for 5 min. Blocking was performed in PBS 2 % BSA (w/v) and 5 % FCS (w/v) for 1 h. NKp30 was then stained with anti-NKp30 (325202, Biolegend) at 1:250 dilution. Secondary immunostaining was done with STAR RED goat-anti mouse (STRED-1001-500UG, Abberior) diluted 1:200. This staining was done in parallel with Alexa488-Phalloidin at 5 U/ml (A12379, Thermo Fisher). Incubations time was 1 h at room temperature using the sitting drop method. Both were preceded and followed by washing 3x with PBS 1 % BSA. Samples were then embedded in Mowiol as described above.

#### Imaging

Imaging was performed on a STEDYCON system (Abberior) installed on the IX83 platform using a UplanXApo 100x 1,45 NA oil immersion objective (Olympus). Alexa488 was excited at 488 nm (f-actin) and DND-99 (lytic granules) was excited at 561 nm. STAR RED (NKp30) was excited at 640 nm and depleted using the 775 nm STED laser. Before and during each imaging session, TetraSpek beads were used to determine whether alignment of beampath and laser output power remained constant across all images taken.

All three channels were acquired in parallel and detected using the single photon counting avalanche photodiodes (APDs) built into the STEDYCON. Two line-averages were recorded at a pixel size of 20 nm. Images were recorded using the Abberior Inspector Software.

### *Image Analysis*

For data analysis, a previously published method was adapted.[113] The position of lytic granules was determined by finding maxima in the lytic granule channel through thresholding. ROIs of 200 nm diameter were placed on the center of these maxima ('valid'). The intensity of the NKp30 signal was then summed ('random'). For comparison, a set of 20 random ROIs were then placed within the outlines of the cell, so that each random ROI is at least 400 nm away from existing ROIs placed over lytic granules. The intensity of the NKp30 signal in them was equally summed. With the sum resulting from each ROI being treated as a single data point, the sums of 'valid' were then plotted against those of 'random' points. Each plot in **Fig. 6 (e)** shows the pooled data from three independent biological replicates for each condition. To determine whether a statistically significant difference was observable, the Mann-Whitney-U test was used. In order to ascertain whether the chosen parameters influenced the outcome of the analysis, the threshold value for lytic granules, the size of ROIs, their number and minimal distance of 'random' ROIs to 'valid' ROIs was varied. The Kruskal-Wallis test was used to perform the multiple comparison needed to determine, if varying these parameters resulted in statistically significant differences.

### *Contributions*

This experiment was performed in cooperation with Katharina Reglinski, Francesco Reina and Felix Hildebrandt, members of the Christian Eggeling group at the Institut für angewandte Optik und Biophysik and the Leibniz Institut für photonische Technologien, both in Jena. M.B. designed the experiment, optimized experimental parameters such as inhibitor/cytokine concentration and staining and prepared all samples. All worked together in choice of imaging setup and imaging parameters. Imaging was performed by F.H. Image analysis was done by and F.H. and M.B.

### **Rac1/CDC42 Assay**

NK-92 cells were exposed, as described above, to either 100 ng/ml leptin for 4 h, 24 and 72 h or 100 ng/ml PMA (524400, Merck) for 1 h. The Rac1/CDC42 activation assay kit (17-441, Merck Millipore) was used according to the manufacturer's instruction for this pull-down assay: The protocol for non-adherent cells was used to obtain lysates, with  $2 \times 10^7$  cells lysed in 200  $\mu$ l of MPER buffer (78503, Thermo Fisher) with added protease inhibitors (04693159001, Sigma-Aldrich). No shearing of genomic DNA was needed, but pre-clearing of lysates with glutathione agarose was performed. Protein concentration was determined by BCA assay as outlined earlier to load equal amounts of whole cell protein in the pull-down. Loading with GDP/ GTP $\gamma$ S, pull-down assay and western blotting were performed as indicated in the manual. Note, this deviates significantly from the western blotting protocol described for leptin earlier. For blotting, a PVDF membrane (10600122, Amersham) was used. Detection via chemoluminescence was done as described earlier.

### **Rho/ROCK – Kinase assay**

$2 \times 10^7$  of NK-92 cells exposed to 100 ng/ml leptin for 4 h, 24 h and 72 h, were harvested from cell culture, washed, pelleted, and lysed in 200  $\mu$ l of MPER Buffer (78503, Thermo Fisher) containing protease inhibitors (04693159001, Sigma-Aldrich). Total protein

concentration was determined via BCA-Assay to use equal amounts of protein per condition in the immunoassay.

Activity of Rho/ROCK Enzyme in the resulting cell lysate was analyzed using the Rho-associated Kinase (ROCK) Activity Assay Kit (CSA0001, Merck Millipore) according to manufacturer's instructions: Using 180 µg of whole protein at 100 µM final concentration of ATP were determined to be ideal parameters by kinase titration with protein lysates and subsequent titration of ATP concentration.

## **Proteomics:**

### *Sample Preparation*

Cultivation of NK-92 cells and leptin stimulation was performed as described above. To obtain lysates of resting cells, these were harvested from cell culture and washed 3x in ice-cold PBS and then lysed in 60 µl of MPER buffer per  $1 \times 10^6$  cells (78503, Thermo Fisher), with protease (04693159001, Sigma-Aldrich) and phosphatase inhibitor (04906837001, Roche) added to the lysis buffer beforehand. After incubation at 25° C for 10 min under mild incubation and centrifuging with 14.000 g for 15 min at 4° C, supernatant was removed and stored at -80° C.

100 µg of protein from each sample was measured using the BCA Protein Assay Kit (as mentioned above). The protein was precipitated overnight with 6x ice-cold acetone and resuspended in 50 mM ammonium bicarbonate and 0.1 % (w/v) RapiGest SF (186002122, Waters). Proteins were then reduced with 10 mM DTT at 80° C for 15 min before being alkylated with 20 mM chloroacetamide for 30 min at room temperature in the dark. LysC/Trypsin was added at a ratio of 1:50 enzyme:substrate and incubated overnight at 37° C. 10 µg of peptides were aliquoted for full proteome analysis. The remaining peptide digests were then completely lyophilized and phosphopeptide enrichment was performed using High-Select TiO<sub>2</sub> Phosphopeptide Enrichment Kit in accordance with manufacturer's specifications (A32993, Thermo Scientific). All peptides were then desalted using C18 spin columns (Pierce C18 Spin Tips, 84850, Thermo Scientific) as recommended by the manufacturer.

### *LC-MS*

Approximately 200 ng of peptides for each sample and replicate were initially trapped (PepMap100 5 µm, 3 x 5 mm, 160454, Thermo Scientific) and separated on a Waters M-Class C18 25 cm analytical column (18600, Acquity UPLC M-Class HSS T3 1.8 µm 75 µm x 250 mm, Waters) over 180 min with an increasing gradient of acetonitrile (125 min between 3-20 %; 25 min between 20-30 %; 2 min between 30-80 %; 5 min at 80 %, and the remaining at 3 %) at 240 nl/min before being injected into a Thermo Scientific Orbitrap Exploris 480 mass spectrometer. Peptides were ionised in positive mode with 2000 V and a transfer capillary temperature of 320° C. Samples were subjected to further separation with FAIMS Pro with 2 compensation voltages (CVs: -45, -60) resulting in 2 separate MS experiments within one data file. Each experiment had the following settings: MS resolution of 120 000 @ 200 m/z, a scan range of 350-1200 m/z, MS AGC target of 300 % for max IT of 50 ms; MS/MS of all the most intense peaks for a total cycle time of 2.5 seconds each with the following settings: Isolation window of 2 m/z normalised collision energy of 30 %, resolution of 15 000 with an AGC target of 100 % and a max. 50 ms IT. Every fragmented precursor within +/- 10 ppm was immediately excluded from reanalysis for 45 seconds.

### *Data Analysis*

Raw data files were analysed within Proteome Discoverer 2.4.0.305 following a LFQ quantification workflow. Searches were performed against the *homo sapiens* database with

decoys using Sequest HT with a precursor tolerance of 10 ppm and a fragment mass tolerance of 0.02 Da, trypsin as a cleavage agent with 2 missed cleavages considered. Carbamidomethylation of Cysteines was set as a static modification, and the following dynamic modifications were investigated: Oxidation (M), Acetylation (K) and Phosphorylation (S, Y, T). IDs were filtered with Percolator at a strict FDR of 0.01. Precursor ion quantification was performed with unique and razor peptides with Top N of 3. Precursor abundance was based upon intensity and normalised over total peptide amount. Regarding the entire method, see also [159]. Proteins or phosphopeptides with a fold-change in abundance of at least 2 and a  $p$ -value  $< 0.0005$  were considered to be significant and of interest. For a phosphopeptide to be considered, the protein it is derived from must also be detected with sufficient confidence.

### *Contributions*

This experiment was performed in cooperation with Matthew Fuszard and the Core Facility Proteomics at the Proteinzentrum Charles Tanford in Halle. M.B. designed the experiment, optimized parameters and made biological samples. Preparation of whole cell lysate from them and BCA-assay was also performed by M.B. All subsequent experimental work, including digest, phosphopeptide enrichment, chromatographic separation and MS/MS was done by M.F. and the core facility. For data analysis, M.F. performed identification and annotation of peptides and proteins and calculated relative abundances and abundance-adjusted  $p$ -values. M.B. performed functional analysis of the resulting dataset, including GO-term enrichment and heat mapping of differentially abundant proteins/phosphopeptides with relevant functions.

### **Statistical analysis, data plotting and figure preparation**

Statistical analysis was performed using Microsoft Excel and GraphPad. All Graphing was performed using GraphPad unless otherwise indicated. FlowJo software (Becton, Dickinson & Company) was used to analyze flow cytometry data and generate associated plots. In all Box-Whisker Plot, the bar represents the median, while the boxes denote quartile ranges, whiskers stretch from minimum to maximum values unless otherwise noted.

Epitope	Species	Clonality	Clone	Conjugate	Source
Integrin $\beta$ -2	Mouse	Monoclonal	TS1/18	-	Thermo Fisher MA1810
Integrin $\beta$ -2	Mouse	Monoclonal	TS1/18	FITC	Miltenyi Biotec 130-120-248
Integrin $\beta$ -2	Rabbit	Monoclonal	hu1124	-	Novus Biologicals NBP2-52686-0.2mg
LAMP1	Mouse	Monoclonal	REA792	FITC	Miltenyi Biotec 130-111-620
LepR	Rabbit	Monoclonal	JA73-01	-	Invitrogen MA5-32685
Mouse IgG	Goat	Polyclonal	-	STAR600	Aberrior ST600-1001-500UG
Mouse IgG	Goat	Polyclonal	-	STAR RED	Aberrior STRED-1001-500UG
Mouse IgG	Goat	Polyclonal	-	Alexa647	Thermo Fisher A-21235
NCAM1	Human recombinant	Monoclonal	REA196	APC	Miltenyi Biotec 130-113-310
NKp30	Mouse	Monoclonal	P30-15	-	Biolegend 325202
NKp30	Human recombinant	Monoclonal	REA823	Biotin	Miltenyi Biotec 130-112-428
Perforin	Mouse	Monoclonal	dG9	-	BioLegend 308102
Rabbit IgG	Goat	Polyclonal	-	HRP	Cell Signaling 7404

**Table 9** Antibodies



# Challenges of using expansion microscopy for super-resolved imaging of cellular organelles

## Introduction

Expansion microscopy (ExM) was shown to be a good tool to increase the resolution when imaging biological samples by embedding them into a swellable acrylamide gel.[160, 161] The sample is fixed, permeabilized and crosslinked to the gel, which, when incubated in water, expands isotropically. ExM has also been successfully combined with super-resolution techniques such as single-molecule switching based technique (STORM).[162] and stimulated emission depletion (STED) microscopy. The latter combination of which has been employed to study microtubules [163-165], cilia and centrioles.[166] The combination of ExM with these techniques provides a promising tool to disclose details beyond the resolution limit of a super-resolution microscope. **Fig. 12** shows an overview of the experimental procedure.

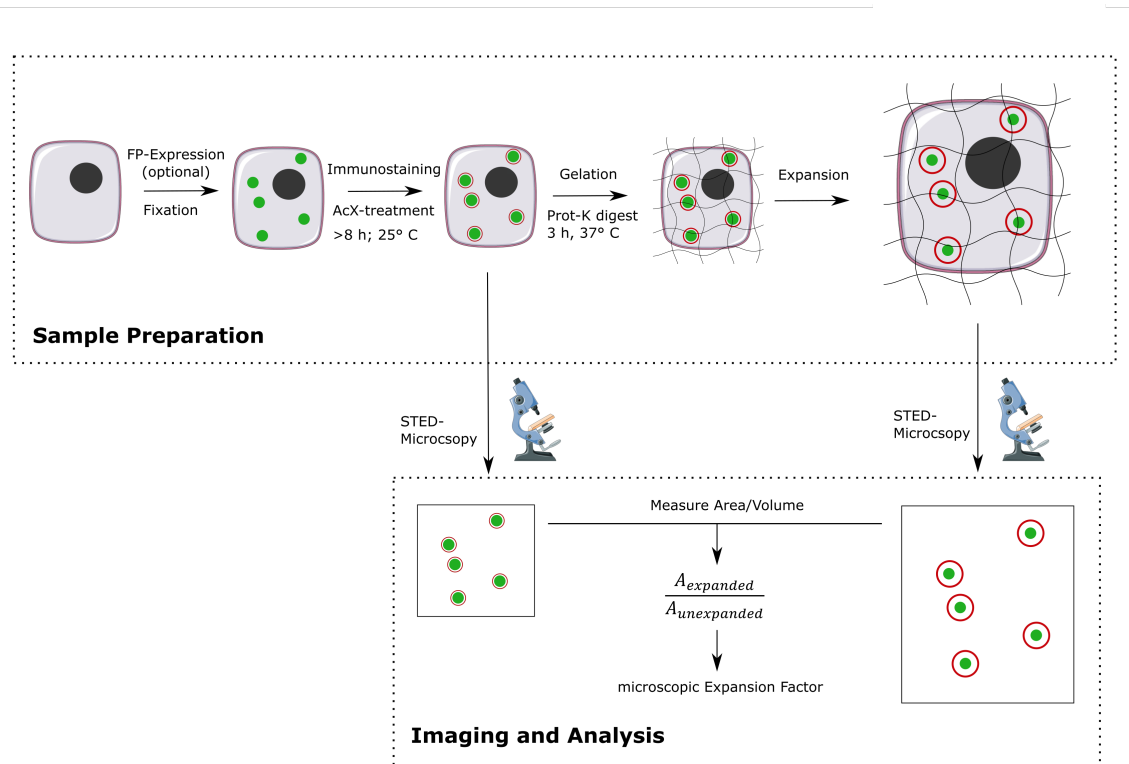


**Figure 12** Expansion microscopy of intracellular organelles. HEK293 cells were grown on glass coverslips and transfected to achieve fluorescent protein (FP)-expression (optional). Cells were then fixed, immunostained, treated with the crosslinking reagent AcX and embedded into the gel. Subsequently, the sample was treated with proteinase K, which digests all cellular proteins to peptides, that are co-polymerized into the gel. This allows them to expand together with the gel when incubated in water. The expanded cells were imaged by conventional confocal or STED microscopy. Unexpanded controls were imaged after immunostaining. The area or volume of the structure of interest was then measured and used to calculate the expansion factor.

## **The peroxisomal import machinery**

The protein import machinery of peroxisomes is one process for which an increase in resolution could aid in the understanding the particulars of its function. Peroxisomes fulfill a broad range of cellular functions, such as  $\beta$ -oxidation, removal of reactive oxygen species and synthesis of lipids.[167] Consequently their dysfunction can be deleterious.[168, 169] All the proteins required to perform these functions must be imported into the peroxisome. As opposed to mitochondria, where proteins are imported as reduced and unfolded precursors[170], peroxisomal proteins can be imported from the cytosol after translation in a folded or even oligomerized state.[171] The import of these rather large protein complexes is facilitated by the PEX14/PEX5 system. The majority of proteins to be imported into the peroxisomal matrix is C-terminally flagged by the peroxisomal targeting signal 1 (PTS1) [168] which is bound by PEX5. The resulting complex then moves through the cytosol to the peroxisomal membrane, where it interacts with PEX14. Together, PEX5 and PEX14 form a transient pore that allows passage of the cargo protein.[172, 173] Ubiquitylation of PEX5 is then followed by its ATP-dependent removal from the peroxisomal membrane.[174, 175]

Several details regarding the function of the mechanism and the organization of these proteins on the membrane are still unknown. Due to their size, localization of proteins in peroxisomes requires super-resolved microscopy. Previous work using STED microscopy identified subsets of peroxisomes with weak colocalization of PEX14 and PEX5 but strong compartmentalization of the imported sterol carrier protein 2 (SCP2). These were opposed to subsets with strong colocalization between the import proteins and a homogenous distribution of SCP2 in the peroxisomal matrix.[113]

A higher level of detail, than was obtainable with STED microscopy, would be helpful to understand the protein distribution and composition of peroxisomal membrane proteins better, which might help to link them to a physiological function. As the density of the epitopes, recognized by antibodies against our proteins of interest, on the peroxisomal membrane is very high, verifying their colocalization is challenging.

The initial aim was therefore to combine ExM with STED, by first expanding peroxisomes within a HEK293 cell to then image it with STED microscopy. This could theoretically result in an increase of the 60 nm STED resolution by the expansion factor of the gel, commonly around 4x, to 15 nm. This technique could then also be helpful for the study of colocalization in other organelles, where the crowded environment makes a separation of signals desirable.

## **Expansion microscopy can increase resolution**

To achieve this goal several problems needed to be addressed. First, the staining of the sample after expansion needed to be bright enough to perform two-colour STED imaging, as a linear expansion factor of 4 (which is in general obtained by ExM) [161] results in a 4<sup>2</sup>-fold increase in area and a 4<sup>3</sup>- fold increase in volume. During expansion, the fluorophores at the epitope thus move away from one another, increasing the dye-to-dye distance and lowering their density. While this is the motivation for performing expansion microscopy, it effectively results in a 1  $\mu\text{m}^3$  cube in the original sample being expanded to 64  $\mu\text{m}^3$  in the gel and the resulting “dilution” of fluorophores per imaged voxel can be challenging, especially for STED. Contrarily, the typically very low background of the gel can result in good signal-to-noise ratio when using sensitive detectors.[161]

Second, the isotropy of the expansion needed to be validated. In the literature, several approaches can be found to validate the isotropic expansion of the sample embedded in acrylamide gels. Often, a vector distortion field is used, which is working well in expanded

tissue slices.[161] Here, the sample is imaged before and after expansion and any distortions become apparent when the images are compared. However, this approach is not appropriate for the imaging of single cells, as exact same cells before and after expansion are difficult to find. Therefore, the aim was to explore the congruence of the expansion factor (EF) when analyzing groups of cells in the same sample before and after expansion. The different organelles of one cell are composed of vastly different proteins and other components that allow their functions. This difference in composition likely results in biochemical heterogeneity. In regard to this method, it could lead to different accessibility for the compounds used in this protocol to the proteins they are supposed to bind. Furthermore, different compositions can result in different mechanical properties during expansion. It was thus necessary to include controls to ensure that the entire cell expands isotropically.

Using confocal and STED microscopy, the size of the nucleus, mitochondria, entire cells, and the peroxisomal matrix and membrane were determined. Variations in the values of EF were observable, indicating that the expansion within a cell can vary, which therefore needs to be validated with carefully chosen controls.

## Results

This study aims to examine the application of expansion microscopy to address cell biological questions, potentially in combination with STED microscopy. The question at the outset was whether the technique could be employed to increase resolution when determining colocalization of PEX14 and PEX5 and the possible compartmentalization of PTS1-bearing SCP2 in peroxisomes.

To ensure that the imaging yielded reliable data, it was necessary to find a method to validate the EF that does not rely on measuring the expansion of the gel and does not require imaging the same cell in the unexpanded and expanded state. It should rather measure a large number of cells to obtain the EF by examining microscopic structures inside the sample. To ensure that the entire cell expands isotropically and reliable colocalization data can be obtained, it was thus necessary to establish the expansion factor of organelles and the cell as a whole. For all experiments, the EF of the macroscopic gel varied between 3.9 and 4.2 with a median of 4.1. This work was done in cooperation with members of the Weatherall Institute for Molecular Medicine. For a detailed list of contributions, see the methods section.

### Expansion of the nucleus

The cellular nucleus was first chosen as a control to measure the EF. The nuclear pore complex in fixed HEK293 cells was immunostained with a primary antibody against nucleoporin 153 (NUP153) and a dye-conjugated secondary antibody. Afterwards, the sample was gelled and expanded **Fig. 13**. Using confocal microscopy, the cells were optically sectioned, and the maximal extent of the nucleus determined and imaged. In these images, the extent of the nucleus was then manually traced, and its area recorded. See **Fig. 13**. By comparing the area from nuclei of expanded **Fig. 13 (a)** and unexpanded **Fig. 13 (b)** cells a microscopic EF was calculated, shown in **Fig. 13 (c)** and **(d)**. The linear expansion factor is calculated by taking the square root of the expansion in area or the third root of the expansion in volume. The volumes can be calculated from a series of images (z-stack) since the distance between the slices is known. **Fig. 13 (d)** shows significant standard deviations for the measured areas, both for expanded and unexpanded cells. The resulting deviation in the EF is therefore large, but the 95 % confidence interval is narrow, suggesting that the EF can be determined in this manner. The EF of the nucleus differs from that of the gel.

### Comparison of cell area and the mitochondrial network

Measuring the microscopic EF by using the volume of the whole cell and the volume of the mitochondrial network was attempted next.

To this end, the plasma membrane was labelled by expression of glycosylphosphatidylinositol (GPI)-anchored green fluorescent protein (GFP) [176] in HEK293 cells and an ATTO488-conjugated single-domain antibody directed against GFP was used to boost this signal. In the same cells, mitochondria were immunostained for TOM20, a marker for the outer mitochondrial membrane.[170] Expanded and unexpanded cells were then imaged as z-stacks on a spinning disc confocal microscope setup. The signal intensity of the GPI-GFP plasma membrane staining after expansion was too low to measure the volume of the cell accurately. This was most likely due to the aggressive permeabilization required for the ExM protocol, which destabilized the plasma membrane.

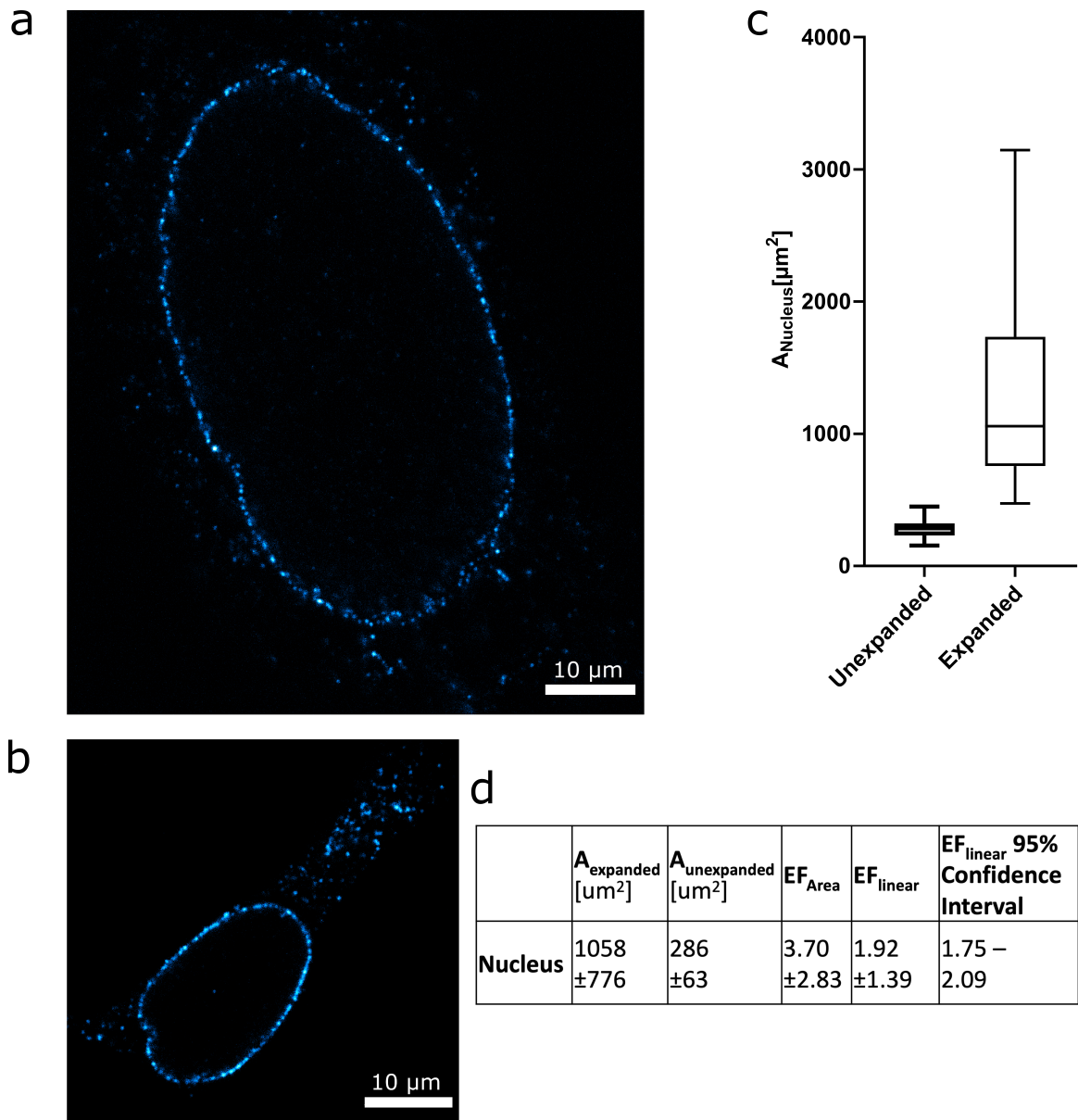


**Figure 13** Expansion of the nucleus **(a)** HEK293 cell, immunolabelled with an antibody against the nuclear pore complex protein NUP153, in an expanded gel. For imaging, the confocal plane with the maximal extent of the nucleus was chosen. The size of the nucleus was measured by manually tracing the NUP153 signal, and the resulting area was recorded for analysis. **(b)** For unexpanded cells treated in the same manner, the analysis was performed analogously. **(c)** Box-whisker plot comparing the measured areas for maximal extent of the nucleus between expanded and unexpanded cells. The median value is denoted by the bar; the box shows the quartile ranges. Whiskers extend from the 5th to the 95th percentile. **(d)** Expansion factor calculated from pooled median areas of unexpanded (n=80) and expanded (n=54) nuclei across two independent replicates. The EF was calculated using median values. Done in cooperation with Katharina Reglinski.

Hence a lot of the GPI-GFP was washed away and after expansion the remaining signal was too weak to enable the reconstruction of a 3D image of the cell that could be used to estimate its volume.

Instead, the z-slice with the maximum extent of the cell was chosen and its area recorded **Fig. 13 (a)**. The antibody-based labelling of the mitochondrial outer membrane using the TOM20 antibody gave a better signal-to-noise ratio. The TOM20 signal was segmented via

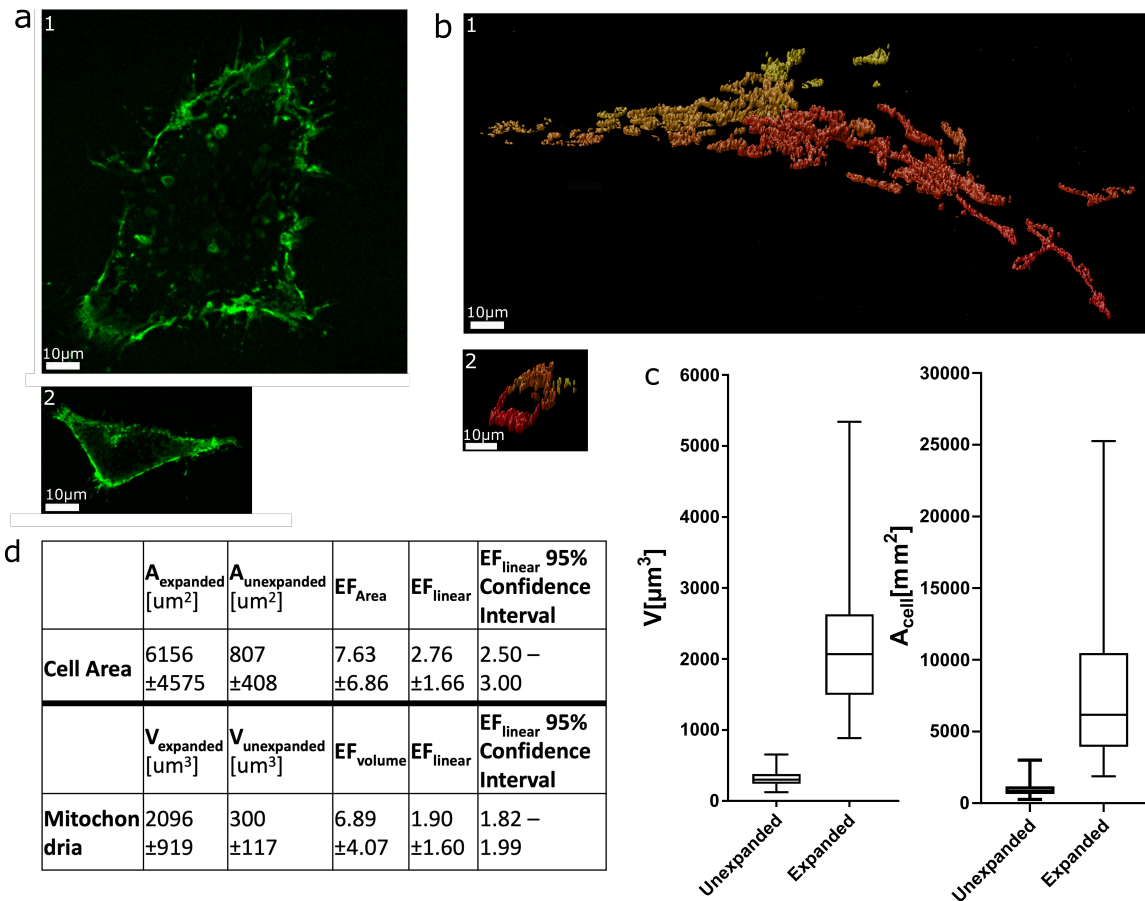


**Figure 14** Expansion of the cell area and mitochondria within the same cells. To stain the plasma membrane, HEK2993 cells expressing GPI-GFP were additionally immunolabelled with antibodies against the mitochondrial outer-membrane protein TOM20. The cells were expanded and imaged as z-stacks on a spinning disc microscope setup. **(a)** Example images of **(a1)** expanded and **(a2)** unexpanded cells expressing GPI-GFP on the cell membrane. The z slice with the maximum extent of the cell was chosen, and the cell area was measured manually. **(b)** Example surface renderings of immunostained mitochondria derived from the z-stacks of **(b1)** expanded and **(b2)** unexpanded cells are shown. The red-to-yellow shading of the surface renderings illustrates the depth, where yellow objects are further away from the viewer. The z-stacks were thresholded, and the volume of all voxels was summed to obtain the volume of the whole mitochondrial network. **(c)** Box-whisker plot showing measured volumes for TOM20 and areas for GPI-GFP. The median value is denoted by the bar; the box shows the quartile ranges. Whiskers extend from the 5th to the 95th percentile. **(d)** Expansion factors calculated from median volumes of the mitochondrial network of unexpanded (n=76) and expanded (n=80) cells. The expansion factor for cell areas was calculated from median areas of unexpanded (n=206) and expanded (n=72) cells. The pooled data shown were obtained from three independent replicates. Done in cooperation with Katharina Reglinski, Christoffer Lagerholm and Dominic Waithe.

thresholding in every stack and then all voxels (dimensions per voxel:  $0.135 \times 0.135 \times 0.370 \mu\text{m}^3$ ) were counted to obtain the volume of the organelle **Fig. 14 (b)**. While comparison of the cell areas obtained a linear EF of 2.7, comparison of mitochondrial volumes between expanded and unexpanded cells yielded a linear EF of 1.9 **Fig. 14 (c)** and **(d)**.

## Peroxisomal membrane and matrix

With notable discrepancies between the EF of the gel and that of the nucleus and mitochondria, determining the EF of the peroxisomes was undertaken next. In order to obtain good signal-to-noise ratios when using ExM, the most common technique is the expression of the protein of interest fused to a fluorescent protein. Then polyclonal, fluorophore-conjugated antibodies are applied that are directed against the fluorescent protein. This approach gives a strong signal and is feasible for staining of whole organelles with specific markers such as the SCP2-GFP containing a peroxisomal targeting signal type 1 (PTS1) for the peroxisomal matrix.

However, this approach using FPs becomes infeasible when colocalization of small, motile proteins on membranes and their interaction partners are to be examined. The bulky, fluorescent protein may change the localization of the protein of interest or may block its binding domain for an interaction partner. Hence the only option here is immunostaining with a primary antibody against the protein of interest. The peroxisomal matrix was thus labelled with SCP2-GFP. The PTS1 signal directed the GFP across the peroxisomal membrane into the lumen of the peroxisomes. Then, an ATTO488-conjugated-anti-GFP single domain antibody was applied to enhance (or boost) this signal.

Staining PEX5 in this application comes with certain limitations, as its role as a carrier protein means it is distributed throughout the cytosol. Using a PEX5 antibody derived from immunizing with a peptide sequence for staining, or using a fusion protein, therefore is not feasible as the result would be a somewhat homogeneously stained cytosol. Instead, a conformer-specific antibody is required that only binds PEX5 when it is attached to the peroxisomal membrane.[177] The conformer-specificity however comes at the cost of reduced binding strength. Unfortunately, the PEX5 signal diminished significantly during digest and expansion, disallowing imaging. A shortened proteinase K digestion was also not able to alleviate this issue (data now shown). To label the membrane, a polyclonal antibody against PEX14 was used. This antibody has a very high affinity to its target and gives a good signal to noise ratio. When used in combination with stable dyes compatible with STED microscopy, such as Abberior STAR RED, the labelling density is sufficient for ExM-STED.

A representative image of the obtained two-colour STED images of peroxisomal matrix and membrane is shown in **Fig. 15 (a)** shows expanded cells in the gel, while **(b)** shows unexpanded cells. The size of the peroxisomal membrane could not be measured automatically, as the signal for PEX14 appeared to be dotted along the membrane. Assigning the PEX14 signal was not possible for clustered peroxisomes **Fig. 15 (a1)**, as it could not be distinguished to which peroxisome the signal belongs. These peroxisomes were thus excluded from further analysis. For peroxisomes whose borders could be defined by the membrane staining **Fig. 15 (a2)**, the PEX14 signal was manually traced to obtain the outline of the peroxisomal membrane and then its extent was recorded. For the peroxisomal matrix, the boosted SCP2-GFP signal was thresholded and then the area of the matrix was measured using the Fiji-Plugin "Particle Analyzer" **Fig. 15 (a3)**. [158] As before, the two sets of areas obtained for expanded and unexpanded cells were employed to calculate the linear EF **Fig. 15 (c)**. The resulting EFs are shown in **Fig. 15 (d)**. With a median expansion factor of 4.1 for the gel, the linear microscopic EF for the peroxisomal membrane was 2.1, while the expansion of the peroxisome matrix was considerably smaller. The linear EF for the peroxisomal matrix was 1.3. There was again considerable variance in the areas determined, but the 95 % confidence interval for the EF of both matrix and membrane are reasonably narrow. As opposed to the mitochondria data, the signal-to-noise ratio for both SCP2-GFP and PEX14 were good for this data set.

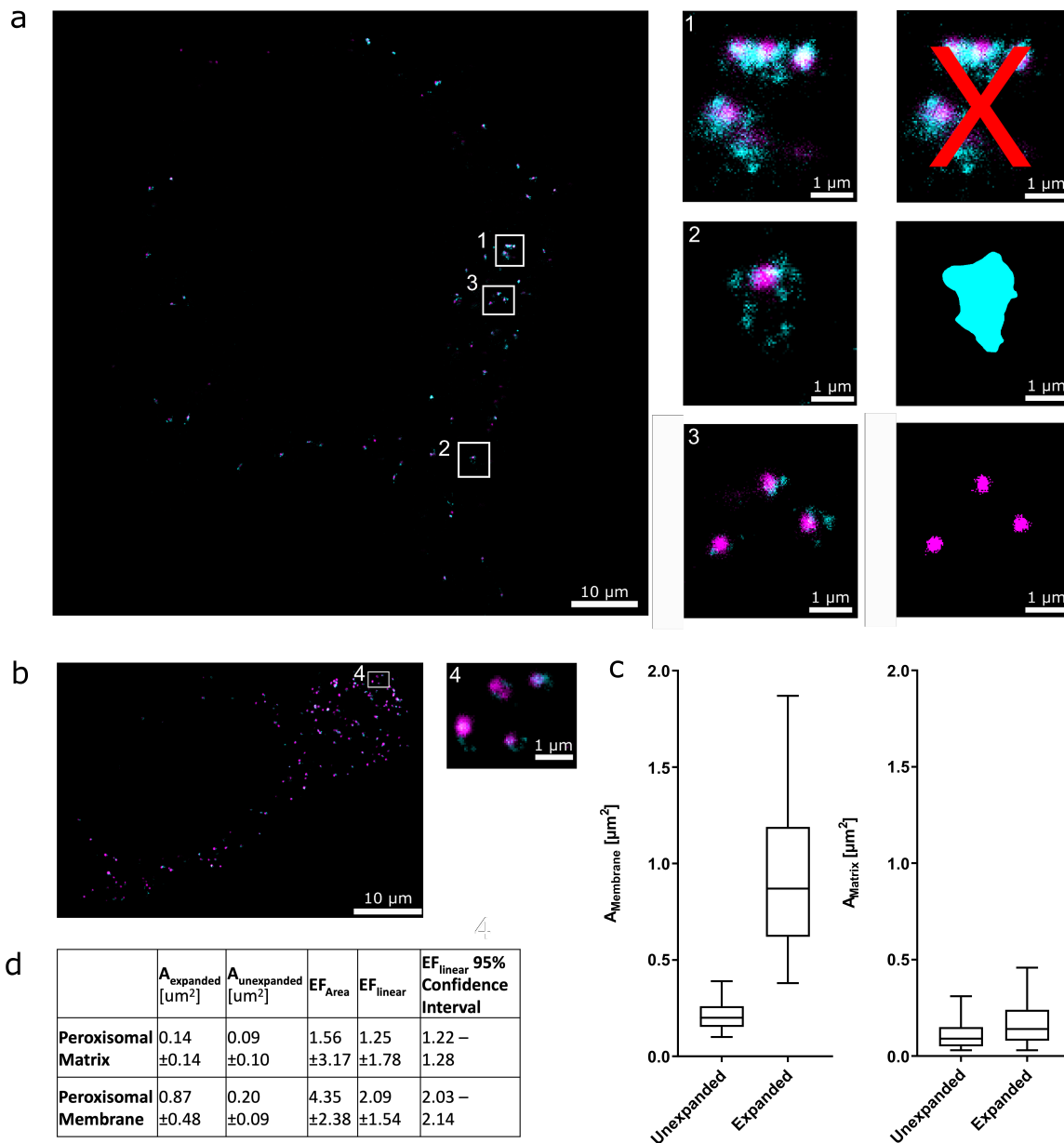


**Figure 15** Expansion of peroxisomes. HEK293 cells expressing SCP2-GFP were immunolabelled with an antibody against PEX14 (cyan), expanded and imaged in two-colour STED. The GFP signal was boosted with an ATTO488-labelled nanobody against GFP (magenta). **(a)** One expanded HEK cell; insets are highlighted on the right with a visualization of the data analysis (right). **(a1)** As clear assignment of the PEX14 signal in clustered peroxisomes was not possible, these were excluded from the analysis. **(a2)** In more isolated peroxisomes, the peroxisomal membrane was manually traced according to the PEX14 signal, and the area was determined for analysis. **(a3)** For the peroxisomal matrix, the SCP2-GFP signal was thresholded, and its area was determined automatically. **(b)** An unexpanded cell treated and stained by the same method was used for the gels. Areas were measured analogously to the analysis of expanded cells. **(c)** Box whisker plots showing areas of peroxisomal matrix and membrane before and after expansion. The median value is denoted by the bar; the box shows the quartile ranges. Whiskers extend from the 5th to the 95th percentile. **(d)** Median areas of unexpanded ( $n=744$ ) and expanded ( $n=654$ ) peroxisomal membranes were used to calculate the expansion factor. Similarly, for the peroxisomal matrix, median areas of unexpanded ( $n=3657$ ) and expanded ( $n=3322$ ) matrices were compared. The pooled data shown were obtained from three independent replicates. Done in cooperation with Katharina Reglinski and Silvia Galiani.



## Discussion

These datasets indicate that the organelles of one cell can expand to different degrees and that the resulting EF is not necessarily the same as that of the gel. Determining the areas for the nucleus in expanded and unexpanded cells yielded datasets with large standard deviations for both. This is due to the inherent variance of biological systems. E.g., in the case of the nucleus, cells are morphologically different and are at different points in the cell cycle at the time of fixation. However, the narrow 95% confidence interval for all determined EFs shows that it can be reliably determined in this fashion if the sample size is sufficiently large.

### **The nucleus expands anisotropically**

The microscopic EF of 1.9 obtained from the NUP153 staining deviated from that determined from the macroscopic EF of 4.1 of the whole gel. Under the assumption of isotropic expansion, this discrepancy is rather surprising and unexpected.

However, Pesce and colleagues reported similar discrepancies when examining nuclear pore complexes as potential intrinsic reporters for the expansion factor.[178] In this study, the EF of the gel was reported to be 5.0, while the EF determined through the distance between nuclear pore complexes was reported as 3.8. The EF calculated from the radii of the NPC before and after expansion was reported as 4.3. The same authors show that a heterogeneous loss of fluorescence can pose a particular challenge in cell biology.[178] They analyzed NUP153, which forms a symmetrical octagon in the nuclear pore complex and noticed heterogeneous loss of signal due to polymerization and digestion in the ExM protocol. For well-explored epitopes like the nuclear pore, other data (mainly from CryoEM) can be consulted to compare the image obtained from an expanded cell. However, for proteins of interest where little prior knowledge exists and where their (co)localization or structure is to be examined, noticing artefacts due to heterogeneous signal loss becomes more challenging.

Another study found a linear microscopic expansion factor of nuclei which matches exactly that of the gel (4.1). This was reported for isolated barley nuclei, but only when employing a slightly modified ExM protocol using heat denaturation, which in turn resulted in impairments in chromatin structure after expansion.[179] In another example, when examining rat hepatocytes, Pernal and colleagues reported an EF of 4.71 for the whole cell, whereas the nucleus only expanded by a factor of 3.86.[180] The same study also examined human primary skeletal muscle cells. Crucially, it showed that the relative ratio of (heterochromatin-containing) DAPI-stained areas of the cell to the area of the whole nucleus changed during expansion because the heterochromatin-containing regions expanded to a lesser degree than the nucleolus. In the same cells, the EF determined via the width of myosin fibres was shown to be 2.7. For these nuclei, the length-to width- ratio also changes during expansion. The authors furthermore list fragmentary pieces of evidence for differential expansion from several other publications employing ExM. In conjunction with this data, this points to the conclusion that the nucleus expands anisotropically and that there are further examples of differences between EFs determined by macroscopic inspection of the whole gel and EFs of cellular structures, which has to be considered for final structure-size determination.

### **Signal loss can impair detection confidence**

A problem for measuring the volume of mitochondria was the loss of fluorescence intensity during the expansion. For measuring the volume of the mitochondria in the reconstructed 3D images, the image was thresholded, which is not easy when the brightness of the two samples (expanded and unexpanded) varies. Although this might have led to false-negative

detection of voxels in the expanded cells, the signal was strong enough to recreate the shape of the organelles quite efficiently. This effect alone cannot explain the difference in the linear EF of mitochondria (1.9) to the one of the gel (4.1), indicating again that the expansion of intracellular structures was much less than that of the gel. Further data with better signal-to-noise ratio would be desirable to confirm the EF of the mitochondria. Use of fusion proteins with mitochondrial proteins resident in matrix and membrane, targeted by fluorophore-conjugated nanobodies might be of use here. Labelling of the mitochondrial matrix could also be considered to compare the expansion factor of the mitochondrial membrane to that of the matrix. However, for the expansion experiments (especially when combined with STED) there is, as also outlined below, a further need for very bright staining, since expansion leads to a “dilution” of signal. For example, even for a usually efficient stain, such as of TOM20 in the mitochondrial membrane, a pronounced lowering of signal after expansion was observed, so that the signal-to-noise ratio of the resulting images was rather low and deconvolution (and thus denoising) became necessary to evaluate the data. Any staining of the matrix would be dispersed throughout the whole mitochondrion and thus be less concentrated after expansion, compared to for example the high concentration of the actively imported peroxisomal membrane marker. Nevertheless, it seems likely that the matrix of mitochondria will probably expand more or less equally to the membrane, as it does in hypotonic solution.[181]

The case of the GPI-GFP and ATTO488 stained membrane illustrates, that the harsh permeabilization protocol required to allow access to the polymer and subsequent protein digest can also considerably attenuate the signal. Differences in EF of whole cells were also encountered when applying ExM to bacteria, due to biochemical heterogeneity of their cell walls. In some cases, it was possible to abolish these differences in EF by digesting the cell wall prior to expansion.[182]

### **The peroxisomal membrane expands more than the peroxisomal matrix**

The initial motivation for the study was to elucidate the protein distribution on organelle membranes, like the peroxisomal membrane, with a combination of ExM and STED. Consequently, the expansion of this organelle was determined next. The matrix and membrane of peroxisomes were labelled and imaged with STED microscopy before and after expansion. Similar to the other organelles, differences between the EF of the peroxisomal matrix, membrane and that of the gel are noticeable.

This result can however not be attributed to a poor signal-to-noise-ratio, since the chosen labelling approach also gave strong fluorescence in the expanded gel. Instead, this result is most likely caused by the dense environment of the peroxisomal matrix, which in some cases even contains a crystalloid protein core.[183] It has also been shown that peroxisomes do not expand like other organelles, including ER, endosomes, lysosomes or mitochondria, upon incubation of cells in hypotonic solution.[181] This is probably also due to the dense protein matrix in the lumen of these organelles. During the digestion step, proteinase K probably cannot cleave proteins in this environment efficiently, resulting in incomplete expansion of these protein structures afterwards. To overcome this issue, it was attempted to prolong the digestion with proteinase K, but this led to significant loss of signal (data not shown).

The use of a monoclonal antibody against PEX5, the peroxisomal import receptor, which is shuttling between the cytosol and the peroxisomal membrane to import PTS1-containing cargo proteins was also attempted. At the membrane, PEX5 is interacting with PEX14, triggering the translocation of the cargo protein.[184-186] The monoclonal PEX5 antibody used here, only binds to PEX5 when it is located at the peroxisomal membrane and not to

the cytosolic pool of the shuttling receptor.[177] Here, good STED images are obtainable using PEX14 and PEX5 in a dual colour STED colocalization study [113] but the signal with the PEX5 antibody was too weak for ExM-STED. This effect is most likely caused by the harsh permeabilization, and digest needed for the expansion. The weak signal might be since monoclonal antibodies bind to only one epitope on their target protein. Another contributing issue might be the need to digest the sample: If the epitope of a monoclonal antibody is surrounded by proteinase cleavage sites, fluorophores bound to it can be lost. Therefore, the use of polyclonals is recommended for ExM-STED, as these can bind multiple epitopes on their target protein. On a note, compared to mitochondria, the crystalloid core of peroxisomes is a very organelle-specific property and therefore the difference of the expansion of peroxisomal membrane and matrix is an extreme example. Nevertheless, this highlights that the differences in expansion can be dramatic and need to be considered in any such experiments.

This data clearly indicates that the EFs of different organelles, and in case of peroxisomes even distinct regions of the same organelle, differ significantly. Although the linear expansion factor of the gel was consistently 4.1, the EF of the measured cellular compartments ranged from 2.7 (cell area) to 1.3 (peroxisomal matrix; **Table 10**). This needs to be considered when interpreting data from single cell measurements in ExM.

Organelle	Expansion Factor Area	Volume	Linear	Linear (95 % confidence interval)
Nucleus	3.70 ± 2.83	-	1.92 ± 1.39	1.75 ± 1.90
Mitochondria	-	6.89 ± 4.07	1.90 ± 1.60	1.82 ± 1.99
Cell area	7.63 ± 6.86	-	2.76 ± 1.66	2.50 ± 3.00
Peroxisomal matrix	1.56 ± 3.17	-	1.25 ± 1.78	1.22 ± 1.28
Peroxisomal membrane	4.35 ± 2.38	-	2.09 ± 1.54	2.03 ± 2.14

**Table 10** Expansion factors of different organelles calculated with median areas or volume and the resulting linear expansion factor

### Direct comparison of individual cells

Comparing the expansion of one organelle in the same individual cell before and after expansion was previously done by training to find the same cell before and after expansion, in analogy to the vector-field-distortion analysis that has classically been used to validate isotropic expansion in ExM (e. g., for microtubules).[163] A number of hindrances made it impossible to realize this in a reliable fashion in this study: When examining a coverslip with HEK cells and the resulting gel, it was difficult to clearly identify the same cell in samples pre- and post- expansion, because most cells were morphologically quite similar. An identification was in addition complicated due to the large difference in fluorescence brightness before and after expansion. Many cells were thus analyzed within large sample sizes independent of pre- and post-expansion instead, to avoid erroneous assignment of single cells. It was also considered to investigate the expansion factor of further organelles. For example, microtubules have been used before to validate isotropic expansion.[163, 165] However, to in detail explore and compare values of the expansion factor, it was found

to be more reliable to employ areas instead of one-dimensional structures such as microtubules.

### **Alternative approaches to increasing the fluorescence intensity**

The loss of fluorescence intensity encountered in ExM-STED, due to a combination of loss of fluorophores and a physical “dilution” of the signal during expansion of the sample, poses a major challenge. Several approaches have been used to increase the labelling density in the pre-expansion sample in order to attain a sufficient labelling density in the expanded gel. One option is to first use primary antibodies conjugated with biotin on the unexpanded cells, followed by treatment with fluorophore-conjugated secondary antibodies directed against these primary antibodies. The expanded gel is then perfused with streptavidin-conjugated fluorophores. This results in an increased labelling density when compared to conventional immunostaining.[165] A variant of this method allows signal amplification through iterative treatment of the sample with biotin- and dye-conjugated secondary antibodies and dye-conjugated streptavidin. While this method gives a fluorophore density high enough to reach the maximum STED resolution in an expanded sample, it also introduces a localization error with each amplification cycle, due to the resulting distance between the protein of interest and the fluorophore.[187] An alternative to expressing the protein of interest conjugated with a fluorescent protein is to attach the AviTag peptide sequence, consisting of only 16 amino acids. The small peptide is less likely to interfere with the protein’s motility and to block binding domains than the bulky structures of a fluorescent protein. This previously demonstrated method [187] then uses the BirA biotin ligase to biotinylate the peptide. The sample can then be treated with the same iterative treatment as outlined above.

### **Conclusion**

Expansion microscopy is a sophisticated tool for the analysis of tissue slices, as the structures can be easily compared between expanded and unexpanded samples. Here a vector-distortion field can be applied to visualize and detect anisotropic expansion due to biomechanical heterogeneity of the sample. Furthermore, different parts of tissue slices often have varying refractive indices. These lead to aberrations that limit the depth to which a slice of tissue can be imaged. This problem is partly overcome by ExM as the gel has almost the same refractive index as water, which alleviates this issue. Therefore, ExM improves deep-tissue imaging. This data points to the conclusion that it might be difficult to define one epitope or structure inside cells as a reference and then generalize isotropy and EF from it. The biochemical heterogeneity of cellular organelles makes it necessary to validate the expansion on exactly the epitope that is to be measured. As the expansion factors measured differ for all analyzed organelles, and in case of peroxisomes even for structures within the same organelle, it becomes clear that ExM on subcellular structures is quite challenging. Peroxisomes are a difficult organelle for ExM as they have a protein-rich crystalline core, which is difficult to expand because of its special biochemical properties. That might explain the very low EF for the peroxisomal matrix, but it is also clear that the big variety of EFs measured with different organelles is a problem for imaging intracellular details with ExM. This underlines the need to validate the isotropic expansion of the structure of interest when using this technique.

## Methods

### Cell culture

HEK293 cells (CRL-1573, ATCC) were maintained in a culture medium consisting of DMEM with 4500 mg/l glucose, 110 mg/l sodium pyruvate supplemented with 10 % fetal calf serum (FCS, F7524 Sigma-Aldrich), 2 mM glutamine (25030081, Thermo Fisher) and penicillin-streptomycin (1 %). The cells were cultured at 37° C and 8.5 % CO<sub>2</sub>. Cells were grown on #1.5 cover slides of 18 mm diameter. For the analysis of the peroxisomal matrix, the cells were transfected with 0.5 µg SCP2-GFP [188] or GPI-GFP (ID 32601, Addgene) per dish using Lipofectamine 2000 transfection reagent (11668027, Invitrogen). Transfected cells were fixed for immunostaining 24 h after transfection.

### Immunostaining

Cells were fixed with 3% *para*-Formaldehyde (28906, Pierce) for 20 min and permeabilized with 0.1% Triton X-100 (85111, Thermo Fisher) for 10 min. Samples were then blocked (2% BSA, 5% FCS in phosphate buffered saline (PBS), for 1 h at RT) and incubated in the primary antibody in dilutions shown in **Table 11**. Subsequently, samples were incubated with the secondary antibody **Table 12** and treated with 0.1 mg/ml 6-((acryloyl)amino) hexanoic acid, succinimidyl ester (AcX, A20770, Thermo Fisher) for at least 12 h.

### Gelation, digest and expansion

Gelation was performed as previously described.[161] Briefly, monomer solution with 1x PBS, 2 M NaCl, 8.625 % sodium acrylate (408220, Merck), 2.5 % acrylamide (A9099, Merck), 0.15% N,N'-methylenebisacrylamide (01702, Merck) was mixed, frozen in aliquots, and thawed before use. Monomer solution was used at 4° C. Concentrated stocks of ammonium persulfate (APS, 248614, Merck) and tetramethylethylenediamine (TEMED, T7024, Merck) were added to the monomer solution up to 0.2 % each. Polymerization was allowed to proceed for 15 min at RT and then 1 h at 37° C to allow complete gelation. The gel was then cut asymmetrically, and the length of its longest side was recorded. Gels were then removed from the gelation chamber and fully immersed in digestion buffer (50 mM Tris (pH 8), 1 mM EDTA, 0.5 % Triton X-100, 1 M NaCl) with 8 U/mL of proteinase K (9210, BioVision) added immediately before use. Digestion was performed for 3 h at 37° C. For expansion, gels were placed in doubly deionized water (ddH<sub>2</sub>O) for 4 h. ddH<sub>2</sub>O was replaced every 30 min until the maximum expansion of the gel was reached. The length of the longest side was recorded again and used to calculate the EF of the gel. This consistently gave an EF ranging between 3.9–4.2 with a median EF of 4.1.

### Mounting

For mounting of gel-embedded cells, FluoroDish glass bottom dishes (FD35-100, World Precision Instruments) were coated with 0.1 mg/ml Poly-L-lysine for 1 h at 37° C and then washed once with ddH<sub>2</sub>O. Expanded gels were placed on the glass and all excess water removed. After allowing adhesion for 5 min, the dish was placed in the sample holder of the microscope. The top of the gel was covered with a small amount of ddH<sub>2</sub>O to prevent shrinkage due to evaporation. For unexpanded controls the cells were grown on glass slides, then fixed, stained and incubated in AcX and subsequently imaged. For imaging, the coverslip was mounted in an imaging chamber and covered with PBS.

### Image acquisition

Images of SCP2-GFP expressing HEK293 cells immunostained for either NUP153 or PEX14 were acquired on a Leica SP8 3x STED Microscope with a HC PL APO 86x 1.2 NA

objective with motorized collar correction. The white-light laser was used for excitation at 488 nm and 640 nm with depletion via the 592 nm and 775 nm STED laser, respectively. NUP153 signal was acquired in confocal mode only. When using two depletion lasers of different wavelengths, only one STED-channel can be acquired at a time. Hence, for SCP2-GFP/PEX14 stained cells, acquisition was performed frame-by-frame. First, PEX14 signal was acquired in STED with parallel acquisition of SCP2-GFP signal in confocal. Then, SCP2-GFP signal was acquired in STED. To correct for any drift in between acquisition of the frames, the Fiji-Plugin “Correct 3D Drift” [158] was used to align the channels according to the SCP2-GFP signal. GPI-GFP expressing HEK293 cells immunostained for TOM20 were imaged on a Zeiss Cell Observer SD with a Yokogawa CSU-X1 M 500 Dual Cam spinning disc, Hamamatsu Orca Flash 4.0 V2 sCMOS camera and a LD C-Apochromat 40Å~ 1.1 NA objective. Excitation of ATTO488-nanobody boosted GFP signal was done at 488 nm, while Abberior STAR RED was excited at 635 nm.

### **Image processing and data analysis**

TOM20 images acquired on the spinning disc setup were deconvolved with Huygens (Scientific Volume Imaging), using classical maximum likelihood estimation (CMLE). All image analysis was performed using Fiji. In particular, the “Particle Analyzer” and “Voxel Counter” scripts were used to obtain areas and volumes respectively.[158] Graphing and statistical analysis was performed using GraphPad. In all Box-whisker plots, the median value is denoted by the bar and the box shows the quartile ranges. Whiskers extend from the 5th to the 95th percentile. The EF in all tables was calculated using median values.

### **Contributions**

This work was performed in contribution with Katharina Reglinski, Silvia Galiani, both members of the Christian Eggeling group, Christoffer Lagerholm of the Wolfson Imaging Facility, as well as Dominic Waithe, all at the Weatherall Institute for Molecular Medicine in Oxford.

K.R. provided expertise about peroxisomes and an initial staining strategy that worked for STED microscopy. K.R. furthermore provided all plasmids, as well as PEX5 and PEX14 antibodies and performed all cell culture work. M.B. performed all sample preparations, as well as adaptation of staining strategy for ExM and optimization of gel preparation. All imaging was performed by M.B. with assistance from S.G for peroxisome data. C.L. helped in choice of imaging setup and parameters for mitochondria/cell area data. Image analysis was performed by M.B. with advice from K.R. D.W. helped with deconvolving mitochondria/cell area data. This project was part of a larger effort studying peroxisomal import. The antibodies for PEX5 and PEX14 were developed in the labs of Ralf Erdmann and Wolfgang Schliebs, who kindly provided them for this study. See also the corresponding publication.[189]

Epitope	Species	Clonality	Clone	Conjugate	Source
aPEX14	Rabbit	Polyclonal	-	-	See ref. [19]
NUP153	Mouse	Monoclonal	QE5	-	Abcam Ab24700
TOM20	Rabbit	Polyclonal	-	-	Santa Cruz Sc-11415

**Table 11** Primary antibodies

Epitope	Species	Clonality	Clone	Conjugate	Source
Rabbit IgG1	Goat	Polyclonal	-	STAR RED	Aberrior 2-0012 011-9
Mouse IgG1	Goat	Polyclonal	-	STAR RED	Aberrior 2-0002-011-2
GFP	Alpaca	Monoclonal	-	ATTO488	Proteintech gba488

**Table 12** Secondary antibodies

## References

1. Vivier, E., et al., *Functions of natural killer cells*. Nature Immunology, 2008. **9**(5): p. 503-510.
2. Dieckmann, N.M.G., et al., *The cytotoxic T lymphocyte immune synapse at a glance*. Journal of Cell Science, 2016. **129**(15): p. 2881-2886.
3. Pennock, N.D., et al., *T cell responses: naïve to memory and everything in between*. Advances in Physiology Education, 2013. **37**(4): p. 273-283.
4. Raghavan, M., et al., *MHC class I assembly: out and about*. Trends in Immunology, 2008. **29**(9): p. 436-443.
5. Kärre, K., et al., *Selective rejection of H-2-deficient lymphoma variants suggests alternative immune defence strategy*. Nature, 1986. **319**(6055): p. 675-678.
6. Ljunggren, H.-G. and K. Kärre, *In search of the 'missing self': MHC molecules and NK cell recognition*. Immunology Today, 1990. **11**: p. 237-244.
7. Hashimoto, G., P.F. Wright, and D.T. Karzon, *Antibody-Dependent Cell-Mediated Cytotoxicity Against Influenza Virus-Infected Cells*. The Journal of Infectious Diseases, 1983. **148**(5): p. 785-794.
8. Wang, W., et al., *NK Cell-Mediated Antibody-Dependent Cellular Cytotoxicity in Cancer Immunotherapy*. Frontiers in Immunology, 2015. **6**(368).
9. Cerboni, C., et al., *The DNA Damage Response: A Common Pathway in the Regulation of NKG2D and DNAM-1 Ligand Expression in Normal, Infected, and Cancer Cells*. Frontiers in Immunology, 2014. **4**(508).
10. Brandt, C.S., et al., *The B7 family member B7-H6 is a tumor cell ligand for the activating natural killer cell receptor NKp30 in humans*. Journal of Experimental Medicine, 2009. **206**(7): p. 1495-1503.
11. Pogge von Strandmann, E., et al., *Human Leukocyte Antigen-B-Associated Transcript 3 Is Released from Tumor Cells and Engages the NKp30 Receptor on Natural Killer Cells*. Immunity, 2007. **27**(6): p. 965-974.
12. Hecht, M.-L., et al., *Natural Cytotoxicity Receptors NKp30, NKp44 and NKp46 Bind to Different Heparan Sulfate/Heparin Sequences*. Journal of Proteome Research, 2009. **8**(2): p. 712-720.
13. Bartolini, B., et al., *Heparan Sulfate in the Tumor Microenvironment*, in *Tumor Microenvironment: Extracellular Matrix Components – Part A*, A. Birbrair, Editor. 2020, Springer International Publishing: Cham. p. 147-161.
14. Joyce, M.G., et al., *Crystal structure of human natural cytotoxicity receptor NKp30 and identification of its ligand binding site*. Proceedings of the National Academy of Sciences, 2011. **108**(15): p. 6223-6228.
15. Li, Y., Q. Wang, and R.A. Mariuzza, *Structure of the human activating natural cytotoxicity receptor NKp30 bound to its tumor cell ligand B7-H6*. Journal of Experimental Medicine, 2011. **208**(4): p. 703-714.
16. Skořepa, O., et al., *Natural Killer Cell Activation Receptor NKp30 Oligomerization Depends on Its N-Glycosylation*. Cancers, 2020. **12**(7): p. 1998.
17. Memmer, S., et al., *The Stalk Domain of NKp30 Contributes to Ligand Binding and Signaling of a Preassembled NKp30-CD3 $\zeta$  Complex*. The Journal of biological chemistry, 2016. **291**(49): p. 25427-25438.
18. Luczo, J.M., S.L. Ronzulli, and S.M. Tompkins, *Influenza A Virus Hemagglutinin and Other Pathogen Glycoprotein Interactions with NK Cell Natural Cytotoxicity Receptors NKp46, NKp44, and NKp30*. Viruses, 2021. **13**(2): p. 156.
19. Björkström, N.K., B. Strunz, and H.-G. Ljunggren, *Natural killer cells in antiviral immunity*. Nature Reviews Immunology, 2022. **22**(2): p. 112-123.
20. Arnaout, M.A., *Biology and structure of leukocyte  $\beta$  (2) integrins and their role in inflammation*. F1000Research, 2016. **5**: p. F1000 Faculty Rev-2433.
21. Urlaub, D., et al., *LFA-1 Activation in NK Cells and Their Subsets: Influence of Receptors, Maturation, and Cytokine Stimulation*. The Journal of Immunology, 2017. **198**(5): p. 1944-1951.
22. Mace, E.M., et al., *Elucidation of the integrin LFA-1-mediated signaling pathway of actin polarization in natural killer cells*. Blood, 2010. **116**(8): p. 1272-1279.
23. Pende, D., et al., *Killer Ig-Like Receptors (KIRs): Their Role in NK Cell Modulation and Developments Leading to Their Clinical Exploitation*. Frontiers in Immunology, 2019. **10**(1179).
24. Hammer, Q., et al., *Peptide-specific recognition of human cytomegalovirus strains controls adaptive natural killer cells*. Nature Immunology, 2018. **19**(5): p. 453-463.
25. Vietzen, H., et al., *Deletion of the NKG2C receptor encoding KLRC2 gene and HLA-E variants are risk factors for severe COVID-19*. Genetics in Medicine, 2021. **23**(5): p. 963-967.



26. Jandus, C., et al., *Interactions between Siglec-7/9 receptors and ligands influence NK cell-dependent tumor immunosurveillance*. The Journal of Clinical Investigation, 2014. **124**(4): p. 1810-1820.
27. Hong, S., et al., *Modulation of Siglec-7 Signaling Via In Situ-Created High-Affinity cis-Ligands*. ACS Central Science, 2021. **7**(8): p. 1338-1346.
28. Pegram, H.J., et al., *Activating and inhibitory receptors of natural killer cells*. Immunology & Cell Biology, 2011. **89**(2): p. 216-224.
29. Sivori, S., et al., *Human NK cells: surface receptors, inhibitory checkpoints, and translational applications*. Cellular & Molecular Immunology, 2019. **16**(5): p. 430-441.
30. Sivori, S., et al., *Inhibitory Receptors and Checkpoints in Human NK Cells, Implications for the Immunotherapy of Cancer*. Frontiers in Immunology, 2020. **11**(2156).
31. Chan, C.J., M.J. Smyth, and L. Martinet, *Molecular mechanisms of natural killer cell activation in response to cellular stress*. Cell death and differentiation, 2014. **21**(1): p. 5-14.
32. Gunesch, J.T., et al., *Genome-wide analyses and functional profiling of human NK cell lines*. Mol Immunol, 2019. **115**: p. 64-75.
33. Zwirner, N.W. and C.I. Domaica, *Cytokine regulation of natural killer cell effector functions*. BioFactors, 2010. **36**(4): p. 274-288.
34. Ostensen, M.E., D.L. Thiele, and P.E. Lipsky, *Tumor necrosis factor-alpha enhances cytolytic activity of human natural killer cells*. The Journal of Immunology, 1987. **138**(12): p. 4185-4191.
35. Sabio, G. and R.J. Davis, *TNF and MAP kinase signalling pathways*. Seminars in Immunology, 2014. **26**(3): p. 237-245.
36. Wang, R., et al., *Natural killer cell-produced IFN- $\gamma$  and TNF- $\alpha$  induce target cell cytotoxicity through up-regulation of ICAM-1*. Journal of Leukocyte Biology, 2012. **91**(2): p. 299-309.
37. Reefman, E., et al., *Cytokine Secretion Is Distinct from Secretion of Cytotoxic Granules in NK Cells*. The Journal of Immunology, 2010. **184**(9): p. 4852-4862.
38. Tilg, H. and A.R. Moschen, *Adipocytokines: mediators linking adipose tissue, inflammation and immunity*. Nature Reviews Immunology, 2006. **6**(10): p. 772-783.
39. Zhang, Y., et al., *Positional cloning of the mouse obese gene and its human homologue*. Nature, 1994. **372**(6505): p. 425-432.
40. Malendowicz, W., et al., *Leptin and leptin receptors in the prostate and seminal vesicles of the adult rat*. Int J Mol Med, 2006. **18**(4): p. 615-618.
41. Pan, W.W. and M.G. Myers, *Leptin and the maintenance of elevated body weight*. Nature Reviews Neuroscience, 2018. **19**(2): p. 95-105.
42. Friedman, J., *20 YEARS OF LEPTIN: Leptin at 20: an overview*. Journal of Endocrinology, 2014. **223**(1): p. T1-T8.
43. Bähr, I., et al., *Obesity-Associated Alterations of Natural Killer Cells and Immunosurveillance of Cancer*. Frontiers in Immunology, 2020. **11**(245).
44. Michelet, X., et al., *Metabolic reprogramming of natural killer cells in obesity limits antitumor responses*. Nature Immunology, 2018. **19**(12): p. 1330-1340.
45. Lamas, B., et al., *Leptin modulates dose-dependently the metabolic and cytolytic activities of NK-92 cells*. Journal of Cellular Physiology, 2013. **228**(6): p. 1202-1209.
46. Nave, H., et al., *Resistance of Janus Kinase-2 Dependent Leptin Signaling in Natural Killer (NK) Cells: A Novel Mechanism of NK Cell Dysfunction in Diet-Induced Obesity*. Endocrinology, 2008. **149**(7): p. 3370-3378.
47. Wrann, C.D., et al., *Short-term and long-term leptin exposure differentially affect human natural killer cell immune functions*. American Journal of Physiology-Endocrinology and Metabolism, 2012. **302**(1): p. E108-E116.
48. Williams, B.A., et al., *A phase I trial of NK-92 cells for refractory hematological malignancies relapsing after autologous hematopoietic cell transplantation shows safety and evidence of efficacy*. Oncotarget, 2017. **8**(51).
49. Brent, A.W., et al., *CD16+NK-92 and anti-CD123 monoclonal antibody prolongs survival in primary human acute myeloid leukemia xenografted mice*. Haematologica, 2018. **103**(10): p. 1720-1729.
50. Chames, P., et al., *Therapeutic antibodies: successes, limitations and hopes for the future*. British Journal of Pharmacology, 2009. **157**(2): p. 220-233.
51. Sterner, R.C. and R.M. Sterner, *CAR-T cell therapy: current limitations and potential strategies*. Blood Cancer Journal, 2021. **11**(4): p. 69.
52. Chong, E.A., et al., *PD-1 blockade modulates chimeric antigen receptor (CAR)-modified T cells: refueling the CAR*. Blood, 2017. **129**(8): p. 1039-1041.

53. Majzner, R.G. and C.L. Mackall, *Tumor Antigen Escape from CAR T-cell Therapy*. *Cancer Discovery*, 2018. **8**(10): p. 1219-1226.
54. Albinger, N., J. Hartmann, and E. Ullrich, *Current status and perspective of CAR-T and CAR-NK cell therapy trials in Germany*. *Gene Therapy*, 2021. **28**(9): p. 513-527.
55. Gong, J.H., G. Maki, and H.G. Klingemann, *Characterization of a human cell line (NK-92) with phenotypical and functional characteristics of activated natural killer cells*. *Leukemia*, 1994. **8** 4: p. 652-8.
56. Tang, X., et al., *First-in-man clinical trial of CAR NK-92 cells: safety test of CD33-CAR NK-92 cells in patients with relapsed and refractory acute myeloid leukemia*. *American journal of cancer research*, 2018. **8**(6): p. 1083-1089.
57. Burger, M.C., et al., *CAR-Engineered NK Cells for the Treatment of Glioblastoma: Turning Innate Effectors Into Precision Tools for Cancer Immunotherapy*. *Frontiers in Immunology*, 2019. **10**.
58. Shannon, M.J. and E.M. Mace, *Natural Killer Cell Integrins and Their Functions in Tissue Residency*. *Frontiers in Immunology*, 2021. **12**.
59. Chen, X., et al., *Many NK cell receptors activate ERK2 and JNK1 to trigger microtubule organizing center and granule polarization and cytotoxicity*. *Proceedings of the National Academy of Sciences*, 2007. **104**(15): p. 6329-6334.
60. Krzewski, K. and J. Coligan, *Human NK cell lytic granules and regulation of their exocytosis*. *Frontiers in Immunology*, 2012. **3**.
61. Ben-Shmuel, A., et al., *The Role of the Cytoskeleton in Regulating the Natural Killer Cell Immune Response in Health and Disease: From Signaling Dynamics to Function*. *Frontiers in Cell and Developmental Biology*, 2021. **9**.
62. Orange, J.S., et al., *Wiskott-Aldrich syndrome protein is required for NK cell cytotoxicity and colocalizes with actin to NK cell-activating immunologic synapses*. *Proceedings of the National Academy of Sciences*, 2002. **99**(17): p. 11351-11356.
63. Goley, E.D. and M.D. Welch, *The ARP2/3 complex: an actin nucleator comes of age*. *Nature Reviews Molecular Cell Biology*, 2006. **7**(10): p. 713-726.
64. Ramoni, C., et al., *Differential expression and distribution of ezrin, radixin and moesin in human natural killer cells*. *European Journal of Immunology*, 2002. **32**(11): p. 3059-3065.
65. Gil-Krzewska, A., et al., *An actin cytoskeletal barrier inhibits lytic granule release from natural killer cells in patients with Chediak-Higashi syndrome*. *Journal of Allergy and Clinical Immunology*, 2018. **142**(3): p. 914-927.e6.
66. Rak, G.D., et al., *Natural Killer Cell Lytic Granule Secretion Occurs through a Pervasive Actin Network at the Immune Synapse*. *PLOS Biology*, 2011. **9**(9): p. e1001151.
67. Mace, E.M. and J.S. Orange, *Dual channel STED nanoscopy of lytic granules on actin filaments in natural killer cells*. *Communicative & Integrative Biology*, 2012. **5**(2): p. 184-186.
68. Hsu, H.-T., et al., *NK cells converge lytic granules to promote cytotoxicity and prevent bystander killing*. *The Journal of Cell Biology*, 2016. **215**(6): p. 875-889.
69. Mace, E.M. and J.S. Orange, *Lytic immune synapse function requires filamentous actin deconstruction by Coronin 1A*. *Proceedings of the National Academy of Sciences*, 2014. **111**(18): p. 6708-6713.
70. Cavini, I.A., et al., *The Structural Biology of Septins and Their Filaments: An Update*. *Frontiers in Cell and Developmental Biology*, 2021. **9**.
71. Phatarpekar, P.V., et al., *The septin cytoskeleton regulates natural killer cell lytic granule release*. *Journal of Cell Biology*, 2020. **219**(11).
72. Voskoboinik, I., J.C. Whisstock, and J.A. Trapani, *Perforin and granzymes: function, dysfunction and human pathology*. *Nature Reviews Immunology*, 2015. **15**: p. 388.
73. Brunner, K.T., et al., *Quantitative assay of the lytic action of immune lymphoid cells on 51-Cr-labelled allogeneic target cells in vitro; inhibition by isoantibody and by drugs*. *Immunology*, 1968. **14**(2): p. 181-196.
74. Lorenzo-Herrero, S., et al., *CD107a Degranulation Assay to Evaluate Immune Cell Antitumor Activity*, in *Cancer Immunosurveillance: Methods and Protocols*, A. López-Soto and A.R. Folgueras, Editors. 2019, Springer New York: New York, NY. p. 119-130.
75. Suhrbier, A., et al., *BLT esterase activity as an alternative to chromium release in cytotoxic T cell assays*. *Journal of Immunological Methods*, 1991. **145**(1): p. 43-53.
76. Mosmann, T.R. and T.A.T. Fong, *Specific assays for cytokine production by T cells*. *Journal of Immunological Methods*, 1989. **116**(2): p. 151-158.
77. Young, H.A., *Cytokine multiplex analysis*. *Methods in molecular biology (Clifton, N.J.)*, 2009. **511**: p. 85-105.

78. Skak, K., K.S. Frederiksen, and D. Lundsgaard, *Interleukin-21 activates human natural killer cells and modulates their surface receptor expression*. *Immunology*, 2008. **123**(4): p. 575-583.
79. Raulat, D.H., R.E. Vance, and C.W. McMahon, *Regulation of the Natural Killer Cell Receptor Repertoire*. *Annual Review of Immunology*, 2001. **19**(1): p. 291-330.
80. Aquino-López, A., et al., *Interferon Gamma Induces Changes in Natural Killer (NK) Cell Ligand Expression and Alters NK Cell-Mediated Lysis of Pediatric Cancer Cell Lines*. *Frontiers in Immunology*, 2017. **8**.
81. Lanier, L.L., *Up on the tightrope: natural killer cell activation and inhibition*. *Nature Immunology*, 2008. **9**(5): p. 495-502.
82. Hwang, J.-R., et al., *Recent insights of T cell receptor-mediated signaling pathways for T cell activation and development*. *Experimental & Molecular Medicine*, 2020. **52**(5): p. 750-761.
83. Liu, H., et al., *A Comprehensive Immunoreceptor Phosphotyrosine-based Signaling Network Revealed by Reciprocal Protein-Peptide Array Screening*. *Molecular & cellular proteomics : MCP*, 2015. **14**(7): p. 1846-1858.
84. Koch, J., et al., *Activating natural cytotoxicity receptors of natural killer cells in cancer and infection*. *Trends in Immunology*, 2013. **34**(4): p. 182-191.
85. Pinheiro, P.F., G.C. Justino, and M.M. Marques, *NKp30 - A prospective target for new cancer immunotherapy strategies*. *British Journal of Pharmacology*, 2020. **177**(20): p. 4563-4580.
86. Garrity, D., et al., *The activating NKG2D receptor assembles in the membrane with two signaling dimers into a hexameric structure*. *Proceedings of the National Academy of Sciences*, 2005. **102**(21): p. 7641-7646.
87. Quatrini, L., et al., *The Immune Checkpoint PD-1 in Natural Killer Cells: Expression, Function and Targeting in Tumour Immunotherapy*. *Cancers*, 2020. **12**(11): p. 3285.
88. Mariotti, F.R., et al., *PD-1 in human NK cells: evidence of cytoplasmic mRNA and protein expression*. *OncoImmunology*, 2019. **8**(3): p. 1557030.
89. Kumagai, S., et al., *The PD-1 expression balance between effector and regulatory T cells predicts the clinical efficacy of PD-1 blockade therapies*. *Nature Immunology*, 2020. **21**(11): p. 1346-1358.
90. Lorenz, U., *SHP-1 and SHP-2 in T cells: two phosphatases functioning at many levels*. *Immunological Reviews*, 2009. **228**(1): p. 342-359.
91. Pedicone, C., et al., *Targeting SHIP1 and SHIP2 in Cancer*. *Cancers*, 2021. **13**(4).
92. Brown, A.C.N., et al., *Super-resolution imaging of remodeled synaptic actin reveals different synergies between NK cell receptors and integrins*. *Blood*, 2012. **120**(18): p. 3729-3740.
93. Dam, T., et al., *Calcium Signaling in T Cells Is Induced by Binding to Nickel-Chelating Lipids in Supported Lipid Bilayers*. *Frontiers in Physiology*, 2021. **11**.
94. Loftus, C., et al., *Activation of Human Natural Killer Cells by Graphene Oxide-Templated Antibody Nanoclusters*. *Nano Letters*, 2018. **18**(5): p. 3282-3289.
95. Toledo, E., et al., *Molecular-scale spatio-chemical control of the activating-inhibitory signal integration in NK cells*. *Sci Adv*, 2021. **7**(24).
96. Orange, J.S., et al., *The mature activating natural killer cell immunologic synapse is formed in distinct stages*. *Proceedings of the National Academy of Sciences*, 2003. **100**(24): p. 14151-14156.
97. Hell, S.W. and J. Wichmann, *Breaking the diffraction resolution limit by stimulated emission: stimulated-emission-depletion fluorescence microscopy*. *Opt Lett*, 1994. **19**(11): p. 780-2.
98. Mace, E.M., et al., *NK Cell Lytic Granules Are Highly Motile at the Immunological Synapse and Require F-Actin for Post-Degranulation Persistence*. *The Journal of Immunology*, 2012. **189**(10): p. 4870-4880.
99. Fish, K.N., *Total internal reflection fluorescence (TIRF) microscopy*. *Curr Protoc Cytom*, 2009. **Chapter 12**: p. Unit12.18.
100. Heintzmann, R. and T. Huser, *Super-Resolution Structured Illumination Microscopy*. *Chemical Reviews*, 2017. **117**(23): p. 13890-13908.
101. Carisey, A.F., et al., *Nanoscale Dynamism of Actin Enables Secretory Function in Cytolytic Cells*. *Current Biology*, 2018. **28**(4): p. 489-502.e9.
102. Pagoon, S.V., et al., *Superresolution Microscopy Reveals Nanometer-Scale Reorganization of Inhibitory Natural Killer Cell Receptors upon Activation of NKG2D*. *Science Signaling*, 2013. **6**(285): p. ra62-ra62.
103. Oszmiana, A., et al., *The Size of Activating and Inhibitory Killer Ig-like Receptor Nanoclusters Is Controlled by the Transmembrane Sequence and Affects Signaling*. *Cell Reports*, 2016. **15**(9): p. 1957-1972.
104. Fritzsche, M., *What Is the Right Mechanical Readout for Understanding the Mechanobiology of the Immune Response?* *Frontiers in Cell and Developmental Biology*, 2021. **9**.

105. Pfannenstill, V., et al., *Quantitative Methodologies to Dissect Immune Cell Mechanobiology*. *Cells*, 2021. **10**(4): p. 851.
106. Lelek, M., et al., *Single-molecule localization microscopy*. *Nature Reviews Methods Primers*, 2021. **1**(1): p. 39.
107. Freud, A.G., et al., *The Broad Spectrum of Human Natural Killer Cell Diversity*. *Immunity*, 2017. **47**(5): p. 820-833.
108. Ferlazzo, G., *Isolation and Analysis of Human Natural Killer Cell Subsets*, in *Innate Immunity*, J. Ewbank and E. Vivier, Editors. 2008, Humana Press: Totowa, NJ. p. 197-213.
109. Poli, A., et al., *Novel method for isolating untouched rat natural killer cells with higher purity compared with positive selection and fluorescence-activated cell sorting*. *Immunology*, 2010. **131**(3): p. 386-394.
110. Liu, D., et al., *Integrin-Dependent Organization and Bidirectional Vesicular Traffic at Cytotoxic Immune Synapses*. *Immunity*, 2009. **31**(1): p. 99-109.
111. Bhat, R. and C. Watzl, *Serial Killing of Tumor Cells by Human Natural Killer Cells – Enhancement by Therapeutic Antibodies*. *PLOS ONE*, 2007. **2**(3): p. e326.
112. Zhitomirsky, B., H. Farber, and Y.G. Assaraf, *LysoTracker and MitoTracker Red are transport substrates of P-glycoprotein: implications for anticancer drug design evading multidrug resistance*. *Journal of Cellular and Molecular Medicine*, 2018. **22**(4): p. 2131-2141.
113. Galiani, S., et al., *Super-resolution Microscopy Reveals Compartmentalization of Peroxisomal Membrane Proteins*. *J Biol Chem*, 2016. **291**(33): p. 16948-62.
114. Nolen, B.J., et al., *Characterization of two classes of small molecule inhibitors of Arp2/3 complex*. *Nature*, 2009. **460**(7258): p. 1031-1034.
115. Wakatsuki, T., et al., *Effects of cytochalasin D and latrunculin B on mechanical properties of cells*. *Journal of Cell Science*, 2001. **114**(5): p. 1025-1036.
116. Platanius, L.C., *Mechanisms of type-I- and type-II-interferon-mediated signalling*. *Nature Reviews Immunology*, 2005. **5**(5): p. 375-386.
117. Gao, Y., et al., *Rational design and characterization of a Rac GTPase-specific small molecule inhibitor*. *Proc Natl Acad Sci U S A*, 2004. **101**(20): p. 7618-23.
118. Truebestein, L., et al., *A molecular ruler regulates cytoskeletal remodelling by the Rho kinases*. *Nature Communications*, 2015. **6**(1): p. 10029.
119. Ashburner, M., et al., *Gene ontology: tool for the unification of biology. The Gene Ontology Consortium*. *Nat Genet*, 2000. **25**(1): p. 25-9.
120. GO-Consortium, *The Gene Ontology resource: enriching a Gold mine*. *Nucleic Acids Res*, 2021. **49**(D1): p. D325-d334.
121. Cervero, P., et al., *Lymphocyte-specific protein 1 regulates mechanosensory oscillation of podosomes and actin isoform-based actomyosin symmetry breaking*. *Nature Communications*, 2018. **9**(1): p. 515.
122. Kim, N., et al., *Filamin A Is Required for NK Cell Cytotoxicity at the Expense of Cytokine Production via Synaptic Filamentous Actin Modulation*. *Frontiers in Immunology*, 2022. **12**.
123. Phatarpekar, P.V. and D.D. Billadeau, *Molecular regulation of the plasma membrane-proximal cellular steps involved in NK cell cytolytic function*. *Journal of Cell Science*, 2020. **133**(5).
124. Gulbranson, D.R., et al., *RABIF/MSS4 is a Rab-stabilizing holdase chaperone required for GLUT4 exocytosis*. *Proceedings of the National Academy of Sciences*, 2017. **114**(39): p. E8224-E8233.
125. Jahn, J., et al., *Decreased NK cell functions in obesity can be reactivated by fat mass reduction*. *Obesity*, 2015. **23**(11): p. 2233-2241.
126. Procaccini, C., et al., *Leptin Signaling: A Key Pathway in Immune Responses*. *Current Signal Transduction Therapy*, 2009. **4**(1): p. 22-30.
127. Korthals, M., et al., *aPIX RhoGEF Supports Positive Selection by Restraining Migration and Promoting Arrest of Thymocytes*. *The Journal of Immunology*, 2014. **192**(7): p. 3228-3238.
128. Schlam, D., et al., *Phosphoinositide 3-kinase enables phagocytosis of large particles by terminating actin assembly through Rac/Cdc42 GTPase-activating proteins*. *Nature Communications*, 2015. **6**(1): p. 8623.
129. Gowrisankaran, S., et al., *Endophilin-A coordinates priming and fusion of neurosecretory vesicles via intersectin*. *Nature Communications*, 2020. **11**(1): p. 1266.
130. Norin, U., et al., *Endophilin A2 deficiency protects rodents from autoimmune arthritis by modulating T cell activation*. *Nature Communications*, 2021. **12**(1): p. 610.
131. Yadav, S., et al., *TAOK2 Kinase Mediates PSD95 Stability and Dendritic Spine Maturation through Septin7 Phosphorylation*. *Neuron*, 2017. **93**(2): p. 379-393.
132. Morley, S.C., et al., *Gelsolin overexpression alters actin dynamics and tyrosine phosphorylation of lipid raft-associated proteins in Jurkat T cells*. *Molecular Immunology*, 2007. **44**(9): p. 2469-2480.

133. Takiguchi, K., S. Yamashiro-Matsumura, and F. Matsumura, *Artificial Phosphorylation Removes Gelsolin's Dependence on Calcium*. Cell Structure and Function, 2000. **25**(1): p. 57-65.
134. Sun, W., et al., *The function of SEC22B and its role in human diseases*. Cytoskeleton, 2020. **77**(8): p. 303-312.
135. Sowerby, J.M., et al., *NBEAL2 is required for neutrophil and NK cell function and pathogen defense*. The Journal of Clinical Investigation, 2017. **127**(9): p. 3521-3526.
136. Considine, R.V., et al., *Serum Immunoreactive-Leptin Concentrations in Normal-Weight and Obese Humans*. New England Journal of Medicine, 1996. **334**(5): p. 292-295.
137. Kazmi, A., et al., *Serum leptin values in the healthy obese and non-obese subjects of Rawalpindi*. J Pak Med Assoc, 2013. **63**(2): p. 245-8.
138. Denisin, A.K. and B.L. Pruitt, *Tuning the Range of Polyacrylamide Gel Stiffness for Mechanobiology Applications*. ACS Applied Materials & Interfaces, 2016. **8**(34): p. 21893-21902.
139. Barbieri, L., et al., *Two-dimensional TIRF-SIM-traction force microscopy (2D TIRF-SIM-TFM)*. Nature Communications, 2021. **12**(1): p. 2169.
140. Sandström, N., et al., *Live single cell imaging assays in glass microwells produced by laser-induced deep etching*. Lab on a Chip, 2022. **22**(11): p. 2107-2121.
141. Fritzsche, M., et al., *Self-organizing actin patterns shape membrane architecture but not cell mechanics*. Nature Communications, 2017. **8**: p. 14347.
142. Sezgin, E., et al., *Measuring nanoscale diffusion dynamics in cellular membranes with super-resolution STED-FCS*. Nature Protocols, 2019. **14**(4): p. 1054-1083.
143. Santos, A.M., et al., *Capturing resting T cells: the perils of PLL*. Nat Immunol, 2018. **19**(3): p. 203-205.
144. Martinez, A.L., et al., *Quantifying Human Natural Killer Cell Migration by Imaging and Image Analysis*. Methods Mol Biol, 2022. **2463**: p. 129-151.
145. Mondal, P.P., et al., *Lightsheet optical tweezer (LOT) for optical manipulation of microscopic particles and live cells*. Scientific Reports, 2022. **12**(1): p. 10229.
146. Küllmer, F., et al., *Next Generation Opto-Jasplakinolides Enable Local Remodeling of Actin Networks\*\**. Angewandte Chemie International Edition, 2022. **61**(48): p. e202210220.
147. Jünger, F., et al., *100 Hz ROCS microscopy correlated with fluorescence reveals cellular dynamics on different spatiotemporal scales*. Nature Communications, 2022. **13**(1): p. 1758.
148. O'Malley, D., A.J. Irving, and J. Harvey, *Leptin-induced dynamic changes in the actin cytoskeleton mediate the activation and synaptic clustering of BK channels*. The FASEB Journal, 2005. **19**(13): p. 1917-1919.
149. Kang, G.M., et al., *Leptin Elongates Hypothalamic Neuronal Cilia via Transcriptional Regulation and Actin Destabilization*. J Biol Chem, 2015. **290**(29): p. 18146-55.
150. Li, Z., et al., *The role of leptin on the organization and expression of cytoskeleton elements in nucleus pulposus cells*. Journal of Orthopaedic Research, 2013. **31**(6): p. 847-857.
151. Gotthardt, D., et al., *JAK/STAT Cytokine Signaling at the Crossroad of NK Cell Development and Maturation*. Frontiers in Immunology, 2019. **10**.
152. Van Acker, T., J. Tavernier, and F. Peelman, *The Small GTPase Arf6: An Overview of Its Mechanisms of Action and of Its Role in Host-Pathogen Interactions and Innate Immunity*. International Journal of Molecular Sciences, 2019. **20**(9): p. 2209.
153. Hausser, A., et al., *Protein kinase D regulates vesicular transport by phosphorylating and activating phosphatidylinositol-4 kinase III $\beta$  at the Golgi complex*. Nature Cell Biology, 2005. **7**(9): p. 880-886.
154. Mullins, R.D., J.A. Heuser, and T.D. Pollard, *The interaction of Arp2/3 complex with actin: Nucleation, high affinity pointed end capping, and formation of branching networks of filaments*. Proceedings of the National Academy of Sciences, 1998. **95**(11): p. 6181-6186.
155. Gwalani, L.A. and J.S. Orange, *Single Degranulations in NK Cells Can Mediate Target Cell Killing*. The Journal of Immunology, 2018. **200**(9): p. 3231-3243.
156. de Beco, S., et al., *Optogenetic dissection of Rac1 and Cdc42 gradient shaping*. Nature Communications, 2018. **9**(1): p. 4816.
157. Brunetti, R.M., et al., *WASP integrates substrate topology and cell polarity to guide neutrophil migration*. Journal of Cell Biology, 2021. **221**(2).
158. Schindelin, J., et al., *Fiji: an open-source platform for biological-image analysis*. Nature Methods, 2012. **9**(7): p. 676-682.
159. Dagley, L.F., et al., *Universal Solid-Phase Protein Preparation (USP3) for Bottom-up and Top-down Proteomics*. Journal of Proteome Research, 2019. **18**(7): p. 2915-2924.
160. Chen, F., P.W. Tillberg, and E.S. Boyden, *Optical imaging. Expansion microscopy*. Science, 2015. **347**(6221): p. 543-8.

161. Tillberg, P.W., et al., *Protein-retention expansion microscopy of cells and tissues labeled using standard fluorescent proteins and antibodies*. Nat Biotechnol, 2016. **34**(9): p. 987-92.
162. Xu, H., et al., *Molecular organization of mammalian meiotic chromosome axis revealed by expansion STORM microscopy*. Proceedings of the National Academy of Sciences, 2019. **116**(37): p. 18423-18428.
163. Gao, M., et al., *Expansion Stimulated Emission Depletion Microscopy (ExSTED)*. ACS Nano, 2018. **12**(5): p. 4178-4185.
164. Zwettler, F.U., et al., *Molecular resolution imaging by post-labeling expansion single-molecule localization microscopy (Ex-SMLM)*. Nature Communications, 2020. **11**(1): p. 3388.
165. Li, R., et al., *Expansion enhanced nanoscopy*. Nanoscale, 2018. **10**(37): p. 17552-17556.
166. Gambarotto, D., et al., *Imaging cellular ultrastructures using expansion microscopy (U-ExM)*. Nat Methods, 2019. **16**(1): p. 71-74.
167. Braverman, N.E. and A.B. Moser, *Functions of plasmalogen lipids in health and disease*. Biochim Biophys Acta, 2012. **1822**(9): p. 1442-52.
168. Nagotu, S., et al., *Molecular basis of peroxisomal biogenesis disorders caused by defects in peroxisomal matrix protein import*. Biochim Biophys Acta, 2012. **1822**(9): p. 1326-36.
169. Waterham, H.R., S. Ferdinandusse, and R.J. Wanders, *Human disorders of peroxisome metabolism and biogenesis*. Biochim Biophys Acta, 2016. **1863**(5): p. 922-33.
170. Wiedemann, N. and N. Pfanner, *Mitochondrial Machineries for Protein Import and Assembly*. Annual Review of Biochemistry, 2017. **86**(1): p. 685-714.
171. Léon, S., et al., *Dynamics of the peroxisomal import cycle of PpPex20p: ubiquitin-dependent localization and regulation*. J Cell Biol, 2006. **172**(1): p. 67-78.
172. Meinecke, M., et al., *The peroxisomal importomer constitutes a large and highly dynamic pore*. Nat Cell Biol, 2010. **12**(3): p. 273-7.
173. Erdmann, R. and W. Schliebs, *Peroxisomal matrix protein import: the transient pore model*. Nat Rev Mol Cell Biol, 2005. **6**(9): p. 738-42.
174. Platta, H.W., et al., *Functional role of the AAA peroxins in dislocation of the cycling PTS1 receptor back to the cytosol*. Nat Cell Biol, 2005. **7**(8): p. 817-22.
175. Miyata, N. and Y. Fujiki, *Shuttling mechanism of peroxisome targeting signal type 1 receptor Pex5: ATP-independent import and ATP-dependent export*. Mol Cell Biol, 2005. **25**(24): p. 10822-32.
176. Rhee, J.M., et al., *In vivo imaging and differential localization of lipid-modified GFP-variant fusions in embryonic stem cells and mice*. Genesis, 2006. **44**(4): p. 202-18.
177. Cizmowski, C., et al., *A monoclonal antibody for in vivo detection of peroxisome-associated PTS1 receptor*. Hybridoma (Larchmt), 2011. **30**(4): p. 387-91.
178. Pesce, L., et al., *Measuring expansion from macro- to nanoscale using NPC as intrinsic reporter*. Journal of Biophotonics, 2019. **12**(8): p. e201900018.
179. Kubalová, I., et al., *Prospects and limitations of expansion microscopy in chromatin ultrastructure determination*. Chromosome Research, 2020. **28**(3): p. 355-368.
180. Pernal, S.P., et al., *Nanoscale imaging using differential expansion microscopy*. Histochemistry and Cell Biology, 2020. **153**(6): p. 469-480.
181. King, C., et al., *ER membranes exhibit phase behavior at sites of organelle contact*. Proc Natl Acad Sci U S A, 2020. **117**(13): p. 7225-7235.
182. Lim, Y., et al., *Mechanically resolved imaging of bacteria using expansion microscopy*. PLoS Biol, 2019. **17**(10): p. e3000268.
183. Smith, J.J. and J.D. Aitchison, *Peroxisomes take shape*. Nature Reviews Molecular Cell Biology, 2013. **14**(12): p. 803-817.
184. Otera, H., et al., *Peroxisomal targeting signal receptor Pex5p interacts with cargoes and import machinery components in a spatiotemporally differentiated manner: conserved Pex5p WXXXF/Y motifs are critical for matrix protein import*. Mol Cell Biol, 2002. **22**(6): p. 1639-55.
185. Saidowsky, J., et al., *The di-aromatic pentapeptide repeats of the human peroxisome import receptor PEX5 are separate high affinity binding sites for the peroxisomal membrane protein PEX14*. J Biol Chem, 2001. **276**(37): p. 34524-9.
186. Schliebs, W., et al., *Recombinant human peroxisomal targeting signal receptor PEX5. Structural basis for interaction of PEX5 with PEX14*. J Biol Chem, 1999. **274**(9): p. 5666-73.
187. Kim, D., et al., *Amplified Expansion Stimulated Emission Depletion Microscopy*. ChemBiochem, 2019. **20**(10): p. 1260-1265.
188. Stanley, W.A., et al., *Recognition of a functional peroxisome type 1 target by the dynamic import receptor pex5p*. Mol Cell, 2006. **24**(5): p. 653-663.

189. Büttner, M., et al., *Challenges of Using Expansion Microscopy for Super-resolved Imaging of Cellular Organelles*. *ChemBioChem*, 2021. **22**(4): p. 686-693.

# Angaben zur Person und zum wissenschaftlichen Werdegang

Herr Maximilian Lothar Wilhelm Büttner  
M. Sc. Biochemie  
Fachgebiet der Promotion: Biochemie



## Werdegang



Juni 2017 – Juni 2023

MARTIN-LUTHER-UNIVERSITÄT HALLE-WITTENBERG, Halle (Saale)  
Institut für Anatomie und Zellbiologie, AG Professorin Heike  
Kielstein

**Wissenschaftlicher Mitarbeiter**



April 2018 – Dezember 2018

UNIVERSITY OF OXFORD, Oxford  
Weatherall Institute for Molecular Medicine, AG Professor Christian  
Eggeling

**Gastwissenschaftler**



Oktober 2014 – Juli 2017

MARTIN-LUTHER-UNIVERSITÄT HALLE-WITTENBERG, Halle (Saale)

**Master of Science in Biochemie**



Oktober 2010 – März 2014

LUDWIG-MAXIMILIANS-UNIVERSITÄT, München  
**Bachelor of Science in Chemie und Biochemie**



August 1997 – Juli 2010

ALBRECHT-DÜRER-GYMNASIUM, Hagen  
**Abitur**

---

Ort, Datum

---

Maximilian Lothar Wilhelm Büttner



# **Eidesstattliche Erklärungen gemäß § 5 Promotionsordnung**

## **Erklärung zum Wahrheitsgehalt der Angaben**

Ich erkläre, die Angaben wahrheitsgemäß gemacht und die wissenschaftliche Arbeit an keiner anderen wissenschaftlichen Einrichtung zur Erlangung eines akademischen Grades eingereicht zu haben. Weiterhin erkläre ich, dass ich bislang keine vergeblichen Promotionsversuche unternommen habe.

## **Eidesstattliche Erklärung**

Ich erkläre an Eides statt, dass ich die Arbeit selbstständig und ohne fremde Hilfe verfasst, keine anderen als die von mir angegebenen Quellen und Hilfsmittel benutzt und die den benutzten Werken wörtlich oder inhaltlich entnommenen Stellen als solche kenntlich gemacht habe.

## **Vorstrafen, Ermittlungsverfahren**

Hiermit erkläre ich, dass ich weder vorbestraft bin, noch dass gegen mich Ermittlungsverfahren anhängig sind.

---

Ort, Datum

---

Maximilian Lothar Wilhelm Büttner